Politecnico di Torino

Master of Science in Biomedical Engineering

Thermo-sensitive and photo-curable polymeric hydrogels as potential drug delivery systems and bioinks

SUPERVISORS
Prof. Gianluca Ciardelli
Dr. Monica Boffito

CANDIDATE
Enea Peretti

December 2019

Table of Content

Abstract

In recent years, the development of innovative microfabrication and rapid prototyping techniques has increased the demand of bioinks with tunable chemical and mechanical properties to target different biomedical applications. In this thesis work, a collection of thermo-sensitive and photo-curable polymeric hydrogels has been designed, based on the combination of an amphiphilic poly(ether urethane) (PEU) entrapped within a photo-crosslinked poly(ethylene glycol) diacrylate (PEGDA) mesh. The rationale underpinning the introduction of a photo-sensitive component lies on the need to increase the overall hydrogel stability in aqueous environment, thus allowing a better answer to the strict requirements of both regenerative medicine and drug delivery applications. On the other hand, the use of a thermo-sensitive component ensured capability to quickly reach a primary stability and initially retain its shape.

Thermo-sensitivity was provided by use of a previously developed amphiphilic poly(ether urethane) (acronym NHP407) based on the commercial Poloxamer P407, 1,6-hexanediisocyanate (HDI) and an amino acid derived diol (N-Boc serinol) as chain extender. After the synthesis, the BOC caging group present in the chain extender was eliminated by deprotection in acidic conditions (acronym of the deprotected PEU SHP407), thus exposing free amines along polymer chains which could be exploited for further functionalization or to provide the developed systems with antibacterial properties. The success of the synthesis and the absence of degradation upon deprotection reaction were confirmed by Attenuated Total Reflectance Fourier Transform Infrared (ATR-FTIR) spectroscopy and size exclusion chromatography (SEC) (weight average molecular weight of NHP407 and SHP407 were 52000 Da and 53000 Da, respectively). A quantification of the exposed amino groups along SHP407 chains was also performed using a Ninhydrin colorimetric assay ($7.24*10^{16}$ NH_2/g).

The gelation properties of NHP407- and SHP407-based hydrogels were investigated by tube inverting test in temperature ramp and isothermal conditions (37 °C) to assess gelation temperature and gelation time in physiological conditions, respectively. Critical micellar temperature (CMT) and temperature-dependent micelle size analysis were also performed on not-gelling systems to assess the effects of the deprotection reaction on polymer chain

arrangement into micelles and micelle aggregates obtaining non relevant differences between the two materials: the decrease of hydrogel concentrations leads to longer times and higher temperatures to undergo sol-gel transitions.

Based on these considerations, a final concentration of 12.5% w/v was selected for SHP407, in order to obtain a gelation temperature within the physiological range (i.e., ~27.5°C) and a gelation time at 37 °C (i.e., ~28 min) suitable for the considered applications.

12.5% w/v concentrated SHP407 hydrogels were then made photo-sensitive adding PEGDA. The end-capping functionalization with acrylate moieties was performed on three poly(ethylene glycol) (PEG) differing in their number average molecular weights (M_n 3350, 4600 and 6000 Da), with the aim to finally obtain different mesh sizes in the final blends between SHP407 and PEGDA (acronyms PEGDA 3350, PEGDA 4600 and PEGDA 6000). Success of PEGDA synthesis was confirmed by ATR-FTIR spectroscopy (appearance of peaks near 172 cm^{-1} and 1637 cm^{-1} relative to acrylate groups) and the acrylation degree of each synthetized PEGDA was estimated by Proton Nuclear Magnetic Resonance (^{1}H-NMR) Spectroscopy (acrylation degree of PEGDA3350, PEGDA 4600 and PEGDA 6000 81 , 86 and 77 %, respectively).

However, PEGDA with a molecular weight of 4600 Da was found to be insoluble in aqueous solvents at concentrations higher than 1.5% w/v, probably because of its high acrylation degree. Hence, SHP407-PEGDA blends were designed considering only PEGDA 3350 and PEGDA 6000. Blend composition was defined with the aim to compare formulations with equal amount of acrylate moieties or equal PEGDA content (i.e., PEGDA % w/v concentration), but different PEGDA molecular weight. Three blend formulations per different PEGDA molecular weight were thus developed: 3, 5.5 and 10% w/v for PEGDA 3350 and 5.5, 10 and 18% w/v for PEGDA 6000. The amount of SHP407 was kept constant at 12.5% w/v as previously discussed.

Sol-gel systems based on SHP407-PEGDA blends were characterized as previously done for the sole SHP407-based systems and a general faster gelation kinetics was found for the blends (e.g. 8 min vs 4 min for SHP407 and SHP407-PEGDA600_10% w/v, respectively) , more relevant for the PEGDA 6000-based hydrogels (e.g. 5 and 4 minutes for SHP407-PEGDA3350_10%w/v and SHP407-PEGDA6000_10%w/v, respectively). Rheological

characterization (temperature ramp, frequency sweep and stain sweep tests) confirmed the qualitative results obtained from qualitative tube inverting tests, with fully developed gels at 37 °C and a progressive embrittlement for compositions containing increasing PEGDA 6000 concentration (linear viscoelastic region width for SHP407-PEGDA6000_10%w/v and SHP407-PEGDA6000_18%w/v: 0.69 and 0.05 % respectively). Printability tests were also performed using a commercially available bioprinter (Inkredible +, CELLINK) using a 27G tip (200 μm), pressures of tens kPa and printing at room temperature, which are conditions suitable to print in the presence of cells. All blends were able to produce continuous filaments and primarily maintain the shape before photo-curing.

To perform swelling and stability tests in physiological conditions (37°C, Phosphate-buffered saline - PBS), circular-shaped samples of approx. 10 mm diameter and 2 mm thickness were produced and photo-crosslinked using UV light (365 nm, 3 min irradiation, 10 mW/cm^2) and lithium phenyl-2,4,6-trimethylbenzoylphosphinate (LAP) at 0.05% w/v concentration as photo-initiator. Although the blends containing PEGDA 3350 were stable for a short period of time (i.e., fews days), samples based on PEGDA 6000 were still present after several weeks of incubation, with a limited weight loss and a good shape maintenance.

Finally, to verify the possibility to use the developed hydrogels as drug delivery platforms, Fluorescein Isothiocyanate-Dextran (FD4) was used as a model biomolecule and absorption and release tests were performed. The systems showed a good ability to absorb the molecule and the release was in general modulated by PEGDA content, with a slower kinetics for the blends containing a higher PEGDA percentage.

The herein developed platform of thermo- and photo-sensitive hydrogels could thus find widespread application in the biomedical field as drug releasing systems or bioinks for 3D printing applications. The compositional versatility of these hydrogels makes them suitable to a variety of applications, with the potential to target the properties of any soft tissue of the body and any desired payload release profile.

Thesis goal

The goal of this exploratory work is focused on the design of novel hydrogels for applications in the tissue engineering and regenerative medicine fields. In recent years, the frontiers of these disciplines led the research toward innovative materials, with appropriate chemical and physical characteristic for the production of scaffolds using microfabrication techniques. In particular, the materials designed to produce printable hydrogels for *in vivo* biomedical applications must be able to be extruded applying physical parameters that avoid cellular damage. For this aim, the viscosity should be sufficiently low to allow easy injection without creating elevate shear stress and a homogeneous drugs and/or cells dispersion. Moreover, the material permeability must allow the exchange of nutrients and waste substances and the degradation rate must avoid an initial burst release of the loaded cells and/or drugs, to maintain a stable environment for cell activity and accompany the tissue regrow.

Hydrogels are ideal candidates in this bioengineering research field, thanks to their ability to absorb a large amount of water or biological fluids and because of their texture similar to biological tissues. Synthetic polymeric hydrogels are particularly suitable for this purpose thanks to their easily tunable properties in terms of mechanical and slow-degradative characteristics. These peculiarities extend the combination of application to a large set of different tissue presenting different mechanical properties. However, synthetic hydrogels can have disadvantages related to low cytocompatibility and/or production of toxic degradation products. For this reason, only a limited collection of synthetic polymers can be applied.

In this thesis work, a set of biocompatible and biodegradable synthetic hydrogels as potential bioinks and drug delivery systems will be designed. The hydrogels will comprise a thermosensitive and a photocurable component: these two elements will be mixed together at different concentrations, in order to obtain a library of different physical and mechanical properties.

The thermosensitive component will be represented by an amphiphilic polyurethane based on a Food and Drug Administration approved polymer (Poloxamer 407®) that will be

synthetized in the first phases of this project, following a protocol previously developed (Boffito et al). A deprotection of the amino groups by Boc cleaving will then be performed to improve the material hydrophilicity and cytocompatibility and to allow further functionalization. The thermo-sensitivity given by this component allows the injection or printability in sol or semi-sol phase and guarantees a gel state at physiological temperature (37°C). These properties will also allow the dissolution of drugs in the hydrogel systems at mild conditions and enable a future cell encapsulation.

On the other hand, the photocurable component will be represented by polyethylene glycol diacrylate (PEGDA), that will be synthetized at three different molecular weights (3350 Da, 4600 Da and 6000 Da) by the reaction of PEG with acryloyl chloride. The photocurable polymer has the purpose to improve the stability of the material and influence the drug release through the different mesh dimension obtained after photocuring.

PEGDA will be added at different concentrations to investigate how the different molecular weight and concentration will influence the physical properties, swelling, degradation rate, drug release, absorption and stiffness. The systems will then be characterized in terms of thermal response and photo-sensitivity, moreover their rheological characteristics will be investigated and the printability using a commercial bioprinter (INKREDIBLE+^{TM}, Cellink) will be assessed.

1 Introduction and State of Art

1. Hydrogels

1.1. Definition

The first studies about hydrogels date back to more than half a century ago [1], with the pioneering work of Wichterle and Lim, that provided one of the first cross-linked hydrogels made by hydroxyethyl methacrylate (HEMA) in 1960 [2]. Nowadays, hydrogels are a topic of great interest for material scientists and biomedical researchers and a lot of innovations have been introduced in the biomedical engineering field in terms of applications and formulations.

Hydrogels are a class of materials with an elastic and gummy consistency composed by a three-dimensional (3D) network that consists of hydrophilic homopolymers or copolymers. Hydrogels are characterized by the ability to retain a significant amount of water or physiological fluids without dissolving in them in the short time term. These materials show good biocompatibility, tunable chemical composition and physical characteristics: due to these properties, they have shown many applications in biomedical field. Their hydrophilic nature allows the uptake of a copious amount of water, which makes them able to mimic the extracellular matrix (ECM) and provides them with tissue-like characteristics in three-dimensions. For these reasons, hydrogels alone or in combination with cells are good candidates to be used as scaffolds in tissue engineering and regenerative medicine. [3] Additionally, they have been also reported as suitable carriers for the localized and sustained delivery of drugs and biomolecules [4]. The wet environment of the hydrogel stimulates the migration of cells and allows the exchange of nutrients and waste substances; moreover, it guides and influences the release kinetics of drugs and biomolecules in the organism. Hydrogels can also be injectable systems; they are able to perfectly fill body cavities or defects and this characteristic makes them interesting materials in minimally invasive surgery applications.

1.2. Hydrogel Characteristics

1.2.1. Swelling: Water in hydrogel

The infusion of nutrients in the hydrogel and the release of substances are influenced by the nature of the water absorbed by the hydrogel. The absorption of water occurs on the hydrogel surface firstly and then in the inner part. This process induces the swelling of the material (**Figure 1**). In detail, three different kinds of water can be identified: primary bound water, secondary bound water and free water (**Figure 2**) [5].

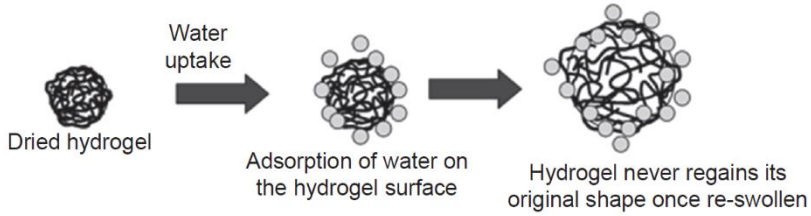

Figure 1: Hydrogel water absorption.

As a dry hydrogel is put in a wet environment, it begins absorbing water, thus increasing its volume. The "*primary bound water"* includes the first group of water molecules that enters in the hydrogel network and hydrates the most polar, hydrophilic chemical groups. After the hydrophilic groups are bound to water molecules, the network swells and this allows the hydrophobic groups to be exposed and interact with the "*secondary bound water"* molecules. The total amount of primary and secondary bound water forms the "*total bound water"*. At this point all polar and non-polar groups are saturated by water molecules and the network imbibes additional water, led by osmotic driving force of the network chains towards infinite dilution. While this *"free water"* continues to enter in the system causing additional swelling, the elastic forces of the structure of the polymeric network oppose to the swelling, until an equilibrium of forces is reached. This *"free water"* fills the void spaces present within the polymernetwrok, without bounding to it.

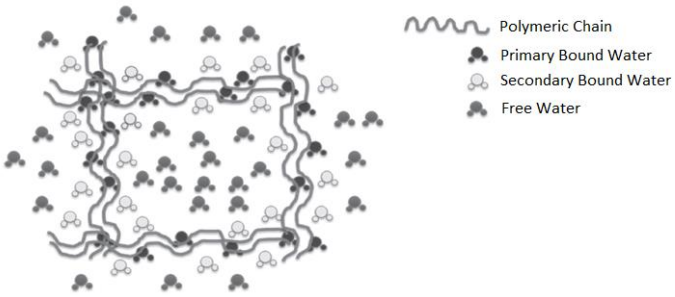

Figure 2: The three physical states of water in a hydrogel [4].

The three types of water in the hydrogel have different behavior at low temperatures:

- the *primary bound water* does not freeze at the usual freezing point because it is strongly linked to hydrophilic segments of the network;
- the *secondary bound water* freezes at temperature lower than the usual temperature of freezing because its behavior is influenced by the bounds with free water and hydrophobic segments of the network;
- the *free water* is the only type of water capable to freeze at 0°C because it does not have any interaction with the material.

There are two main methods to estimate the amount of free and bound water as fraction of the total water absorbed by the hydrogel: Differential Scanning Calorimetry (DSC) and probe molecule method.

A Differential Scanning Calorimetry instrument measures the amount of heat required to increase the temperature of a sample and a reference, and considers the differences as a function of temperature [6]. The rational of this method is based on the hypothesis that only free water in the hydrogel can form ice crystals; according to this, it is assumed that the endothermic energy measured when the gel is defrosting characterizes the melting of free water. The bound water is calculated by difference between all the water absorbed by the hydrogel and the obtained free water.

The *probe molecule method* uses a solution of a particular probe and is based on several hypothesis: (i) only free water can dissolve the solute; (ii) the solute has no effect on the distribution of free and bound water in the hydrogel; (iii) the entire free water is accessible to the solute; (iv) the concentration of the solute outside and inside the hydrogel is equal

after equilibrium is reached; and (v) the solute does not influence the gel matrix chains. During the test, the hydrogel is put in a solution of a fluorescent probe molecule until equilibrium is reached. Then, the volume absorbed by the hydrogel is measured. Knowing the concentration of the solution before and after the equilibrium and the volume absorbed, the molecule amount is derived and the volume of free water is calculated. Then bound water is obtained as difference between absorbed water and free water. The use of a fluorescent probe allows to spectrophotometrically evaluate the concentration of the solution.

From another point of view, swelling is considered as the property of the material to absorb water and keep it for a long time period. It can be quantified measuring the dry weigh and the swollen-state weight and calculating the swelling either as a weight variation or as a volume of solvent that has been absorbed [6] (**Figure 3**).

$$W.U. = \frac{swollen\ weight - dry\ weight}{dry\ weight} \times 100 \qquad V.A.S. = \frac{swollen\ weight - dry\ weight}{water\ density} \times 100$$

Figure 3: Water Uptake and Volume of Absorbed Solvent

The capacity of the hydrogel to swell depends on the nature of the polymer that constitutes the network, on the crosslinking agents and therefore on the crosslinking degree [7]. The swelling degree is influenced by the presence of a crosslinking agent because its polarity can modify the hydrophilicity of the material and because it constrains the polymeric chains, acting as bridge. The addition of a big amount of crosslinkers increases the stiffness and rigidity of the material; for example, this characteristic is exploited in pharmaceutical devices to disrupt capsules and tablets containing drugs. The more the hydrogel is crosslinked, the less it is able to absorb water: in general, the swelling evaluation is the simplest way to classify a hydrogel as crosslinked or not crosslinked [8].

In the deswelling process, caused by heating or lyophilization, the three classes of water leave the hydrogel in a specific order: free water, secondary bound water and then primary bound water in the last phase (**Figure 5**). This mechanism causes dehydration and therefore

the shrinking of the hydrogel, which is caused by the unbinding of the water molecules from the polymeric chains (**Figure 4**).

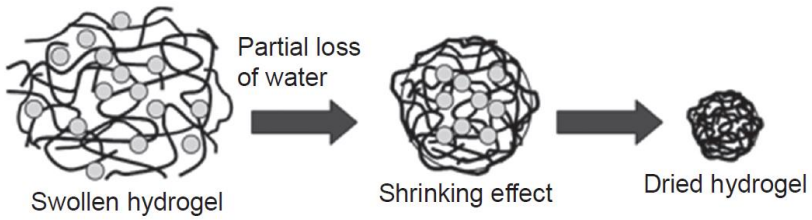

Figure 4: Deswelling mechanism [4].

Following an increase in temperature, at first the free water evaporates from the hydrogel, then the secondary bound water begins to leave the interstitial spaces between different chains. At this point, the system becomes a sort of intermediate material between a gel and a glass and under a certain boundary level of water content, the material transforms into a glassy state with few traces of water in it.

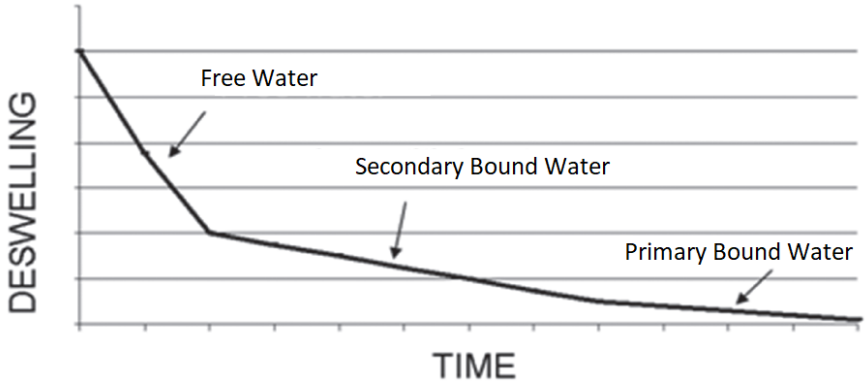

Figure 5: Deswelling mechanism in time [4].

1.2.2. Mesh size and porosity

A hydrogel is formed by statistically distributed polymeric chains dispersed in a liquid phase; as a result, this architecture creates a combination of fluctuating pores and micro-channels. The network does not exhibit a static configuration and its pores are formed and removed following the thermal motion of the polymeric chains. The presence of pores is very important for tissue engineering applications, because it influences cellular behavior and proliferation and the release profile of an encapsulated payload. [9]

Porosity can be generally defined as the presence of cavity in the bulk material. It can be interconnected or closed, and this morphological feature is important because it influences many phenomena as cell migration, osmosis and molecule release.

A method to quantify the porosity measures the total volume of pores in the hydrogel through the solvent required to fill the hollow parts of the scaffold [10]. The hydrogel is put in a graduated cylinder with a known volume of ethanol (V_1). The total volume after the hydrogel immersion is recorder (V_2). The hydrogel is removed after the solvent fills all the cavities and the remaining volume in the cylinder is registered (V_3). The total amount volume (V_T) and then the porosity (χ) are calculated using the formulas reported in **Figure 6**.

$$\chi = \frac{(V_1 - V_3)}{V_T} \times 100 \quad ; \; V_T = V_2 - V_3$$

Figure 6: Porosity quantification.

Pores in the hydrogels can be considered at different scales. Micro-porosity is constituted by the spaces among the single polymer chains and depends on the solvation of the hydrophilic segments during water uptake. These pores have a dimension between 10 and 100 nm and they are responsible for the diffusion and release of small molecules, water, oxygen, salts and metabolites with low molecular weight. Macro-porosity, on the other hand, presents pores between 1 and 100 µm and influences cell behavior and homing, as well as the formation of a new tissue.

As mentioned before, micro-porosity influences molecule release. The release kinetics depends on the relative dimension between the encapsulated molecule and the hydrogel mesh. If the molecule is smaller than the porosity, it will be released easily and in a short time; if the dimension is comparable to the pore diameter, the substance will be released more slowly. Lastly, if the molecule is significantly bigger that the pores, it will not be able to pass through the mesh of the hydrogel and will be retrained by the hydrogel, or eventually released if swelling phenomena sufficiently enlarge the mesh size.

The mesh dimension is often studied using dextran markers of different molecular weight as macromolecular drug model [11]. Dextran fluorescent molecules are encapsulated in the hydrogel and the diffusion rates in aqueous media are obtained measuring the concentration of dextran released in the solution by UV-visible spectroscopy. The mesh dimension can then be derived knowing the dimension and hydrodynamic diameter of the model molecules.

The dimension of the hydrogel mesh can also be obtained through a mathematical model, based on Flory-Rehner theory [12], that considers the thermodynamic of the interactions between the polymer and the water molecules.

The pore-size distribution is then dependent on:

- The concentration of chemical cross-links between the polymeric chains, quantified by the initial ratio of crosslinker to monomer;
- The concentration of physical entanglements in the polymeric network, quantified by the initial concentration of polymerizable monomers;
- The presence of a net charge in the hydrogel, which can result in repulsion between chains with the same charge.

1.2.3. Degradation and dissolution

When the hydrogel is maintained in a wet environment for a long time period, it can run into a progressive process of destruction caused by two main phenomena: degradation and dissolution.

Degradation is a chemical phenomenon that occurs when the polymeric chains are progressively cut in shorter chains through a chemical reaction, such as hydrolysis. *Dissolution* is a physical phenomenon that consists in the gradual dispersion of the polymeric chains from the hydrogel to the liquid solution in which the material is included. Both processes are closely linked to the concept of stability that defines the hydrogel's attitude to maintain its chemical and physical characteristic when exposed to external stimuli over a long time period.

Hydrogel biodegradability is a required property for biomedical applications and it can be regulated by introducing weak bonds within the polymer backbone, that can be broken in physiological conditions. One of the main biodegradation processes is hydrolysis, in which water takes part in the material disaggregation thanks to his polarity. This process produces secondary compounds that can be metabolized into safety products or directly expelled from the organism by renal filtration (**Figure 7**) [13].

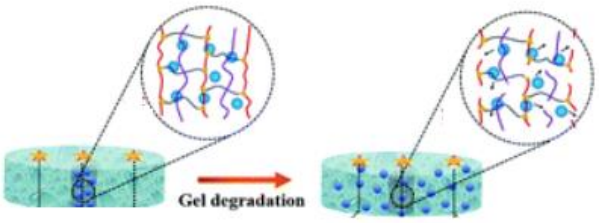

Figure 7: Hydrogel Degradation [13].

The metabolism and degradation of the polymers used as forming-materials in hydrogel design are important factors to consider because, in addition to biocompatibility, the degradation process must not induce local acidity that could damage cell survival and accelerate some degradation processes.

Hydrogel degradation rate is also important because it influences the release rate of drugs or biomolecules. Biodegradation is exploited to control drug release over an extended time period [14]. While the hydrogel absorbs water, the mesh size is increased and the encapsulated molecules are allowed to pass through the polymeric chains. The release can also be mediated by degradation, since the progressive disruption of the hydrogel structure causes the dispersion of the payload along with the polymer debris.

While *in vitro* dissolution/degradation studies are generally conducted evaluating weight loss, an example of an *in vivo* degradation test is the one based on Bolton-Hunter reagent. In this test, biomolecules are labelled with a radioactive molecule and the time course of radioactivity resting in the tissue of a mouse after subcutaneous implantation is monitored.

The degradation rate is an important factor also in tissue engineering applications, because it must be compatible with the generation of a new tissue, providing a proper support to

the cells involved in the process but at the same time permitting the gradual formation of natural structures such as the extracellular matrix (ECM).

1.3. Natural and synthetic hydrogels

According to their origin, hydrogels can be categorized in two classes: natural and synthetic hydrogels [6]. In both cases, the main component is represented by polymers, which are molecular compounds characterized by high molecular weight and composed by repetitive chemical units called monomers. The nature of the polymer reflects on the hydrogel category.

Natural hydrogels include systems based on gelatin, collagen, hyaluronic acid, agarose, fibrin, elastin and derivatives of natural materials such as chitosan, alginate and silk fibers. Most of these polymers are components of the extracellular matrix and for this reason this class of hydrogels is considered to be the most biomimetic and physiological. Their high biocompatibility is especially due to the endogenous signals they provide and that encourage cellular interactions and guide the formation of a new tissue [15]. However, they also show some disadvantages: 1) their mechanical characteristics and their dependence on gelation and polymerization conditions are not totally understood yet, 2) their great batch-to-batch variability caused by the natural origin and 3) their immunogenicity risk derived from the use of animal sources. For these reasons, the production of natural hydrogels is not easily scalable and it is difficult to control and reproduce their final properties and microstructures.

Synthetic hydrogels comprise poly(vinyl alcohol) (PVA), poly(N-isopropylacrylamide) (PNIPAm), poly(2-hydroxyethyl methacrylate) (PHEMA), poly(acryl amide), poly(ethylene glycol) diacrylate (PEGDA), and poly(2-hydroxypropyl methacrylate) (PHPMA). The first application of synthetic hydrogels dates back to the late 1950s', when contact lenses were produced for the first time [16]. These materials have predictable chemical and mechanical properties and are characterized by a more consistent composition, which make them more reproducible. However, they usually do not possess specific functional sites to promote cell interactions and for this reason they are less biocompatible than natural hydrogels. The properties of synthetic polymers can be controlled through the process parameters, as the production method, the use and combination of different monomer

units to form copolymers, the control of amorphous and crystalline regions and the cross-linking grade.

In some cases, the characteristics of natural and synthetic hydrogels are combined into bioartificial hydrogels.

1.4. Physical and Chemical hydrogels

Hydrogels can be stable or degrade/dissolve in a short time period. This characteristic usually depends on the nature of the interactions existing among the polymer chains: in view of this, hydrogels can be classified as physical or chemical hydrogels (**Figure 8**).

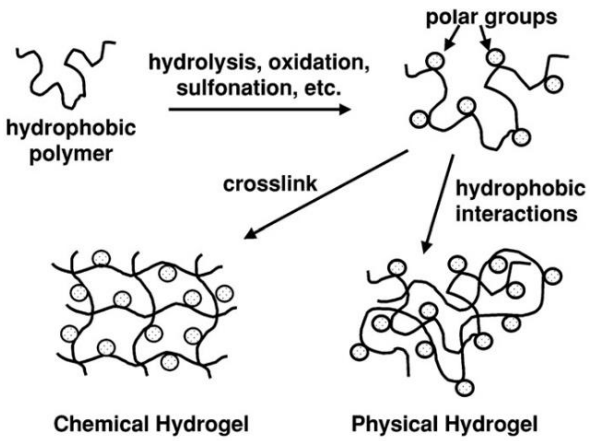

Figure 8: Chemical and Physical Hydrogels [17].

Chemical hydrogels (also called "permanent") are characterized by the covalent crosslinking of the polymeric monomers or chains of the network. They are considered permanent because covalent bonds among the polymer chains prevent the dissolution of the network structure when it is put in aqueous environment. Chemical hydrogels can be synthesized via radical polymerization reaction of low molecular weight monomers that present polymerizable groups. The functional groups (for example -COOH, $-NH_2$ and -OH) of different monomers react together to create a link between different polymer chains. This type of polymerization requires the presence of an initiator and a crosslinking agent that acts like a bridge between two different chains (**Figure 9**).

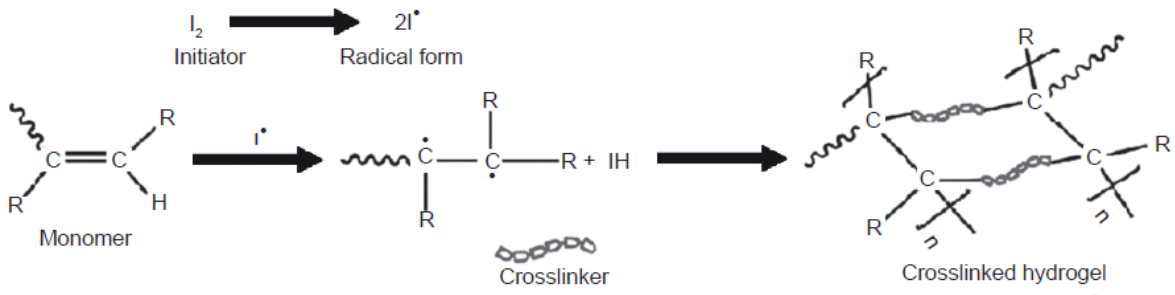

Figure 9: Radical reaction of monomers with initiator and crosslinker [18].

In alternative, high-energy radiations can be used to polymerize unsaturated compounds in the polymeric chains to obtain a permanent mesh.

Physical hydrogels (also called *"*reversible") are hydrogels whose polymeric chains are kept together by entanglements of the chains and/or secondary forces, such as ionic, hydrophobic, H-bonding forces and electrostatic interactions. A physical hydrogel appears as a non-homogeneous system, because it is composed by clusters of entangled chains and/or hydrophobic-hydrophilic domains, that create a gel-like structure by interacting together [19]. This class of hydrogels also include "smart" materials, that are able to spontaneously form a gel system in response to different types of environmental stimuli [20]. These hydrogels are reversible and able to become instable and dissolve under specific external conditions, leading to a growing interest in their development. The variable environment of the human body can indeed be exploited to induce changes in the hydrogel network to lead phase transformations, tunable degradation/dissolution and controlled drug release.

1.4.1. Stimuli-sensitive hydrogels

1.4.1.1. pH-sensitive hydrogels

Although the pH of blood in physiological conditions is comprised between 7.35 and 7.45 [21], different tissues, organs and cellular compartments and pathological states feature changes in the pH values. This variation has a potential as targeting for hydrogel drug delivery systems. pH-sensitive hydrogels are formed by polymers exposing functional groups capable to accept or donate protons (H^+), making them weak acids or bases. The most common functional groups are -COOH for weak acids and -NH_2 for weak bases.

The presence of the protonated or deprotonated form depends on local pH and on the strength of the acid/base involved in the equilibrium reactions. These are represented by the acid dissociation constant K_a and the basic disassociation constant K_b (**Figure 10**).

$$K_{\mathrm{a}} = \frac{[\mathrm{A}^-][\mathrm{H}^+]}{[\mathrm{HA}]} \qquad K_{\mathrm{b}} = \frac{[\mathrm{BH}^+][\mathrm{OH}^-]}{[\mathrm{B}]}$$

Figure 70: Dissociations Constants

In case of weak acid groups (-COOH), the equilibrium is moved to the deprotonated (COO-) form when the pH value is greater than the pK_a value and the group is negatively charged. On the contrary, in case of weak basic groups ($-NH_2$), the equilibrium is moved to the protonated form ($-NH_3^+$) when the pH value is lower than pK_b and the group is positively charged. In both cases, the presence of an electrical charge increases the hydrophilicity of the hydrogel and causes an electrostatic repulsion between the polymeric chains. As a consequence, the pores of the mesh become larger, thus allowing for example the release of encapsulated molecules. A fine modulation of the grade of swelling and, as a consequence, the drug release rate can be achieved by varying the concentration of weak acid and basic groups in the material.

1.4.1.2. Ionic hydrogels

There are two main classes of ionic hydrogels: ionotropic hydrogels and complex coacervates (**Figure 11**) [19].

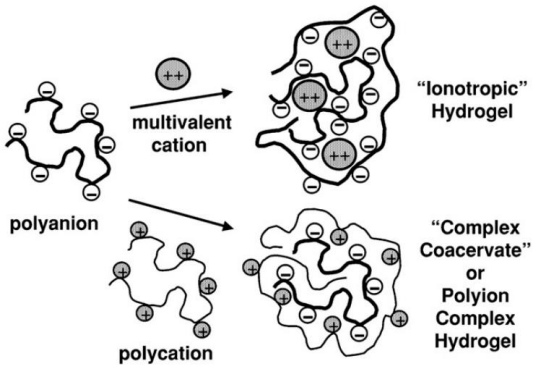

Figure 11: Ionotropic Hydrogel and Complex Coacervate

In this case, the transition from a solution to a gelation state of the polymeric system is driven by a charge combination. This type of hydrogels is constituted by polyelectrolytes that are polymers owing some weak acid or basic groups: in a certain range of environmental pH, they acquire a positive charge if the group is basic or a negative charge if the group is acid.

Ionotropic hydrogels are constituted by the combination of a polyelectrolyte and a multivalent ion with opposite charge, which acts as crosslinker between the polymeric chains. A common example of ionotropic hydrogels are hydrogels formed by calcium alginate. Alginate is a polysaccharide that exposes -COOH groups (polyanion), while calcium is present as a multivalent cation (Ca^{2+}). This hydrogel is reversible and when the ions move out the system, for example following environmental conditions such as the solution pH, the system dissolves and turns back to sol state.

Complex coacervate or polyion complex hydrogels include a blend of polyelectrolytes of opposite charge, that form a precipitate based on their concentrations, pH of the solution and ionic strength. The balance of charge between the two polyelectrolytes gets polymeric chains closer and leads to the hydrogel formation. Also in this case, the system is reversible as a consequence of pH variations. An example of these systems is given the mixture of alginate and chitosan. In a certain pH range, chitosan is positively charged and alginate is negatively charged, thus generating electrostatic interactions among the polymer chains and the formation of a gel.

1.4.1.3. Analyte-sensitive hydrogels

Analyte-sensitive hydrogels are designed to mimic the molecular recognition process that is present in nature. Analyte recognition can be achieved by including in the hydrogel formulation some biomolecules that own inert recognition properties, such as peptides, enzymes and nucleic acids [22]. The interaction between the analyte and the biomolecule probe triggers a chemical reaction able to modify some physical or chemical parameters in the hydrogel, resulting in a response that can be exploited for drug delivery or sensing (**Figure 12**).

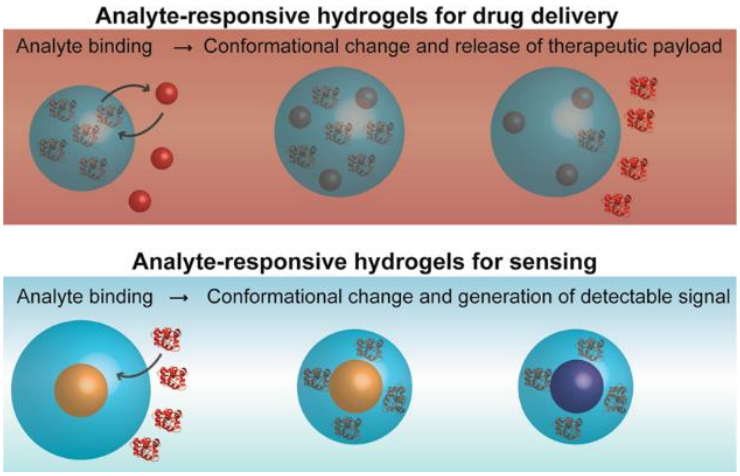

Figure 12: Analyte-responsive hydrogels [22].

An example of analyte-sensitive hydrogel is a system used to release insulin when the blood concentration of glucose is high. In a pH responsive hydrogel, glucose oxidase and insulin are entrapped. When the glucose present in blood diffuses in the hydrogel, glucose oxidase converts it into gluconic acid, thus raising the pH value. As response, the hydrogel starts to swell, dilating its pores and permitting the release of insulin in the blood. In this case, crosslinking is usually necessary to avoid the complete dissolution of the hydrogel over a short period of time [23].

1.4.1.4. Temperature-sensitive hydrogels

Over the last decade, thermally induced gelling systems have gained major importance because of their promising and innovative biomedical applications. They are usually injectable formulations, also allowing solubilization of hydrophilic and hydrophobic drugs, time-release of biomolecules, delivery of genes and proteins and cell encapsulation [24].

A particular type of temperature-responsive hydrogels is the one based on amphiphilic block copolymers, which aqueous solutions at a concentration higher than the “critical gelation concentration” (CGC) exhibit a phase transition from sol to gel state or vice versa in response to a change in temperature. These thermo-sensitive hydrogels are divided in two classes, depending on their behavior following a temperature variation, as shown in the phase diagrams reported in **Figure 13**.

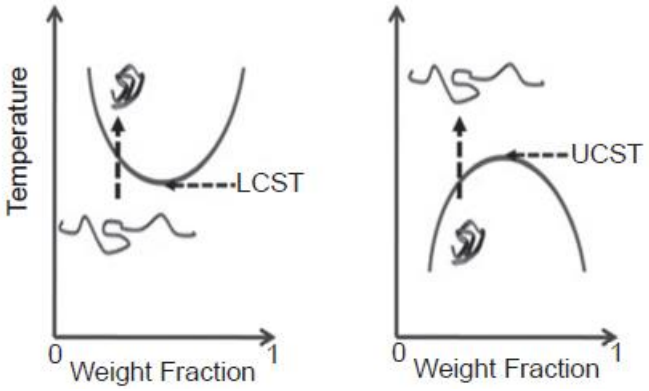

Figure 13: Lower Critical Solution Temperature (LCST) and Upper Critical Solution Temperature (UCST) hydrogels [18].

LCST hydrogels are characterized by a lower critical solution temperature: by increasing the temperature, the system passes from a sol state to a gel state. On the other hand, **UCST** hydrogels are associated to an upper critical solution temperature, suggesting that the sol-to-gel transition occurs by cooling the system below a critical value. In both cases, the transition temperature depends on the polymeric concentration in the solution.

The transition mechanism depends on the ratio between hydrophilic and hydrophobic blocks. When dissolved in water, these polymers assume a micellar conformation, with the polymeric chains arranged so that the hydrophilic blocks are oriented toward the aqueous solution and the hydrophobic blocks are oriented inward, forming a hydrophobic core. The differences that can occur in the transition behavior can be explained by the length of the copolymer chains. In the so called *gel-sol hydrogels*, the polymeric chains have longer hydrophilic than hydrophobic blocks: the system presents a gel state at low temperature because hydrophilic parts are in an entangled form. On the other hand, in *sol-gel-sol hydrogels* (**Figure 14**) hydrophilic blocks are shorter and the system is in the sol phase at low temperatures.

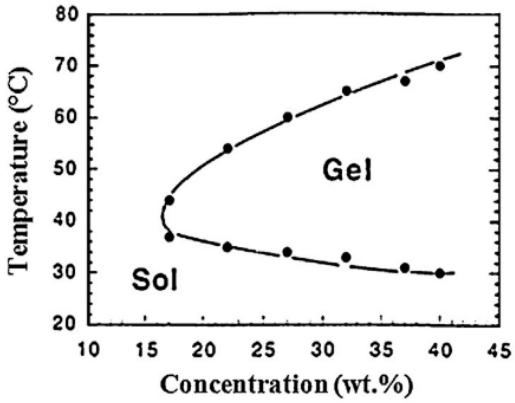

Figure 14: sol-gel-sol hydrogel [24].

The sol-to-gel transition is then driven by the interaction between the micelles. With increasing the temperature of the polymeric solution, the affinity of the polymer chains with water decreases and the micelles, which are individually dispersed in water at low temperature, begin to interact. The hydrophobic interactions among the cores of the micelles trigger a process of micellar aggregation that proceeds with the increase of temperature. Once the affinity between the hydrophobic cores overcomes the affinity between water and the hydrophilic parts of the polymer, the sol-to-gel transition occurs (**Figure 15**). The gel that forms is stable in a certain range of temperatures, but if the temperature is raised above a critical value, called the upper critical solution temperature, the micelles aggregate stronger and closer and the water is expelled from the gel. The two phases of the gel separates and a turbid non gel solution is obtained (syneresis).

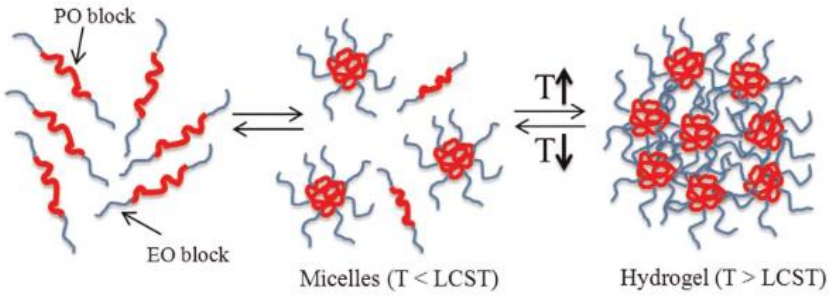

Figure 15: Representation of micellization mechanism: hydrophilic segments in blue and hydrophobic segments in red [24].

Beside the hydrophobic and hydrophilic ratio in the polymer composition, the transition from the sol to the gel state also depends on other parameters. A key feature is the concentration of the polymeric solution, as shown in the phase diagram reported in figure 14: an increase in the amount of the polymer dissolved causes a decrease in the LCST. The use of additives, plasticizers and particular solvents can also change the hydrophilicity of the solution, which influences the interaction between the liquid phase and the polymer and can impact the LCST value.

In general, thermo-sensitive hydrogels present many advantages compared to traditional chemical hydrogels: they are ideal candidates for drug and cell release because their formation occurs in mild conditions. Indeed, their gelation does not required neither high temperatures nor potentially toxic chemical agents, such as organic solvents, that could denature drugs or biomolecules and damage encapsulated cells or the tissue where the system is injected. Crosslinkers that are generally toxic are not required, because the gelation is induced only by temperature. Furthermore, the easy injectability of many of these systems makes them able to completely fill body defects and cavities and suitable for minimally invasive surgery procedures. The transition temperature of sol-gel-sol hydrogels can be finely engineered so as to observe gelation at temperatures close to physiological temperature. This allows to handle the system at room temperature when in a sol/semi-gel state and, thanks to its low viscosity, to inject it through a syringe directly in the body, where the sol-to-gel transition takes place induced by the physiological temperature.

Another important advantage of micellar systems is their use in drug delivery applications. During the formation of micelles, hydrophobic drugs are encapsulated into micelle core, while hydrophilic drugs interacts with the exposed hydrophilic segments and, when the gel state is reached, are entangled between micelles. These characteristics lead to a different release kinetics for the two types of drugs, allowing to control it in a fine way.

1.5. Thermosensitive hydrogels based on synthetic polymers

Thermosensitive hydrogels can be based on natural polymers (such as polysaccharides, polypeptides and cellulose derivatives) or synthetic polymers. Considering the previously mentioned properties, synthetic polymers are more chemically adaptable and permit to

obtain better physical characteristics for biomedical applications. Hence, in this work attention has been focused in hydrogels of synthetic origin.

1.5.1. N-isopropylacrylamide based systems

One of the first synthetic thermosensitive hydrogels used for biomedical applications have been based on poly(N-isopropylacrylamide) (pNiPAAm) copolymers (**Figure 16**). The most interesting characteristics of pNiPAAm hydrogels are their sol-gel transition temperature at approx. 32 °C, i.e., close to the physiological level, and their solubility in water at room temperature.

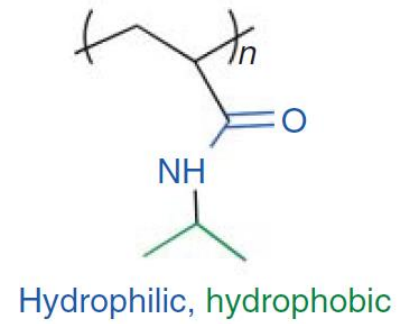

Figure 16: N-isopropylacrylamide Chemical Structure [22].

In addition, the LCST of pNiPAAm-based hydroges can be tuned by incorporating hydrophobic/hydrophilic co-monomers; in general, the value also depends on the polymer molecular weight and structural architecture, inclusion of additives and solvent selection. In particular, it can be decreased by including hydrophilic monomers such as acrylic acid or hydroxyethyl methacrylate, that promote the bound of water to the polymer chains, or increasedbyadding hydrophobic monomers such as butyl methacrylate. In drug release applications, different release profiles of encapsulated hydrophilic and hydrophobic drugs have been obtained: hydrophilic drugs (e.g., nadolol) release is greatly dependent on the molecular weight of the polymer, while hydrophobic drugs (e.g., propranolol and tacrine) exhibit a release profile dependent on solubility [24].

1.5.2. poly(ethylene oxide)-b-poly(propylene oxide)-b-poly(ethylene oxide) triblock copolymers and derivatives

The nonionic triblock copolymers based on poly(ethylene oxide)-b-poly(propylene oxide)-b-poly(ethylene oxide) (PEO–PPO–PEO) are commercially known as Pluronics ® since the late 1950s. According to the block size, these systems in aqueous solution can have different complex states of aggregation (i.e., solid, liquid or paste). Poly(ethylene oxide) (PEO) represents the hydrophilic block, while poly(propylene oxide) (PPO) the hydrophobic part (**Figure 17**).

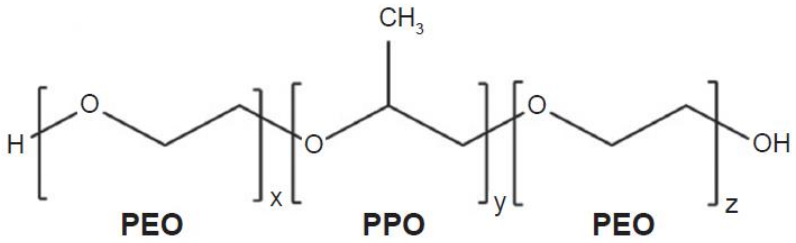

Figure 17: PEO/PPO/PEO triblock copolymer chemical structure [23].

Depending on the PEO/PPO molar ratio and the molecular weight of both PEO and PPO blocks, the copolymer acquires a different name [25]. The dissolution rate of the hydrogels produced starting from Pluronics® is influenced by the copolymer composition and molecular weight. The dissolution is faster as the PEO ratio and molecular weight decrease and this result is probably explained by the degree of hydrogen bonding between the copolymer chains.

The critical micellization concentration (CMC) is the minimum polymer concentration required to observe micelle formation. When the copolymer solution concentration is above its CMC, it configures itself in micelles equilibrated at low temperature with unimers. However, at a concentration lower than CMC, both PEO and PPO blocks are hydrated, and PPO is partially soluble in water. Micelle formation is triggered by the dehydration of PPO blocks that become less soluble in water with increasing temperature (**Figure 15**).

At higher temperatures, there is a reduction of unimers dispersed in solution and the micelle volume fraction increases. This process goes on until the micelle volume fraction reaches the value of 0.53, when they come in contact and aggregate together, progressively

forming a gel. Nowadays, there is not an absolute agreement on Poloxamer gelation mechanism: in some researchers' opinion, it is justified by a micelle packing process and micelle entanglements guided by temperature increasing [26], while for others the process is correlated to the shrinkage of PEO shell and the interactions between PEO chains and PPO core [27]. The formation and disaggregation of the gel is thermally reversible.

Among all the different available formulations, **Poloxamer® 407** (P407, registered trademark of Pluronic F127 - BASF laboratories, Wyandotte, MI, USA), is the most commonly studied hydrogel-forming material for drug delivery applications. It is characterized by a theoretical molecular weight around 12,600 Da, with a PEO/PPO ratio of 2:1 and a PEO percentage of about 70% w/w. The presence of hydrogen bonds at low temperature causes P407 to be more soluble in cold water than in hot water: for this reason, it is a free-flowing liquid at low temperatures. At a concentration higher than 20% w/v the sol-gel transition occurs at 25°C [28]. Thanks to these characteristics, it has remarkable properties to be used in thermally induced *in situ* forming gelling systems, such as in parenteral applications (especially subcutaneous and intramuscular). This material is also studied to produce injectable delivery matrices for biopharmaceuticals products, that due to their polarity and high molecular weight are difficult to be administered orally [24].

Poloxamer® 407 is also a Food and Drug Administration (FDA) approved product. However, its hydrogels show some defects that limit their applications *in vivo*. For example, P407-based gels show low stability *in situ*, because of P407 fast dissolution in contact with an aqueous environment, weak mechanical properties and high permeability [29].

1.5.3. Poly(ε-caprolactone)-poly(ethylene oxide)-poly(ε-caprolactone) (PCL–PEO–PCL) triblock copolymers

The triblock copolymer composed by poly(ethylene oxide) (PEO) and poly(ε-caprolactone) (PCL), with a PEO/PCL ratio of 1:2 (**Figure 18**), has a micellization mechanism different from PEO-PPO-PEO because the hydrophilic/hydrophobic block ratio influences micelle configuration and in turn the behavior of the thermosensitive hydrogel (**Figure 19**).

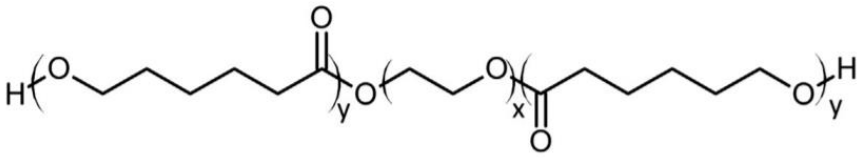

Figure 88: PCL-PEO-PCL chemical structure

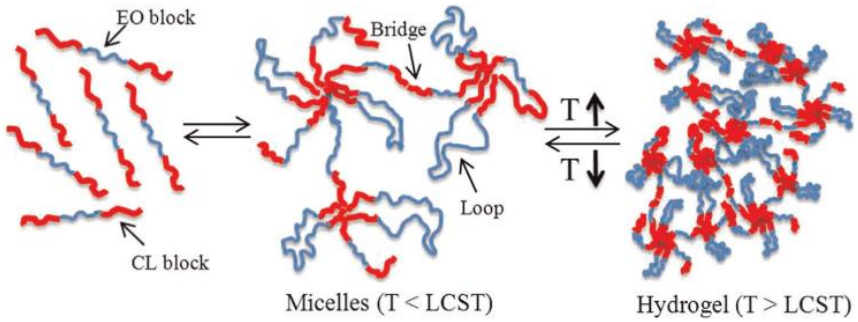

Figure 19: PCL-PEO-PCL solution micellization process

PCL blocks are highly hydrophobic and tend to aggregate together in aqueous environment to reduce their surface of contact with the hydrophilic environment, thus forming micelles. In this case, micelles consist of a hydrophobic core constituted by PCL blocks coming from different polymeric chains and a shell represented by PEO blocks, that arrange themselves in loops. Some micelles are therefore interconnected, because they share a polymeric block that acts like a bridge. The micellization process is again temperature dependent: below the LCST, hydrogen bonds between PEO blocks and water molecules are predominant and the system is a free-flow sol containing micelles. When the temperature is raised above the LCST, the hydrogen bound become weaker and a gel is formed, guided by micelle aggregation induced by hydrophobic bridges between micelles, formed by PCL blocks.

1.5.4. Polyurethanes

After almost half a century of use, poly(urethane)s (PURs) are considered one of the best groups of synthetic biomedical materials, due to their chemical "block" structure, that gives them tunable physical properties. Indeed, poly(urethane)s are recognized as polymers with excellent fatigue resistance and mechanical properties, especially in terms of tensile strength. Moreover, biocompatible, biodegradable PURs can be synthesized to be applied in the biomedical field, with particular regard to tissue engineering and regenerative

medicine. In particular, it is possible to optimize the degradation rate and avoid any risk of cytotoxicity from the degradation by-products and the material itself.

PURs are bock copolymers containing urethane bonds, obtained by the reaction between an isocyanate (terminal functional group of the diisocyanate) group and a hydroxyl group (terminal functional group of the diol). Isocyanate groups can also react with or amine group (terminal functional group of a diamine, leading to "urea" bond formation (**Figure 20**).

The synthesis is often performed through a two-step reaction. In the first step, a polyisocyanate (typically a diisocyanate) reacts with a bi- or multi-functional polyol with two or more hydroxyl terminal groups (typically a diol): a pre-polymer already containing urethane bonds is thus obtained. In the second step, the prepolymer reacts with a chain extender, which can be either a diol or a diamine, to increase the molecular weight and improve the mechanical properties of the resulting polymer.

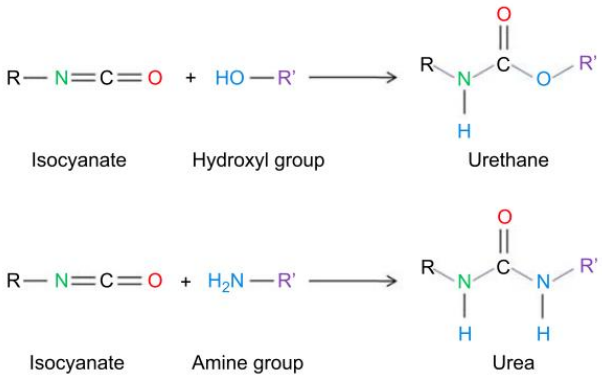

Figure 20: Urethanes and Ureas [27]

PURs can be used to design scaffold for soft (skin, muscle, nerve) or hard tissue (bone) engineering, thanks to their two-domain configuration. The blocks formed by reacting the di- or multi-functional isocyanate with the chain extender are responsible of the hard domains, while the polyol-based segments are responsible of the soft matrix (**Figure 22**) [30].

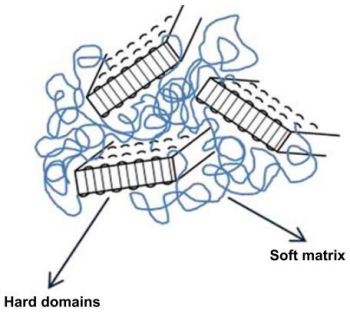

Figure 92: Polyurethanes two-domain configuration.

As previously mentioned, Poloxamer 407 is one of the triblock copolymers mostly used to produce thermo-responsive hydrogels. Many studies showed that increasing the molecular weight of the polymer or modifying it with functional groups for chemical crosslinking during the gelation process are strategies to improve the hydrogel stability in a wet environment, such as the human body. A novel hydrogel injectable platform for the delivery of therapeutic ions in situ was designed incorporating mesoporous bioactive glass particles loaded with therapeutic ions entrapped in a polyurethane thermosensitive hydrogel based on P407 [31]. Boffito et al. [31] synthesized an amphiphilic PUR named NHP407, by a two-step reaction, based on P407 as macrodiol, 1,6-hexamethylene diisocyanate (HDI) and N-Boc serinol as chain extender (**Figure 23**). The authors demonstrated that chain extending P407 through poly(urethane) chemistry could be a valuable tool to design thermo-sensitive hydrogels with improved mechanical strength and stability in aqueous environment; moreover, by exposing the protected -NH_2 group, it is also possible to further functionalize the material to obtain a more pronounced bioactivity.

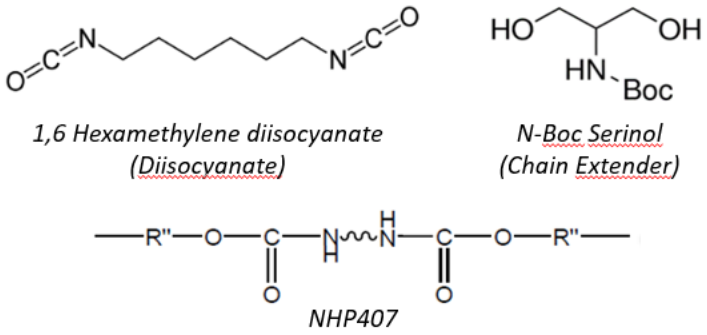

Figure 103: HDI, N-Boc Serinol and NHP407 Chemical Structures.

1.6. Photocurable hydrogels

Since the 1970s, researches have exploited the energy provided by a light source in the UV or visible region to induce the polymerization or crosslinking of particularly sensitive materials [32].

Photopolymerizable systems have many advantages, such as temporal and spatial control of the reaction kinetics, reduced production of heat that could otherwise damage the tissue, possibility to encapsulate cells homogenously and adaptability of the polymerization process by tuning light sources to meet clinical requirements. Furthermore, the development of these materials has reduced the cost and invasiveness of some surgical techniques [33].

For instance, photo-sensitivity can be exploited to improve the stability of thermo-sensitive hydrogels. Two main strategies can be implemented:

1) The polymeric material can be modified by exposing photocurable lateral groups along its backbone, thus obtaining a chemical irreversible hydrogel after light irradiation;
2) A second material with photocurable properties can be blended with a thermosensitive one thus obtaining a new material based on a thermo-sensitive reversible component and a photocurable one.

In the first case (**Figure 24**), the hydrogel can be injected in the sol state at low temperature and when it comes in contact with physiological temperature, the gelation transition occurs. After that, the gel is stabilized by photo crosslinking that creates covalent bonds and makes the gel no more reversible.

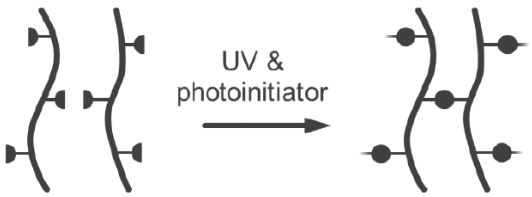

Figure 24: Scheme of photocurable polymer with pendant photosensitive groups [18].

In the second case (**Figure 25**), the system can be injected as in the previous case and gelation occurs induced by the temperature stimulus. However, only the photocurable part

of the blend reacts upon irradiation and this results in a system composed by a still reversible thermosensitive part, penetrated by a three-dimensional mesh of chemically crosslinked polymer.

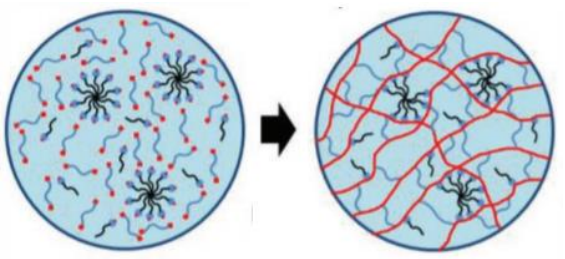

Figure 25: Blend scheme

Among the different available curing strategies, photocuring is characterized by high speed and high polymerization rate. Furthermore, the process can be applied at room temperature and does not require toxic solvent. However, in some cases the process involves partially toxic reagents [32].

In both the cases described, a photoinitiator and a light source (UV or Vis) are needed and play important roles in the crosslinking process.

1.6.1. Photoinitiators

Photo-sensible polymers do not usually have the ability to crosslink by directly absorbing the light energy. Photoinitiators are chemical substances able to absorb energy from light at specific wavelengths, generating reactive species that then interact with the photo-sensitive polymers to induce photopolymerization. Reactive species are atomic or molecular chemical species that own an unpaired electron: for this reason, they are chemically instable and very reactive.

The selection of the photoinitiator is an important step in the set-up of a photocuring process because it influences the properties of the final product in terms of curing speed, by-products and structure [32]. The selection should take into account some critical aspects:

- The absorption peak, concentration of the photoinitiator and light exposure time/intensity must be compatible with the final application (for example photo crosslinking through human tissues);
- The solubility of the photoinitiator should be considered because it influences the stability of the final product;
- The toxicity of the photoinitiator and any sub-products should be controlled to avoid a damage to the tissue;
- The molecule should be easy to handle and storage;
- The economic cost of the reaction should be minimized.

In biomedical applications, photoinitiators must meet strict requirements, such as water-solubility, low cytotoxicity and high efficiency. **Table 1** summarizes the most widely used photo-initiators in bioengineering with their most significant parameters.

Table1: Photoinitiators [29]

Initiators	Name	Type	Wavelength for curing	Curing time	Intensity	Solubility	Concentration for cell encapsulation
Irgacure 2959 (I2959)	2-Hydroxy-4′-(2-hydroxyethoxy)-2-methylpropiophenone	1	365 nm	5~15 min	1~20 mW/cm^2	Water (≤ 0.5%), ethanol (10%)	~0.1%
VA-086	2,2'-Azobis[2-methyl-N-(2-hydroxyethyl) propionamide]	1	365 nm			Water (≤ 5%)	~1.5%
LAP	Lithium phenyl-2,4,6-trimethylbenzoyl phosphinate	1	365 or 405 nm			Water (≤ 8.5%)	~0.1%
Eosin Y	2-(2,4,5,7-Tetrabromo-6-oxido-3-oxo-3H-xanthen-9-yl)benzoate	2	519 nm			Water (≤ 5%)	~0.01%

Most of the photoinitiators described have a wavelength for curing that belongs to the UV spectrum; this is a disadvantage because exposure to UV light can potentially induce DNA damage in cells [33]. Despite this, the use of a restricted concentration of photoinitiator, a proper UV radiation intensity and a short exposure time can ensure safe conditions for cells. For example, using LAP as photoinitiator the material is irradiated with a UV LED at a 365 nm wavelength, with an intensity of 10 mW/cm^2 for 3 minutes [34].

In general, free-radical photoinitiators are classified in two main categories (Type I and Type II photoinitiators), which mechanism of action is schematically represented in **Figure 26** [29].

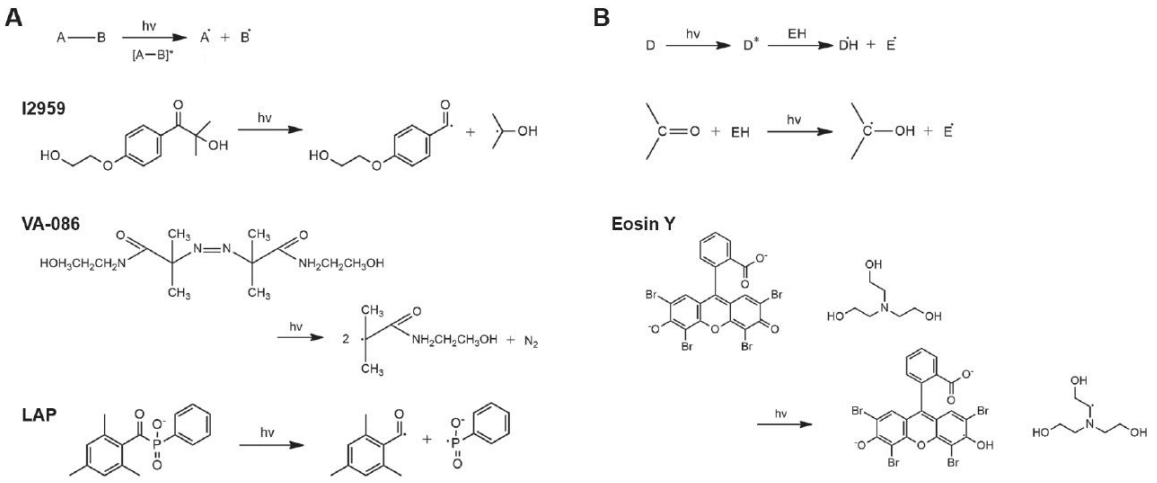

Figure 26: Photo initiators start radical polymerization. (A) Type 1 photo initiators (B) Type 2 photo initiators.

1.6.1.1. Type 1 photoinitiators

After exposure to light, **Type 1** photoinitiators produce two free radicals through a homolytic bond cleavage process. The free radicals then react with photo-sensitive groups in the polymer chains and initiate the polymerization process. Cleavage is typical of weak bonds, but generally takes place at the α-position of the -C=O group, while the β-cleavage is less probable. In most cases, the most photolabile site is the -C-O-C- bond of the aromatic carbonyl compounds, such as benzoin and acetophenone compounds and hydroxylalkylphenone [32].

The most commonly used type 1 photoinitiator is 2-hydroxy-1-[4-(hydroxyethoxy)phenyl]-2-methyl-1-propanone (**Irgacure 2959** – I2959, **Figure 27**).

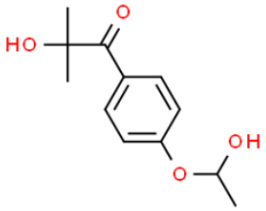

Figure 117: Irgacure 2959 Chemical Structure [29].

Its wavelength for curing is 365 nm, which is comprised in the UV region. It is used for its polymerization efficiency, but suffers from low solubility in water (0.01 mg/mL of solution); for this reason, it is often dissolved in ethanol, in which its solubility increases up to 10 g/100g of solution. Furthermore, it has cytotoxic effects, but in small concentrations (0.03-0.1% w/v) it is well tolerated by a broad range of mammalian cell types [33]. The intensity and time of exposure to UV light, which can be a source of further damage for cell DNA, depends on Irgacure 2959 concentration. In scientific literature, many works use Irgacure 2959 as photoinitiator in the photo-crosslinking of poly(ethylene glycol) (PEG) ([35], [36], [37]) and polyvinyl alcohol-methyl acrylate (PVA-MA) ([38], [39] , [40]).

Lithium phenyl-2,4,6- trimethylbenzoylphosphinate (**LAP**, **Figure 28**) is another commonly used type 1 photoinitiator.

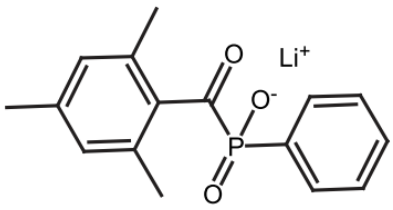

Figure 28: lithium phenyl-2,4,6- trimethylbenzoylphosphinate chemical structure [37].

As shown in **Figure 29**, LAP has a maximum absorbance peak at approximately 375 nm and significant absorbance at 365 nm. In addition, this photoinitiator absorbs weakly in the visible region in the range between 400 nm and 420 nm: this enables also an efficient visible light polymerization. While Irgacure 2959 suffers for its low absorption at 365 nm, that makes the photopolymerization in the UV spectrum delayed, LAP has an increased polymerization rate at 365 nm. Moreover, it shows higher water solubility (0.038 mg/ml) than Irgacure 2959.

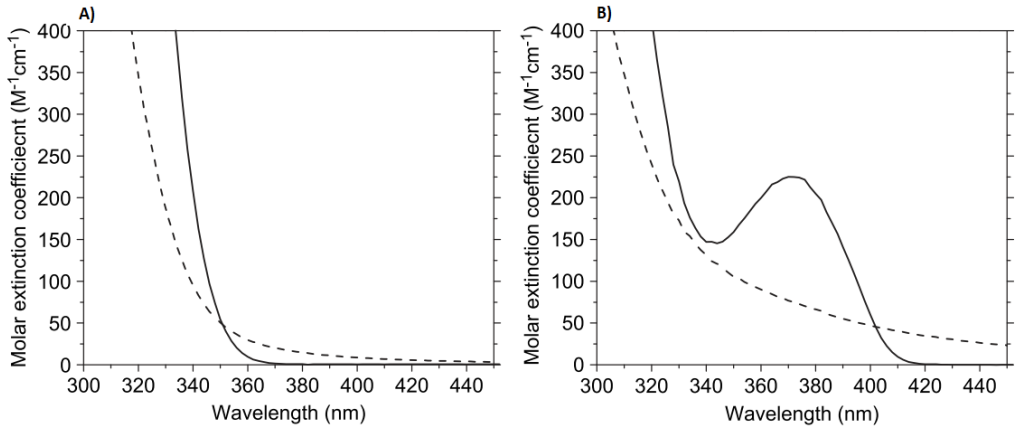

Figure 29: (A) Molar absorptivities of the I2959 (solid line) and cleavage products (dashed line). (B) Molar absorptivities of LAP (solid line) and cleavage products (dashed line). [37].

Another advantage of LAP compared to Irgacure is a bleaching characteristic. Following the photocleavage, a change in absorption is notable, caused by the loss of the chromophore. This is relevant for the irradiation of polymeric films that are not optical thin: during the light exposure, the initiator contained in the exposed surface is consumed and this allows the light to penetrate in the deeper layer and provide the maximum cure of the bulk material [41].

1.6.1.2. Type 2 photoinitiators

In contrast to type 1, **type 2** photoinitiators cannot spontaneously generate radicals through light exposure and therefore need a co-initiator. Indeed, they contain CO-aryl bonds that cannot be broken by UV energy, because their bond energy is too high. The main disadvantage of this type of photoinitiators is the long triplet lifetime that makes them very sensitive to quenching. Moreover, type 2 photoinitiators are generally less efficient than type 1 because of (i) biomolecular nature of the reaction, (ii) solvent cage influence in aqueous media, and (iii) back electron transfer [32].

The co-initiators are classified in two classes, based on their electronic behavior: they can act like hydrogen abstractors or like electron transferors (an electron donor step followed by a proton transfer step). The most used co-initiators are tertiary amines that also act as oxygen scavengers. Other alternatives compounds used can be alcohols, thiols and ethers, but they are generally less efficient. For tertiary amines, the efficiency is inversely proportional to the ionization potential, so the most active radicals are generated from the

weakest amines. Moreover, incorporating hydroxyl groups in the chains can improve efficiency and reactivity [32].

An interesting example of a type 2 photoinitiator is **riboflavin** (7,8-dimetil-10- ((2R,3R,4S)-2,3,4,5-tetraidrossipentil) benzo[g]pteridina-2,4 (3H,10H)-dione). It is also known as vitamin B2, and for this reason it is a molecule with a promising potential use as biological photoinitiator. Thanks to its chemical structure (**Figure 30**), it is able to absorb photon and form either the singlet- or triplet-excited states; triplet states are characterized by a longer lifetime in solution and a better molecular interaction than single state.

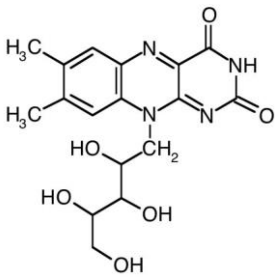

Figure 30: Riboflavin Chemical Structure [38].

Being a type 2 photoinitiator, riboflavin needs a co-initiator. Indeed, triplet riboflavin quenched by a monomer was not found to result in polymerization, but the photopolymerization takes place if riboflavin is associated with the addition of tri-ethanolamine (TEOHA). This synthetic co-initiator (**Figure 31**) was found to be one of the most efficient between the evaluated molecules [42].

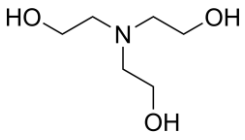

Figure 31: Tri-ethanolamine (TEOHA) Chemical Structure[38].

It is believed that TEOHA oxidizes the triplet state riboflavin, producing the semi-oxidized radical of riboflavin and the semi-reduced amine. It was found that the initiation of the polymerization reaction is attributable to the long-lived neutral amine radical, that is formed by the donation of a proton from the amine to the riboflavin radical [42].

Riboflavin can be defined a versatile photoinitiator thanks to its particular UV-visible absorption spectra (**Figure 32**), that shows two high absorption peaks. The first one is

centered at 365 nm (UV light) and the second one at 448 nm (VIS light), with no significant absorption below 300 nm and above 500 nm. This double-peak spectrum allows to use either a UV or VIS light source in the photopolymerization procedure, avoiding the disadvantage of using UV light that is linked to genotoxicity.

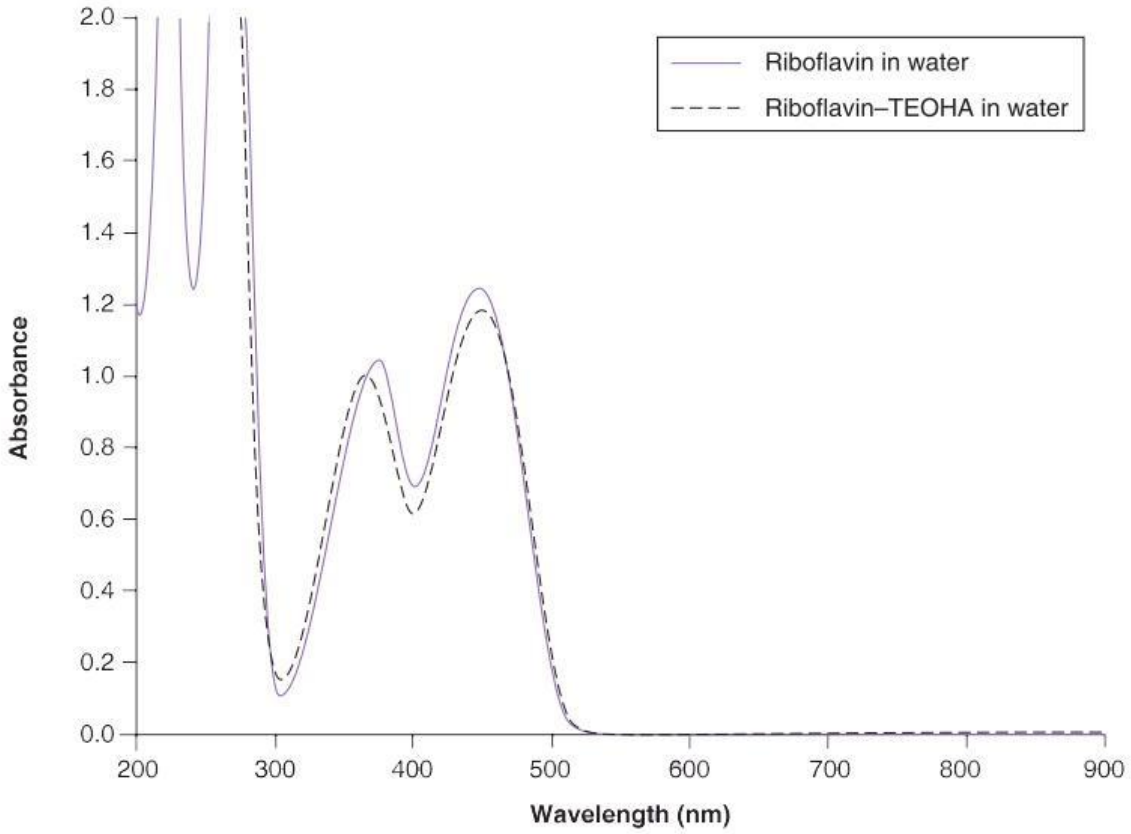

Figure 32: UV-visible absorption spectra of riboflavin and the riboflavin–triethanolamine mixture in distilled water.

Visible light photoinitiators, including also Eosin Y, generally have good water solubility, but they show low photoreactive efficiency in photopolymerization. The selection of the concentration of both riboflavin and TEOHA is a critical point and must be a good compromise between water solubility (riboflavin is slightly water soluble: 2.25×10^{-4} M [43]) and photo-crosslinking efficiency [44]. Furthermore, in the selection of riboflavin concentration, it is important to consider that riboflavin is a colored molecule (yellow): the presence of color generally requires an increase in the intensity of exposure to obtain a good photo-crosslinking efficiency.

The main advantage of using riboflavin as photoinitiator is its non-toxicity. It has already been demonstrated that even at high doses or with UV exposure in therapy applications, it is compatible with living organisms and its addition to tissue engineering structures is hypothesized to not significantly change the biocompatibility [42].

1.6.2. Synthetic polymer-based photocurable hydrogels

The development of photocurable hydrogels of synthetic origin is generally based on a modification of a polymer with the exposure of photosensitive groups, such as acrylates. This presents many advantages in the biomedical field, such as (i) the possibility to a mass-production at a low cost, (ii) tunable mechanical properties by properly selecting molecular weight and degree of polymer modification, and (ii) the incorporation of biological molecules to provide biological features. The most widely studied synthetic hydrogel precursor are poly(ethylene glycol) (PEG) and poly(vinyl alcohol) (PVA).

1.6.2.1. Poly(ethylene glycol)-based photocurable hydrogels: PEG diacrylate (PEGDA) and PEG dimethacrylate (PEGMA)

Poly(ethylene glycol) (PEG) is a synthetic, hydrophilic, anti-fouling, biocompatible, FDA-approved, generally non-immunogenic polymer. It has a widespread use in biomedical applications, such as tissue engineering, bio-printing and drug delivery systems.

From a chemical point of view, it is composed by the repetition of the ethylene glycol -(O-CH_2-CH_2)- unit. PEGs are synthesized using a ring-opening polymerization of ethylene oxide, to produce a broad range of molecular weights and molecular weight distributions. Generally, in order to obtain photocurable versions of PEG, it is modified by binding to the terminal hydroxyl groups acrylate groups (by reaction with acryloyl chloride) or methacrylate groups (by reaction with methacryloyl chloride). PEG diacrylate (PEGDA) or PEG dimethacrylate (PEGMA) are respectively obtained, as depicted in **Figure 33** [45].

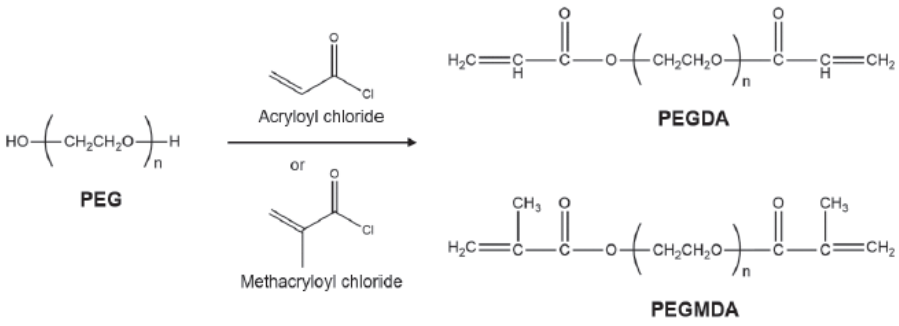

Figure 33: PEGDA and PEGMDA synthesis

The photo-crosslinking of these materials can be performed in the presence of a photoinitiator (and adding a co-initiator if a type 2 photoinitiator is used).

PEGDA hydrogels are characterized by a slow *in vivo* degradation and for this reason they are studied in long term biomedical implantable applications. Degradation probably results from the progressive oxidation of the ether backbone or hydrolysis of the esters in the end acrylate groups (**Figure 34**), which are relatively long degradation processes. Both of them can occur in the foreign body response (FBR) process to implanted devices [45].

Figure 34: PEGDA degradation [41].

1.6.2.2. Poly(vinyl alcohol)(PVA)-based photocurable hydrogels

Another widely used synthetic photocurable hydrogel class is based on poly(vinyl alcohol) (PVA) (**Figure 35**). PVA is a biocompatible and antifouling water soluble material with pendant hydroxyl groups, derived by poly(vinyl acetate) hydrolysis. The pendant hydroxyl groups of PVA can be substituted using acrylic acid, methacrylic acid, glycidyl acrylate, and 2-isocyanotoethyl methacrylate (ICEMA) to make it photocurable. By modifying the concentration and number of photocurable groups per chain, it is possible to control the mechanical properties of the final material [18]. This class of hydrogel can be used to produce scaffolds in tissue engineering or to design drug delivery systems ([46], [47], [48]).

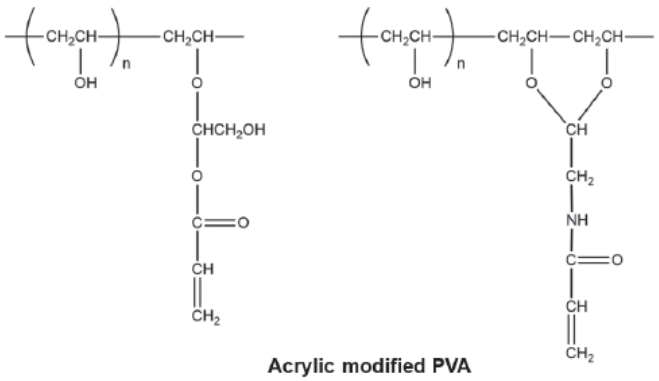

Figure 35: Photocurable poly(vinyl alcohol)-based polymers.

1.7. Biomedical applications of hydrogels

1.7.1. Hydrogels in Tissue Engineering

Tissue engineering (TE) is an interdisciplinary discipline that employs the knowledge of biomedical engineering and biology to develop biological substitutes able to restore and maintain tissue functionality [49].

The use of synthetic materials in TE represents a promising alternative to the traditional clinical solutions that are affected by many limitations. In particular, materials of human or animal origin can have immunogenicity issues and are usually available in limited quantities and at a high cost.

In this field, hydrogels are particularly suitable materials to be used to produce soft scaffolds. In particular, their characteristics are optimal for *in vitro* tissue regeneration, in which cells extracted from the patient are combined with the polymeric material and cultured *in vitro*, until the system is set to be implanted. In this case, hydrogels mimic the function of the native ECM, the non-cellular part of tissues that supports cells by providing anchorage and division between different tissues. The ultimate goal is to replace the original damaged tissue and this artificial ECM, with the addition of proper growth factors and metabolites, helps to bring cells together and direct the new-forming tissue structure and development.

Scaffolds produced in this way should have a porous structure, with a pore size compatible with living cells accommodation. They should also have a degradation rate appropriate to

new tissue formation rate, with the ability to release growth factors and leave space for living cells to penetrate and form a new healthy tissue.

The application of hydrogels in tissue engineering provides benefits such as a biocompatibility, efficient transport of nutrients to the tissue, easy modification with ligands for cells adhesion and protection of cells and biomolecules (growth factors, proteins, peptides, nucleotides). However, there are also some disadvantages, such as generally poor mechanical properties and difficulty in handle the material, sterilize and load drugs and cells and crosslink *in vitro* [6].

In the case of injectable thermo-sensitive hydrogels, cells and biomolecules can be incorporated in the formulation in mild conditions and the material can also be injected directly *in situ*, as illustrated in **Figure 36** [50].

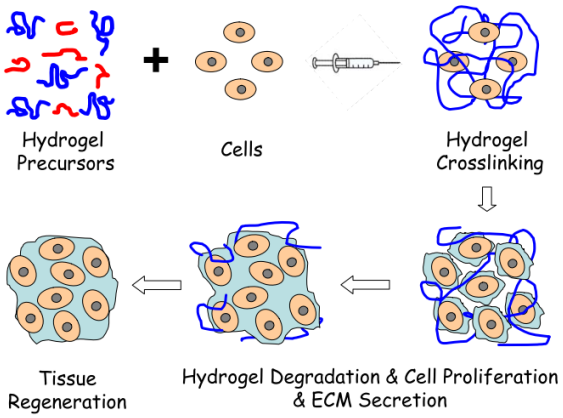

Figure 36: Application of injectable thermosensitive hydrogel in TE

Moreover, injectable hydrogels have many advantages over conventional scaffolds, as summarized in **Table 2**:

Table 2: Conventional scaffolds and injectable hydrogels comparison.

Conventional Scaffolds	Injectable Hydrogels
Comparatively less ease of handling	Easier handling
Invasive surgeries are needed	Minimally invasive application
No proper defect margin adaptation	Excellent defect margin adaptation
Incomplete defect filling leading to vascularization failure	Complete defect filling leading to neovascularization from healthy tissues
Cannot reach very deep tissue defects	Can reach very deep tissue defects

To summarize, the materials designed to produce injectable hydrogels for *in vivo* biomedical applications must satisfy some requirements:

- The material and its degradation products should be biocompatible.
- Before gelation transition, the viscosity should be sufficiently low to allow injection and a homogeneous dispersion with drugs and/or cells.
- Mild gelation conditions after *in vivo* injection, to prevent toxicity provided by heating or use of toxic solvents/reagents.
- The material should have a proper stability and tenancy to be injected with cells and drugs, avoiding a burst release, matching the tissue strength, maintaining a stable environment for cell activity and supporting the internal and external load given by neighboring soft tissue invasion.
- The hydrogel porosity and size and interconnectivity of the cavities should be adequate to allow cell migration and easy exchange of nutrients and waste substances.
- Materials should be biodegradable, in order to leave space for cell growth and rearrangement in the newly formed tissues.

1.7.2 Bioprinting of photocurable hydrogels

The main goal of tissue engineering (TE) is to promote with different strategies the restoration of damaged or diseased human tissues and organs [51]. Additive manufacturing techniques, such as 3D bioprinting, are computer controlled and can be associated to medical image systems (e.g., magnetic resonance imaging, computed tomography) and computer-aided design (CAD) or computer-aided manufacturing (CAM) tools. This makes them useful strategies for the deposition of materials and cells to build patient specific tissue engineered structures [52]. The main requirements a bioink for 3D-bioprinting should match are suitability to micro extrusion and quick stabilization (with temperature or photo-crosslinking), to avoid losing of the the printed structure [53].

For this reason, photo-crosslinkable hydrogels have a great potential as bioinks providing fast polymerization of the material under cell compatible conditions. For example, an important parameter to consider in bioprinting is the bioink viscosity. A viscous bioink maintains the structure better after the extrusion, but the shear stress generated during the printing process can damage the encapsulated cells. Photocurable hydrogels generally present an initial low viscosity, making printing easy, but their polymerization is fast enough to preserve the printed structure. In this work, the thermosensitive part of the hydrogel has also the function to increase the precursor viscosity thanks to temperature getting better printable conditions. However, the balance between printability and biological functionality is still a challenge. Bioprinting technologies exploit an automated process to produce cell-laden constructs through a layer-by-layer approach both *in vitro* and *in vivo* ([54] [55]). For bioprinting of curable materials, the crosslinking pattern is of the utmost importance, because it influences gelation kinetics, mechanical properties, shape fidelity and viability of encapsulated cells [56]. The important parameters in photopolymerization are light intensity, exposure time and the irradiated area and they directly influence the final construct properties such as crosslink density and matrix stiffness [57].

The most used bioprinting technologies are illustrated in **Figure 37**.

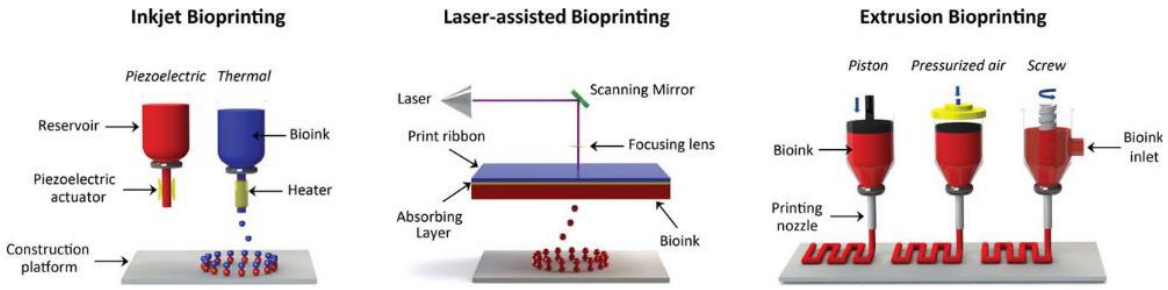

Figure 37: 3D bioprinting processes [56].

Inkjet Bioprinting:

Inkjet bioprinting is a non-contact method that deposits the bioink in form of droplets (1-100 picolitres) with a diameter of 10-50 µm on a surface producing a construct with micrometre resolution [58]. In thermal inkjet printing, the ejection of the droplet is obtained vaporizing a small volume of bioink contained in the reservoir using a heating element. In this case, cells are subjected to high temperatures (~ 300°C) for few microseconds (~ 2 µs) with no consequences on cell viability [59]. In piezoelectric inject printing the droplet is obtained by the application of an external voltage on a piezoelectric element that deforms itself inducing droplet formation and precluding temperature increase. A limitation of these methods is that the bioink must have low viscosity (1-10 mPa) and cell density (<106 cells/mL) [52].

Laser-Assisted Bioprinting:

This process includes the application of a high-energetic pulsed laser on a print ribbon covered with the bioink to induce an ejection of a droplet. The laser shines on a substrate transparent to laser light (e.g., quartz or glass), coated with a metal (for example, titanium or gold) layer that upon absorption of the laser energy generates a bubble in the bioink that is ejected in a droplet form on the receiving substrate. From a biological point of view this process can be dangerous for cells because of the high temperature that is reached (higher than 50 °C). The advantages of this method are its unique resolution that is of 10-100 µm and the possibility to work with a bioink with high cellular density [56].

Extrusion Bioprinting:

In extrusion bioprinting a syringe is filled with a prepolymer containing cells and this bioink is extruded on a surface by applying a pressure driven by a force or pressurized air that pulls a piston or by a rotating screw [52]. The important parameters that need a fine optimization are (i) the cartridge and printing platform temperatures that influence the gelation and viscosity of the material before and after extrusion, and (ii) the applied shear stress and compression forces that affect cellular viability. In this method a hydrogel filament is produced with a diameter in range of 150-300 µm depending on the forces at work and the tip dimension. The main advantage is the possibility to print viscous materials containing high cell density. However, this technique shows a lower resolution (200 µm) compared to previously described methods [56].

1.7.3 Hydrogels in drug delivery systems

The traditional methods of drug administration, enteral (oral, sublingual, rectal), parenteral (percutaneous, inhalatory, ocular or by injection) and topical, consist in a multiple dosing strategy to maintain the drug concentration within the therapeutic window (**Figure 38**).

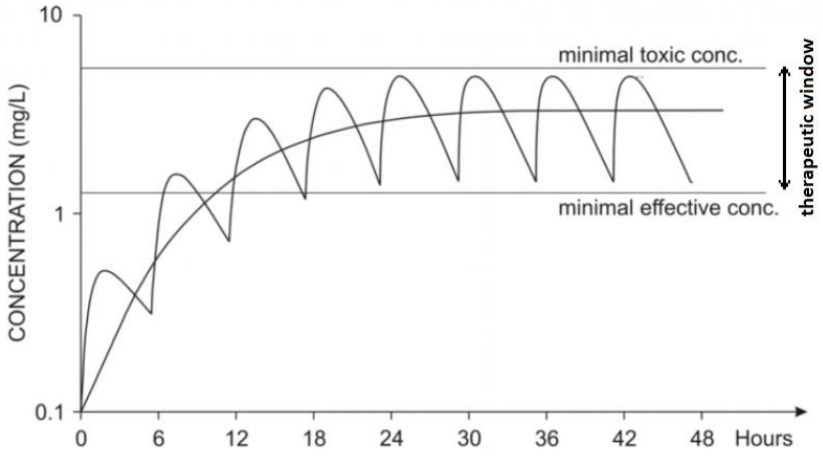

Figure 38: Therapeutic window [22].

As a consequence, the drug concentration in the plasma floats in a range of values that includes ineffective and toxic values, leading to unpleasant side effects. Furthermore, the multiple administration of drug via injection in patients that require daily doses for a long period of time treatment can become a disease itself.

Therefore, it would be desirable to have a constant drug level comprised within the therapeutic window during the entire treatment. Hydrogels are ideal candidate to serve this purpose, because of their controlled drug release connotation and the possibility to avoid the dispersion of the active agent in the body immediately after administration. In particular, injectable systems forming or gelling *in situ* are acquiring interest as platforms apt for local, controlled and prolonged drug and gene delivery, with also the possibility for cell encapsulation in the tissue engineering field [24].

2 Materials and Methods

2.1 Polyurethanes (PUs) synthesis

2.1.1 Reagents for NHP407 Synthesis

Kolliphor® P407 (P407, M_n =12 600 Da, 70% w/w PEO, **Figure 39A**), 1,6-hexamethylene diisocyanate (HDI, **Figure 39B**), dibutyltin dilaurate (DBTDL) and N-Boc serinol (**Figure 39C**) were purchased from Sigma-Aldrich, Milano-Italy. In order to remove residual water N-Boc serinol were dried overnight under reduced pressure at room temperature, while P407 was first heated at 100 °C under vacuum for 8 hours and then cooled down at 30 °C while keeping the oven at a pressure of approx. 200 mbar. HDI was distilled under reduced pressure before use. Glassware and metal accessories were dried in a laboratory oven at 120 °C overnight. All solvents were purchased from CarloErba Reagents (Italy) in analytical grade. The solvent used to perform polyurethane synthesis, i.e., 1-2,dichloroethane (DCE), was anhydrified overnight over activated molecular sieves (activation at 120 °C overnight, Sigma Aldrich, Italy) under N_2 flow, at room temperature.

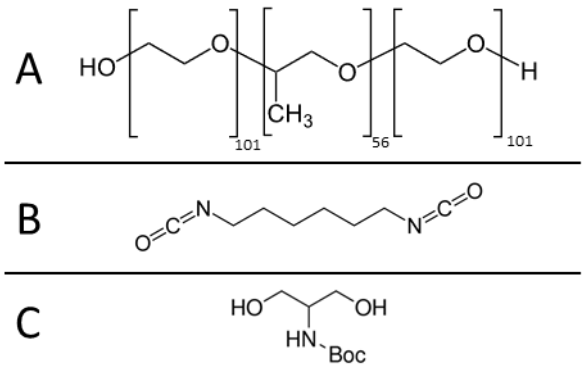

Figure 39: Formula structure of (A) Poloxamer® 407 (P407), (B) 1,6-hexamethylene diisocyanate (HDI) and (C) N-Boc serinol.

2.1.2 NHP407 synthesis

The polyurethanes NHP407 was synthesized through a two-steps reaction according to Boffito et al. [29] (**Figure 40**). The synthesis was conducted in inert atmosphere (continuous nitrogen flow) and anhydrous 1,2-dichloroethane (DCE) was used as solvent.

The polyurethane acronym “NHP407” is derived from its components:

- Macrodiol: Poloxamer® 407 (M_n=12600 g/mol, 70% PEO), abbreviated with P407 in the acronym;
- Diisocyanate: 1,6-Diisocyanatohexane (HDI), abbreviated with H in the acronym;
- Chain Extender: N-Boc Serinol, abbreviated with N in the acronym;

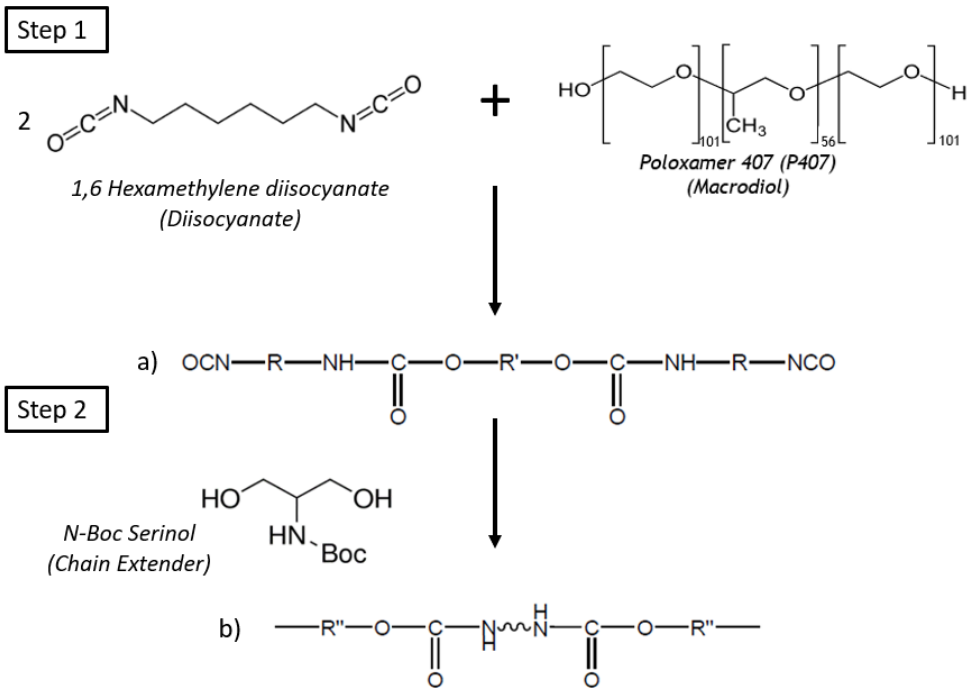

Figure 40: NHP407 synthesis protocol. a) prepolymerization, b) chain extension reaction to gel the final polyurethane.

In the first step, P407 was solubilized in anhydrous DCE at a 20% w/v concentration. Once the polymer was dissolved and equilibrated at 80 °C, HDI in 2:1 molar ratio with respect to P407 was added to the solution and the reaction was carried out for 2.5 hours at 80 °C. This reaction was performed in the presence of DBTDL as catalyst, at a 0.1% w/w concentration with respect to P407.

The second step consisted in the chain-extension through N-Boc serinol. The chain extender was solubilized at 3% w/v concentration in anhydrous DCE and then added to the synthesis system to reach a final 1:1 molar ratio with respect to P407. The addition was carried out upon cooling of the reaction system at 60 °C and the reaction lasted 1.5 hours. After that, the system was cooled at room temperature and the reaction was stopped using methanol and keeping the solution under stirring for 15 minutes. **Figure 41** schematically represents the structures formed during the two steps of the synthesis process.

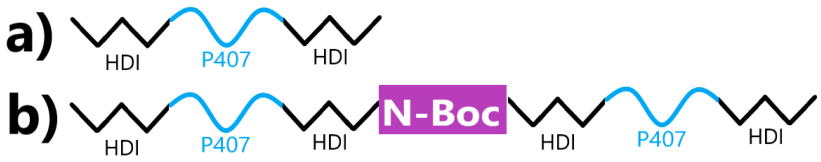

Figure 41: Schematic representation of the prepolymer resulting from the first step of the reaction (a) and the final polymer resulting from the chain extension step (b)

The collection of the synthesized polymer was performed by precipitation in petroleum ether (4:1 volume ratio with respect to DCE) and the material was then purified by dissolution in DCE (35% w/v) and subsequent precipitation in a mixture (5:1 volume ratio with respect to DCE) of diethyl ether (DEE) and methanol (98:2 volume ratio). Finally, the polymer was collected by centrifugation (6000 rpm, 0 °C, 20 min, MIKRO 220R - Hettich), dried overnight at room temperature under the fume hood and stored under vacuum at 4°C.

2.1.3 NHP407 Deprotection to Obtain SHP407

The removal of the Boc caging group present in the N-Boc serinol used during NHP407 synthesis exposes amino groups that enable the polyurethane to be further biofunctionalized [29]. Amines can indeed establish a chemical conjugation with biomolecules, such as carbohydrates and peptides, forming peptide bonds. Moreover, amine protonation can provide the material with an antibacterial effect [60].

N-Boc Serinol deprotection reaction was carried out following a modified literature protocol [61]. The previously synthesized NHP407 (10 g) was dissolved in 225 ml of chloroform (Carlo Erba, Italy) and stirred for 2 h at room temperature under nitrogen flux. Then, 25 ml of trifluoroacetic acid (TFA, Sigma Aldrich, Italy) were added and the solution was stirred for 1 h. The excess TFA and chloroform were eliminated by rotary evaporation (Rotavapor®- BUCHI Italia). Three rotary evaporation cycles were applied, adding 100 ml of chloroform after the first and second cycle in order to completely evaporate TFA traces. The third cycle was carried out until the polymeric solution appeared viscous and waxy; then 200 ml of demineralized water were added. This final solution was kept overnight at 4 °C under stirring and then dialyzed (M_w cutoff 12-14 kDa) against demineralized water (ddH_2O) at 4 °C for 2 days (complete dialysis medium refresh three times/day) and finally lyophilized (Alpha 2-4 LSC, Martin Christ, Germany). The obtained polymeric sponges were

washed with DEE to eliminate residual TFA traces, dried under the fume hood and stored under vacuum at 4 °C. The obtained material after the Boc cleavage reaction was referred to with the acronym SHP407.

2.2 PUs chemical characterization

2.2.1 Attenuated Total Reflectance Fourier Transform Infrared (ATR-FTIR) spectroscopy

Attenuated Total Reflectance Fourier Transform Infrared (ATR-FTIR) spectra were obtained for P407, NHP407 and SHP407 to verify the success of both the synthesis and the deprotection protocols (i.e., formation of urethane bonds and absence of evident degradation during acidic treatment with TFA/chloroform). Analysis were performed at room temperature in the spectral range from 4000 to 600 cm^{-1}, using a Perkin Elmer (Waltham, MA, USA) Spectrum 100 equipped with an ATR accessory (UATR KRS5) and a diamond crystal. Each spectrum, obtained as a result of 32 scans with a resolution of 4 cm^{-1}, was analyzed using the Perkin Elmer Spectrum software.

2.2.2 Size Exclusion Chromatography (SEC)

Number Average and Weight Average molecular weights ($\overline{Mn}$ and $\overline{Mw}$), and molecular weight distribution (M_w/M_n) of P407, NHP407 and SHP407 were estimated by Size Exclusion Chromatography (SEC) (Agilent Technologies 1200 Series, USA). The instrument was equipped with a Refractive Index Detector (RID) and two Waters Styragel columns (HR1 and HR4) conditioned at 55 °C. N,N-Dimethylformamide (DMF, Chromasolv Plus, HPLC grade, 99.8%, Carlo Erba, Italy) with lithium bromide (LiBr, 0.1% w/v, Sigma Aldrich, Italy) was used as eluent at a flow rate of 0.5 ml/min (resulting pressure within the columns approx. 24 bar). M_n and M_w were determined by the Agilent ChemStation Software, referring to a calibration curve based on PEO standards (averaged molecular weight range 982-205500 Da). The samples were dissolved in the same DMF/LiBr mixture used as mobile phase (2 mg/ml) and filtered through a 0.45 µm syringe filter (Whatman) before analysis. The injection volume set on the instrument was 20 µl.

2.2.3 Quantification of exposed amino groups

The number of amino groups present in SHP407 chains was quantified using the Ninhydrin test, known also as Kaiser test. This colorimetric test allows to quantify the concentration of primary amines groups in a polymeric solution. The solution is originally yellow, but an intense blue/purple color is generated by the reaction of Ninhydrin with free primary amines. The color change is correlated to the concentration of amines present in the sample, which can be quantified by UV-Visible spectroscopic analyses. The kit was purchased from Sigma Aldrich, Italy and the analyses were performed according to supplier's instructions.

NHP407 (control) and SHP407 poly(urethane)s were first weight (10 mg) into glass test tube and the following reagents were added:

1. Phenol 80% in ethanol (75 µl)
2. KCN in H_2O/pyridine (100 µl)
3. Ninhydrin 6% in ethanol (75 µl)

Each sample was then mixed with a vortex and heated at 120 °C for 5 minutes. An aliquot of 250 µl of each sample was then collected and diluted 1:2 with EtOH/ddH_2O 60:40 v/v to avoid saturation phenomena during the spectrophotometric analysis. The obtained diluted samples (400 µl) were then analyzed using an UV-Visible spectrophotometer (PerkinElmer Lambda 365 UV/VIS spectrometer), quartz cuvettes and EtOH/ddH_2O 60:40 v/v as blank. The main absorbance peak was observed at 570 nm. The number of free amines was quantified using Lambert-Beer law ($A = c \cdot \varepsilon \cdot l$; ε = 15000). Analyses were conducted in triplicate and results reported as mean ± standard deviation.

2.3 PUs-based sol-gel systems characterization

2.3.1 Sample preparation

Sol–gel systems based only on the synthesized PUs were prepared by solubilizing NHP407 and SHP407 at predefined w/v concentrations in phosphate-buffered saline (PBS, pH 7.4, Sigma-Aldrich Milano, Italy) in Bijou sample containers (CarloErba Reagents, Italy). Samples were kept at 4°C to allow solubilization and avoid undesired gelation.

2.3.2 Micelle size analysis - Dynamic Light Scattering (DLS)

To investigate the mechanism of polymeric structure formation (i.e., the progressive micelle formation and their aggregation) as a function of solution concentration and temperature [29], Dynamic Light Scattering (DLS) analysis were performed. Only very diluted formulations were analyzed with this method, in order to avoid sample turbidity and gelation phenomena that could compromise the measurement.

A Zetasizer Nano S90 (Malvern Instruments, Worcestershire, UK) was used to estimate the average hydrodynamic diameter of the micelles and the micellar aggregates present in NHP407 and SHP407 solutions at a 0.1%, 0.5% and 1% w/v concentration. Each sample (1 ml) was tested at 25 °C, 30 °C, 37 °C and 45 °C with an equilibration time of 15 minutes, following a literature protocol [62]. All the measurements were repeated three times and the micelles size was calculated as the average of the single analysis results.

2.3.3 Critical micellar temperature (CMT)

The Critical Micellar Temperature (CMT) of NHP407 and SHP407-based solutions was estimated following the protocol described by Alexandridis et al. [63]. Solutions of NHP407 and SHP407 were prepared at very low concentrations (0.1%, 0.5% and 1% w/v) to avoid sol-gel transition.

The fluorescent dye 1,6-diphenyl-1,3,5-hexatriene (DPH, Sigma-Aldrich, Milano-Italy) was solubilized in methanol at 4×10^{-4} mol L^{-1} concentration and an aliquot (10 µl) was added to the samples (1 ml). As soon as the polymeric solution starts forming micelles, DPH molecules interact with micelles cores and this results in a signal measurable using UV–visible absorption spectroscopy. DPH spectrum has a main absorption peak at 350-360 nm (**Figure 42**), whose intensity is directly proportional to the amount of micelles present in solution.

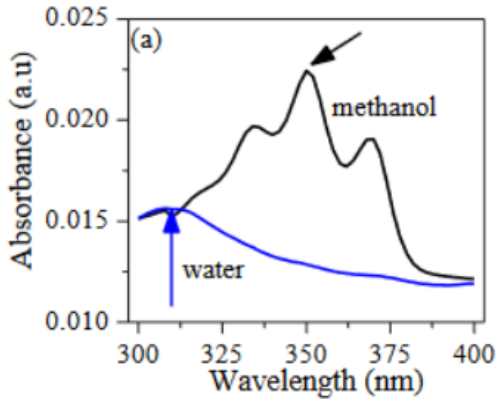

Figure 122: DPH absorbance in water and methanol [64].

Analysis were performed using a Perkin Elmer Lambda 25 UV/VIS spectrophotometer (Waltham, MA, USA), in the temperature range from 4 °C to 40 °C at a rate of 1 °C/step, equilibrating the sample for 5 min at each temperature. Measured absorption intensity at 356 nm were then plotted in function of temperature, obtaining a sigmoidal curve. CMT value was estimated at the first inflection of the curve (**Figure 43**).

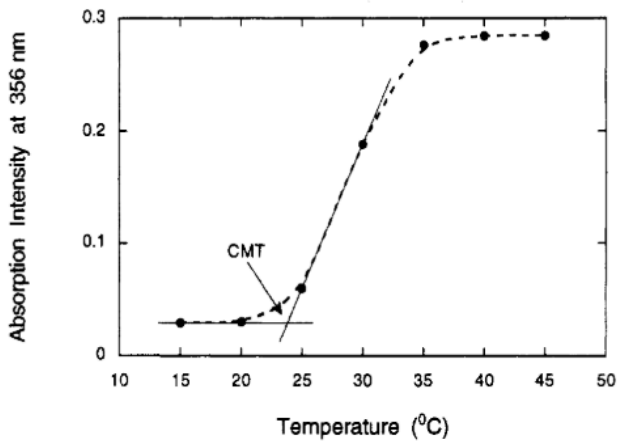

Figure 43: Determination of the critical micellar temperature from the data [63].

2.3.4 Tube Inverting Test

Tube inverting test allows to estimate the temperature at which the sol-gel transition of the samples occurs by relying on a visual inspection performed by the operator. NHP407 and SHP407 aqueous solutions (1 ml) were prepared in a Bijoux sample container at different concentrations (between 5 and 15% w/v), solubilizing the PUs powder in PBS. The controlled temperature increase was performed from 4 °C to 46 °C at 1 °C/step. For each step, the samples were maintained at constant temperature for 5 minutes, then a tube

inversion was performed to allow a visual inspection of the state of the sample. The system was then observed for 30 seconds: if a flow was still present, it was considered as “flow liquid sol”, on the contrary, if it was stationary it was defined as “no flow solid gel”.

2.3.5 Gelation time test at 37°C

Gelation time test allows to estimate the time required for the sol-gel transition to occur at physiological conditions (temperature = 37 °C, pH = 7.4). Samples were prepared as for tube inverting test and incubated at 37 °C (IF 75 Incubator, Memmert). The transition was evaluated at 1-minute intervals, until all sample exhibiting a gelation temperature below 37 °C were classified as “no flow solid gel” as previously described.

2.4 Poly(ethylene glycol) Diacrylate (PEGDA) synthesis

2.4.1 Synthesis reagents

Poly(ethylene glycol) (PEG, M_w 3350, 4600, 6000 Da), acryloyl chloride (AC), triethylamine (TEA), potassium carbonate and magnesium sulfate were purchased from Sigma-Aldrich, Italy. Dichloromethane (DCM) was purchased from Carlo Erba, Italy. Before the synthesis, both PEG, magnesium sulfate and DCM were anhydrified according to the following approaches: PEG was dried under vacuum at 100 °C for 8 hours and then cooled down at 40 °C at a pressure of approx. 200 mbar; DCM was anhydrified over activated molecular sieves overnight in inert atmosphere; magnesium sulfate was dried in a vacuum desiccator at room temperature overnight. Glassware and metal accessories were dried in a laboratory oven at 120 °C overnight.

2.4.2 Synthesis protocol

PEG diacrylate (PEGDA) synthesis reaction (**Figure 44**) was carried out for PEG with different molecular weights (M_w 3350, 4600 and 6000 Da), using the same protocol. The three obtained polymers have been defined with the acronym PEGDA 3350, PEGDA 4600 and PEGDA 6000, depending on the molecular weight of the starting poly(ethylene glycol).

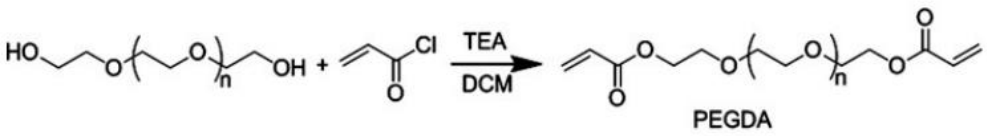

Figure 44: Poly (ethylene glycol) diacrylate synthesis [65].

In order to obtain PEG diacrylate, PEG was functionalized with acrylate groups by reacting its hydroxyl end groups with acryloyl chloride. TEA was used to both catalyze the reaction and to neutralize the solution pH (i.e., TEA neutralizes the drop in pH induced by the HCl molecules resulting from the grafting of AC to –OH groups of PEG).

Before starting the reaction, three "vac-refill" cycles (2 minutes under vacuum – 1 minute under nitrogen) were applied to the synthesis apparatus to completely eliminate any residual water molecule. Then, the dried PEG (50 g) was added to the system and three other "vac-refill" cycles were applied as previously described. After DCM was added to obtain a final PEG concentration of 30% w/v. Three "vac-refill" cycles (1 minutes under vacuum – 1 minute under nitrogen) were again applied. TEA and AC were solubilized in DCM under N_2 flux at a molar ratio with respect to PEG of 2:1 and 4:1, respectively, and then added to the system using a syringe (first TEA was added followed by AC). "Vac-refill" cycles were repeated every time a new reagent was added to the system (1 minutes under vacuum – 1 minute under nitrogen). The reaction was then conducted for 24 h under nitrogen flux keeping the system protected from the light. The solution was then transferred into a separatory funnel. A potassium carbonate solution (1.5 M in deionized water) was added with a 1:4 volume ratio with respect to the DCM total volume, to neutralize the hydrochloric acid formed during the reaction. The separatory funnel was shaken vigorously and uncorked to allow the produced carbon dioxide to get out; then the system was let to rest for 20 h. Two different phases formed: an upper aqueous phase containing potassium carbonate, TEA and not functionalized PEG and a bottom phase containing PEGDA dissolved in DCM. The PEGDA solution was collected and dried magnesium sulfate was added to absorb residual water. The solution was then filtered with a Büchner funnel to collect and eliminate the salt. For PEGDA 6000, the separation was carried out by centrifugation (6000 rpm at 0°C for 20 minutes) because of the high viscosity of the solution which did not allow filtration through the Büchner funnel. The collected solution was then concentrated through rotary evaporation and precipitated in DEE (5:1

volume ratio with respect to DCM). Precipitated PEGDA was finally collected using a Büchner funnel, dried overnight under a chemical hood and stored under vacuum at 4 °C until use.

2.5 PEGDA Chemical Characterization

2.5.1 Attenuated Total Reflectance Fourier Transform Infrared Spectra (ATR-FTIR) Spectroscopy

Attenuated Total Reflectance Fourier Transform Infrared (ATR-FTIR) spectra were registered for the synthesized PEGDA 3350, 4600 and 6000 and the corresponding non-functionalized PEGs. Analyses were conducted following the same protocol as previously described for NHP407 and SHP407, to verify the presence of acrylate groups as a result of the functionalization procedure.

2.5.2 Size exclusion chromatography (SEC)

To verify if any degradation occurred during the functionalization process, Size Exclusion Chromatography (SEC) on PEGs and PEGDAs was performed following the same protocol previously described.

2.5.3 Proton Nuclear Molecule Resonance Spectroscopy (^{1}H-NMR)

PEGDA 3350, 4600, 6000 and their PEG counterparts were dissolved in anhydrous deuterated dimethyl sulfoxide (DMSO-d6, 99.8% D with 0.03% TMS, Sigma Aldrich, Italy) and characterized via Proton Nuclear Magnetic Resonance (^{1}H-NMR, Avance III 500 MHz; Bruker, Billerica, MA, Germany). Spectra were obtained as the average of 12 runs, with 10 s of relaxation time and using tetramethylsilane (TMS) at 0 ppm as reference. The test was conducted to determine the degree of PEG acrylation, by comparing PEG and PEGDA spectra considering that in the PEGDA spectra a set of characteristic peaks located at 5.9-6.4 ppm appears. The intensity of these peaks is related to the amount of acrylate groups in the material.

2.6 PEGDA Solubility test

The solubility of PEGDA 3350, 4600 and 6000 in aqueous media was tested by diluting PEGDA solutions in PBS starting from 20 %w/v, until reaching a concentration that avoided material sedimentation.

2.7 PU-PEGDA blends

2.7.1. Blends selection

The concentration of the thermosensitive component (SHP407) was chosen relying on previous works [66] and fixed for all the blends at 12.5% w/v.

For the photo-curable component, only PEGDAs that presented a solubility limit in the range of concentrations useful to produce photo-crosslinkable systems (i.e., at least few % w/v to allow the formation of a PEGDA network entrapping SHP407 micelles) and to develop blends comparable to each other (i.e., with the same SHP407: PEGDA molar ratio o with the same SHP407 and PEGDA % w/v concentration) were considered. The PEGDA concentrations were selected considering two different criteria of comparison (i.e., same SHP407: PEGDA molar ratio o same SHP407 and PEGDA % w/v concentration).

For blend nomenclature, the SHP407 was not considered since its content was the same for each developed blend. Blends were thus identified with the acronym EDA, followed by the PEGDA molecular weight and its concentration. For example, the blend containing SHP407 at a 12.5% w/v concentration and PEGDA 3350 at a 3% w/v concentration was identified with the acronym EDA3350_3%. **Table 3** summarizes the compositions of the blends investigated in this thesis work.

Table 3: compositions of the investigated blends.

BLEND nomenclature	SHP407	PEGDA
EDA3350_3%	12.5 % w/v	3350 Da, 3% w/v
EDA3350_5.5%		3350 Da, 5.5% w/v
EDA3350_10%		3350 Da, 10% w/v
EDA6000_5.5%		6000 Da, 5.5% w/v
EDA6000_10%		6000 Da, 10% w/v
EDA6000_18%		6000 Da, 18% w/v

In order to make the develop hydrogel formulations sensitive to light irradiation (365 nm, approx. 10 mW/cm^2), a catalytic amount of the Type I photoinitiator Lithium phenyl-2,4,6-trimethylbenzoylphosphinate (LAP, TCI Europe) were added to each SHP407/PEGDA hydrogel. LAP concentration was fixed to 0.05% w/v based on previous evidence of quick photocuring and biocompatibility of similar systems ([67], [68], [56], [66]). From a technical point of view, the hydrogels developed in this work were prepared by first solubilizing the required amount of PEGDA in a 0.05% w/v LAP solution in PBS, according to the concentrations reported in **Table 3**. These solutions were then used to solubilize the amount of SHP407 powders required to reach a final PU concentration of 12.5% w/v in the resulting blend. Samples were mixed using a vortex and kept at 4°C overnight, to avoid micellization and gelation during the solubilization.

2.7.1.1 Blends comparison criteria

The first comparison between blends was carried out as following:

- EDA3350_3% ↔ EDA6000_5.5%
- EDA3350_5.5 % ↔ EDA6000_10 %
- EDA3350_10 % w/v ↔ EDA6000_18 %

The symbol "↔" indicates in this case that the two blends maintain the same molar ratio between thermo- and photo-sensitive species. In this way, the only difference among the different formulations is the size of the mesh produced after the photo-crosslinking phase,

whereas the number of acrylate groups available to react is comparable. The investigated SHP407:PEGDA molar ratios are reported in **Table 4**

Table 4

PEGDA 3350		PEGDA 6000	
% w/v	**SHP407 : PEGDA molar ratio**	**% w/v**	**SHP407: PEGDA molar ratio**
3	1:4	5.5	1:4
5.5	1:7.2	10	1:7.2
10	1:13.2	18	1:13.2

Secondly, blends with the same PEGDA concentrations were compared, to evaluate the effect of the total concentration of the polymeric system (SHP407+PEGDA) on the behavior of the final hydrogels. The comparisons carried out in this case were:

- EDA3350_5.5% ↔ EDA6000_5.5 %
- EDA3350_10 % ↔ EDA6000_10 %

2.7.2 Micelle size analysis

Micelle size analysis was performed as described above for the PU-based solutions (paragraph 12.3.2). To investigate the effect of PEGDA addition on the micellization process, the concentration of SHP407 was fixed at 1% w/v and the relative PEGDA concentration for each blend was calculated to maintain the original ratio between the two components. The final concentrations used in these tests are reported in **Table 5**:

Table 5: DLS blend compositions.

Blend	Sample composition for DLS analyses	
	SHP407	**PEGDA 3350 Da**
EDA3350_3%	1 % w/v	0.24 % v/w
EDA3350_5.5%	1 % w/v	0.44 % w/v
EDA3350_10%	1 % w/v	0.8 % w/v
EDA6000_5.5%	1 % w/v	0.44 % v/w
EDA6000_10%	1 % w/v	0.8 % w/v
EDA6000_18%	1 % w/v	1.44 % w/v

2.7.3 Critical micellar temperature (CMT)

The effect of PEGDA addition to SHP407 solutions was investigated also in terms of Critical micellar temperature (CMT). To this aim, the same formulations investigated through DLS (**Table 5**) were investigated following the same procedure described for the PU-based samples (paragraph 12.3.3).

2.7.4 Thermal characterization of SHP407/PEGDA-based sol-gel systems

2.7.4.1 Tube Inverting test and Gelation Time test in physiological conditions (37°C)

To investigate if the addition of the PEGDA component had an effect on the thermic response of the blends when compared to the pure PU-based systems, tube inverting test and gelation time at 37°C were performed. The procedure and conditions for the tests are the same described for NHP407- and SHP407-based hydrogels (paragraph 12.3.4).

2.7.5 Rheological characterization

The rheological properties of all the developed blends were determined with a stress-controlled rheometer (MCR302, Anton Paar GmbH). The measurements were performed with a 50 mm parallel plate geometry and the temperature control was guaranteed by a Peltier system.

Strain sweep tests were conducted to define the linear viscoelastic (LVE) region, which provides information about sample resistance to applied deformation. Analyses were performed at 37 °C at a frequency of 10 Hz with variable applied deformation (amplitude strain γ) in the range from 0.01% to 500%. Hydrogel temperature-dependent gelation kinetics was investigated by frequency sweep tests. These tests were conducted at different temperatures (25, 30, 37 °C) applying a constant deformation within the LVE region and a variable angular frequency (range from 0.1 to 100 rad/s). Each sample was prepared as described and poured in sol phase at 0 °C on the lower plate. Then, the sample was heated at the set temperature and maintained for 15 minutes to reach stable thermal conditions.

Temperature ramp tests allowed to study hydrogel viscosity (η) trend as a function of temperature variation. Tests were conducted at constant shear rate (0.1 Hz) and within a temperature range from 0 °C to 40 °C at 2°C/minute rate. Each sample was poured in sol phase at 0 °C on the lower plate, equilibrated at this temperature for 15 minutes and then tested. For all the carried out analyses the gap between the plates was set at 0.8 mm.

2.7.6 Characterization of the photo-curing process of SHP407/PEGDA-based sol-gel systems

2.7.6.2 Photo-rheological characterization

The hydrogel behavior in response to photo-curing was examined through photo-rheological tests, to investigate the mesh formed by PEGDA during UV exposure. In this case, the rheometer (MCR302, Anton Paar GmbH) was equipped with a quartz lower plate transparent to UV light and a 25 mm diameter parallel plate geometry was employed. The measurements were conducted at 37 °C with a 0.25 mm gap. Each sample was poured on the lower plate in sol phase at 15 °C (to avoid plate fogging). A portable UV lamp (LIGHTNINGCURE Spot light source LC8, L9588-01A, 300-450 nm) was equipped with a light filter to allow only the passage of UV light at 365 nm and connected under the lower plate at the distance required to obtain a 10 mW/cm^2 irradiation intensity. The tests were performed at constant oscillatory frequency (1 Hz) and strain within the linear viscoelastic region. Before each analysis, an equilibration phase of 6 minutes at 37 °C was set to allow the thermo-sensitive sol-to-gel transition. The analysis was conducted by switching on the lamp 60 seconds after the measurement began, then irradiating the sample for 90 seconds, switching off the lamp and concluding the analysis after 60 additional seconds.

2.8 Study of photo-cured hydrogel swelling, stability and permeability in physiological conditions

2.8.1 Sample preparation

The geometry of the samples produced follows a protocol of a previous thesis work [69]. A metal toroidal mold was used to obtain circular shaped samples with an approximate 2 mm thickness and 10 mm diameter. Samples were then irradiated with a UV LED at 365 nm wavelength, with an intensity of 10 mW/cm^2 for 3 minutes at room temperature (to ensure

a complete photo-polymerization of the samples). The parameters relative to photopolymerization were selected and optimized according to literature studies [34], to avoid a potential cellular damage induced by UV light in future applications. These samples were then transferred into Bijou sample containers (CarloErba Reagents, Italy) and used for permeability (absorption and release of a model molecules), swelling and stability tests.

2.8.2 Swelling and stability in physiological conditions

Hydrogel stability and swelling were tested using the circular shaped samples previously described. For each time step (6 h, 1 day, 3 days, 1 week, 2 weeks, 3 weeks, 4 weeks and 6 weeks) 4 samples for each selected formulation were produced. All samples were weighted immediately after production (w_{gel_i}) and put in a Bijou sample container, then 1 ml was added above each sample and they were incubated at 37 °C for the predefined time. The medium was refreshed every 3 days. At the end of the time step, the residual PBS was removed and the sample was weighted (w_{gel_f}). Then, the samples were freeze dried and weighted again ($W_{freeze\ dried\ gel\ \_f}$). A control set of 4 samples was also prepared, freeze dried and weighted ($W_{freeze\ dried\ gel\ \_i}$). The PBS absorption (%) and weight loss (%) for each time step were calculated using the following equations (**Eq.1** and **Eq.2**):

$$PBS\ absorption\ (\%) = \frac{(W_{gel\_f} - W_{gel\_i})}{W_{gel\_i}} \cdot 100 \qquad \text{Eq. (1)}$$

$$Hydrogel\ dissolution\ (\%) = \frac{(W_{freeze\ dried\ gel\_i} - W_{freeze\ dried\ gel\_f})}{W_{freeze\ dried\ gel\_i}} \cdot 100 \qquad \text{Eq. (2)}$$

In addition, the swelling ratio of each blend formulation was calculated using the following equation (**Eq.3):**

$$swelling\ ratio = \frac{W_s - W_d}{W_d} \qquad \text{Eq. (3)}$$

W_s and W_d represent the weight of hydrogel photocured disk after 24 h of swelling in PBS and the weight of dried hydrogel disk after swelling at 24 h. The swelling ratio is defined as the fractional increase in the weight of the hydrogel due to water absorption.

2.8.3 Permeability test: Fluorescein Isothiocyanate-Dextran (FD4) absorption and release

To verify the possibility to use the developed hydrogels as drug delivery platforms or cell carriers, Fluorescein Isothiocyanate-Dextran with an average molecular weight of 4000 Da (FD4, Sigma Aldrich, Italy) was used as a model biomolecule and absorption and release tests were performed to evaluate absorption and release kinetics. FD4 is commonly used as model of large biomolecules [70] and the fluorescein linked to the molecule allows its quantification using UV-Visible spectroscopy.

For each blend formulation, 4 circular shaped samples were produced as described before and put in a Bijou vial. A FD4 solution (1 mg/ml in PBS) was added above 3 of them and then they were incubated (IF 75, Memmert) at 37 °C. The fourth sample was used as control and PBS without FD4 was added. Two different time steps (24 and 72 h) were considered. After the set incubation time, the eluates were withdrawn from the vials and analyzed using UV-Visible spectroscopy (Perkin Elmer - Waltham, MA, USA) in the range from 400 to 700 nm since the main absorption peak of FD4 is found at 493 nm. Each sample was centrifuged to remove polymeric material from the solution to avoid interferences and a 1:2 dilution was performed for all samples to avoid saturation. Absorbance at 493 nm obtained for the control samples was subtracted to that measured for loaded samples and the FD4 concentration was estimated using a calibration curve based on standard solutions of FD4 in PBS (1-0.1 mg/ml). FD4 absorption was measured as difference between the initial (1 mg/ml) and final FD4 concentrations in the eluates. Results are reported as mean ± standard deviation.

The hydrogel ability to release a payload was also defined using Fluorescein Isothiocyanate-Dextran (FD4). However, in this case, samples were prepared by adding FD4 at a 1mg/ml concentration to the LAP-containing PBS solution used to solubilize the polymers to obtain the blends previously described. Four circular-shaped samples were produced and irradiated for 5 minutes, considering that a new photo-sensitive molecule (i.e., FD4) has been added to the systems. A control sample without FD4 was also produced. After curing, 1 ml of PBS was added above each sample, placed in a Bijou vial, and they were incubated at 37 °C. At predefined time points (1h – 3h – 5h – 1d – 2d – 3d – 7d) the eluates were

collected and fresh PBS was added. Effective release of FD4 was assessed by visual inspection.

2.9 Printability

In order to verify the printability of the blends, preliminary tests were performed using a commercially available bioprinter (Inkredible +, CELLINK). Different tests were performed changing the parameters of pressure (30-100 kPa), syringe temperature (17-25 °C), tip dimension (200-250 μm) and bed temperature (25-37 °C). The model used during the printing phase was developed in a previous work [66] and consisted in a 15x15 mm multi-layered scaffold composed by 4 layers with a 90/90° grid pattern. The possibility to photo-crosslink the entire structure after the printing phase was also evaluated.

2.10 Cytotoxcity test

Cytotoxicity of all the blends based on PEGDA 3350 Da and PEGDA 6000 Da was assessed on extracts of the biomaterials in complete medium, as reported in ISO 10993 “Biological evaluation of medical devices”. Extract obtained by incubating photocured hydrogels disks into complete cell growth medium (DMEM, Sigma Aldrich) with a ratio of 250 mg/2.5 mL for 24 hours at 37°C. The obtained extracts of hydrogels were put in contact with cultures of 3T3 cells (20000 cell/well) placed in a 96 well plate (100 ul/well). After 24 hours a resazurin solution (1X) was added in each well with cells (100 ul/well). Finally, the absorbance of each well was measured with a plate reader (Sirio S, SEAC, Florence, Italy) at 535nm excitation and 595 emission.

3 Results and discussion

3.1 NHP407 – SHP407 Chemical characterization

3.1.1 Attenuated Total Reflectance Fourier Transform Infrared spectra

Attenuated Total Reflectance Fourier Transform Infrared (ATR-FTIR) spectroscopy was performed to verify the success of the PU (NHP407) synthesis. **Figure 45** shows the ATR-FTIR spectra obtained for NHP407 before and after deprotection (SHP407) reaction compared to the macrodiol (P407).

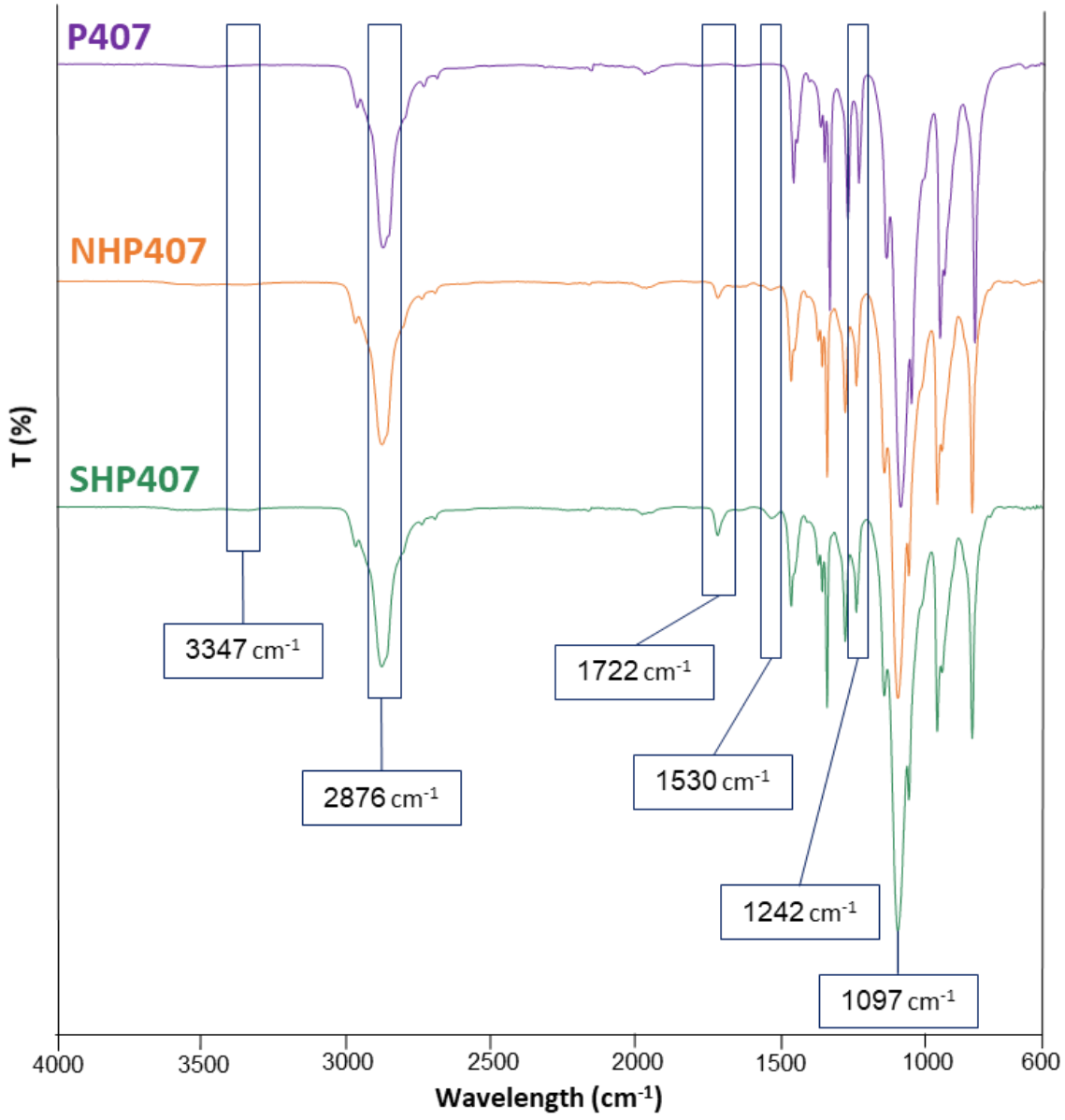

Figure 45: ATR-FTIR spectra of the polyurethanes and P407.

NHP407 and SHP407 spectra are characterized by the presence of specific absorption peaks of PEO-PPO-PEO triblock copolymers, derived from the P407 presence within the materials: CH_2 stretching and rocking vibrations at 2876 and 1242 cm^{-1} respectively and -C-O-C- stretching at 1097 cm^{-1}, due to the repeated $–OCH_2CH_2$ PEO units in the macrodiol.

The polyurethanes synthesis was verified by the appearance of new bands of absorbance found in NHP407 and SHP407 spectra, that testify the correct formation of the urethane bonds: N-H bonds (amide II) stretching vibration at 3347 cm^{-1}, C=O of free urethane carbonyl groups (amide I) at approximately 1722 cm^{-1}, N-H (amide II) bending and CN stretching vibrations at about 1530 cm^{-1}. The absence of unreacted diisocyanate is testified by the lack of peaks at 2200 cm^{-1}.

3.1.2 Size exclusion chromatography (SEC)

Size exclusion chromatography (SEC) allowed to determine the molecular weights of each material. The weight average molecular weight (M_w) and number average molecular weight (M_n) of NHP407 and SHP407 were found to range between 52 and 53 kDa and between 23 and 27 kDa, respectively, and the polydispersity index (D) was between 1.8 and 1.9. The similarity of the molecular weights for both the materials demonstrated that the deprotection treatment on native polyurethane was not degradative.

These values of molecular weights have been compared to P407 molecular weights (M_w= 9500 Da; M_n= 8000 Da; D = 1.2), proving an increase in molecular weight after the polyurethane synthesis, that suggested the success of the reaction.

Figure 46 show the synthetized NHP407.

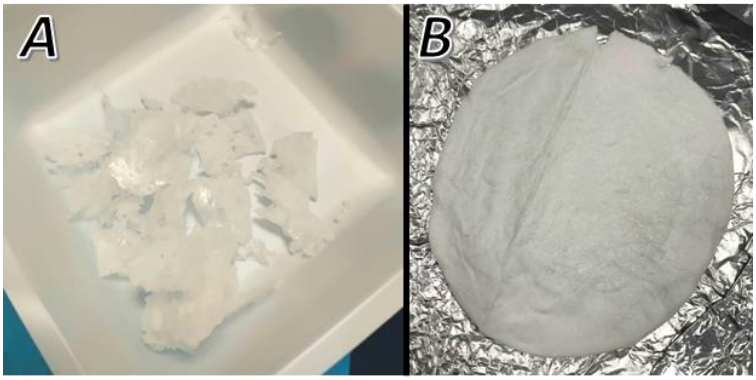

Figure 46: Left-to-right, synthetized NHP407 before and after deprotection.

3.1.3 Amino groups quantification

The ninhydrin assay (Kaiser test) was applied to quantify the amount of free amine groups in the material after N-Boc serinol deprotection reaction. For this purpose, both NHP407 and SHP407 were analyzed and compared. An evidence of BOC cleavage results in a color variation (**Figure 47**) from yellow for the material with protected amines groups (NHP407), to purple for the material with free amines (SHP407).

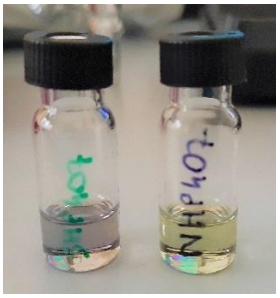

Figure 47: Kaiser test colour variation (left-to-right SHP407 and NHP407).

Samples were analyzed with UV-VIS spectrometer considering the main peak of absorbance around 560 nm. **Figure 48** shows how, compared to NHP407, SHP407 spectrum is characterized by a more intense peak in the region considered. The concentration was then

calculated and referred to the sample volume, then the amount of -NH_2 groups per grams of polyurethane (-NH_2/g_{PU}) was obtained.

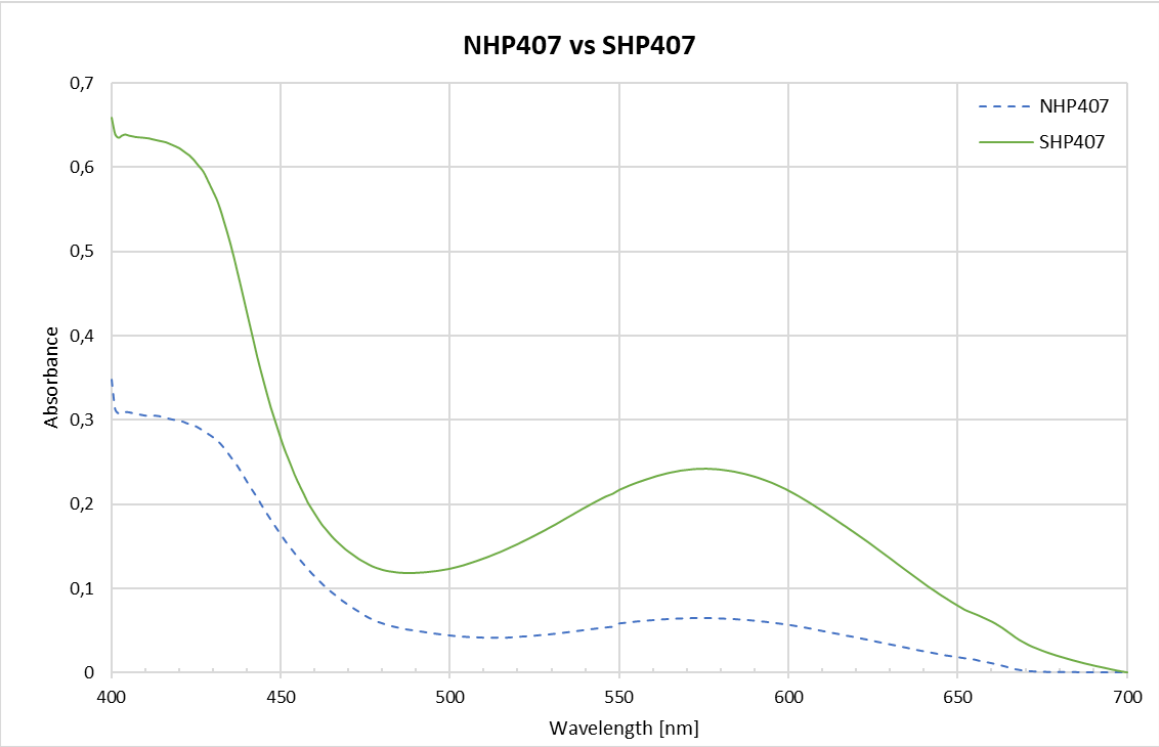

Figure 138: NHP407 vs SHP407 Kaiser UV spectra.

The amount of free amines resulted 7.24 * 10^{16} -NH_2/g_{PU}

This result is in line with previous works.

3.2 PUs-based sol-gel systems characterization

3.2.1 Micelle size analysis - Dynamic Light Scattering (DLS)

NHP407 and SHP407 have amphiphilic properties and for this reason they are expected to form micelles in aqueous environment with hydrophilic shells and hydrophobic cores. The micelle size analysis of PU-based solutions was performed with Dynamic Light Scattering (DLS) to measure the hydrodynamic diameter of the polymeric structures formed and assess the influence of temperature and concentration on micelle formation and dimension. NHP407 and SHP407 solutions were tested at the concentrations of 0.1%, 0.5% and 1% w/v at 25°C, 30°C, 37°C and 45°C, as previously described.

As an example, **Figure 49** shows the DLS results of one for NHP407 at the concentration of 1% w/v at 25, 37 and 45°C. It was decided to report this concentration because of the better stability of the spectra compared to the other tested. It is possible to observe how the increase of temperature lead to a shift of the main peak of the spectra. This behavior means that the increase of temperature guided the micelles formation from unimers (at 25°C), to micelles (37°C) and then to aggregates of micelles (45°C).

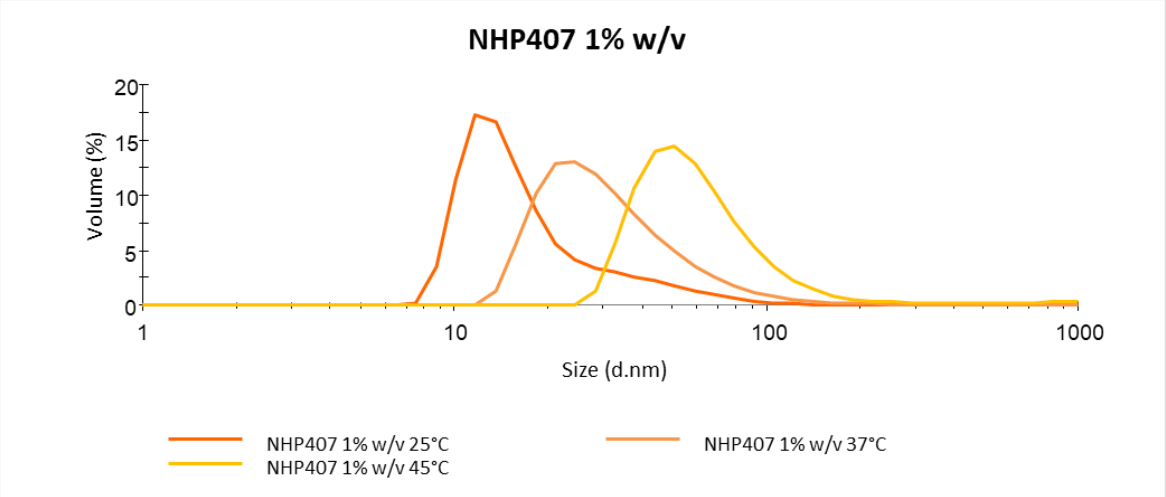

Figure 49: DLS graph of NHP407 1% w/v at 25, 37 and 45°C.

Table 6 reports the hydrodynamic diameters of the main peak of the spectra represented in **Figure 49**.

Table 6: Hydrodynamic diameters relative to the peaks of NHP407 1% w/v at 25, 37 and 45°C.

NHP407 1% w/v	
Temperature (°C)	**Diameter size (nm)**
25	19.81
37	34.73
45	64.79

Figure 50 shows the DLS spectra relative to SHP407 solution at the concentration of 1 % w/v at 25, 37 and 45°C. The distribution obtained for this solution is generally less dispersed than what was observed for NHP407. This can be explained by the formation of more stable micellar structures, with a more definite spherical form. In this case, such as for NHP407,

the shift of the main peak at the increase of temperature proves the micelles formation and aggregation, as explained above.

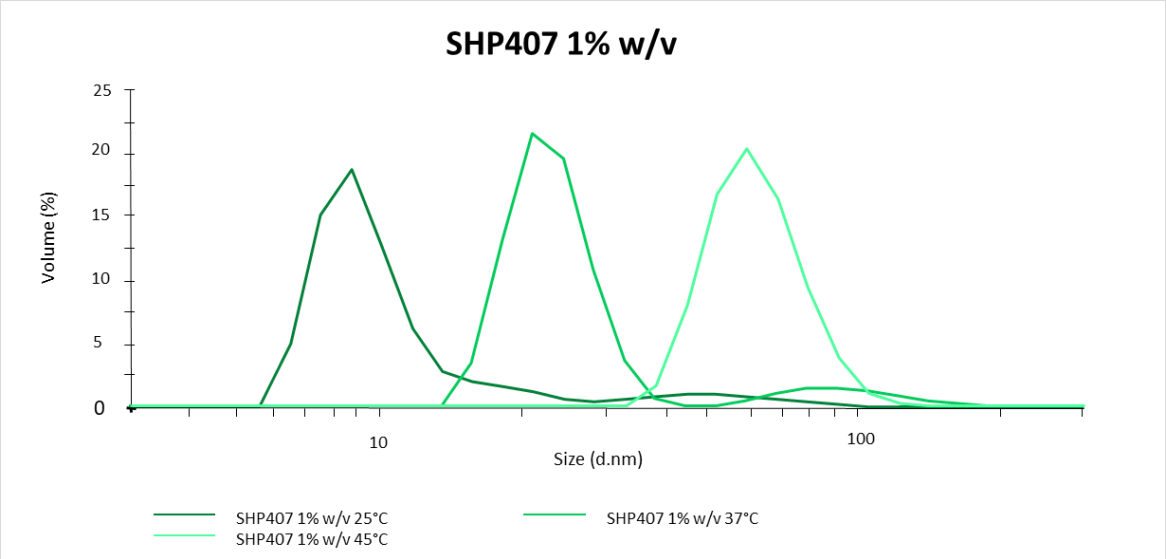

Figure 50: DLS graph of SHP407 1% w/v at 25, 37 and 45°C.

Table 7 resumes the SHP407 diameter sizes relative to the main peaks represented in **Figure 50.**

Table 7: Hydrodynamic diameters relative to the peaks of SHP407 1% w/v at 25, 37 and 45°C.

SHP407 1% w/v	
Temperature (°C)	**Diameter size (nm)**
25	9.97
37	24.96
45	57

Figure 51 shows the comparison of NHP407 and SHP407 at 1% w/v at 37°C. In this picture, it is evident that SHP407 forms more stable and less dispersed aggregates, while the distribution registered for NHP407 is more widespread.

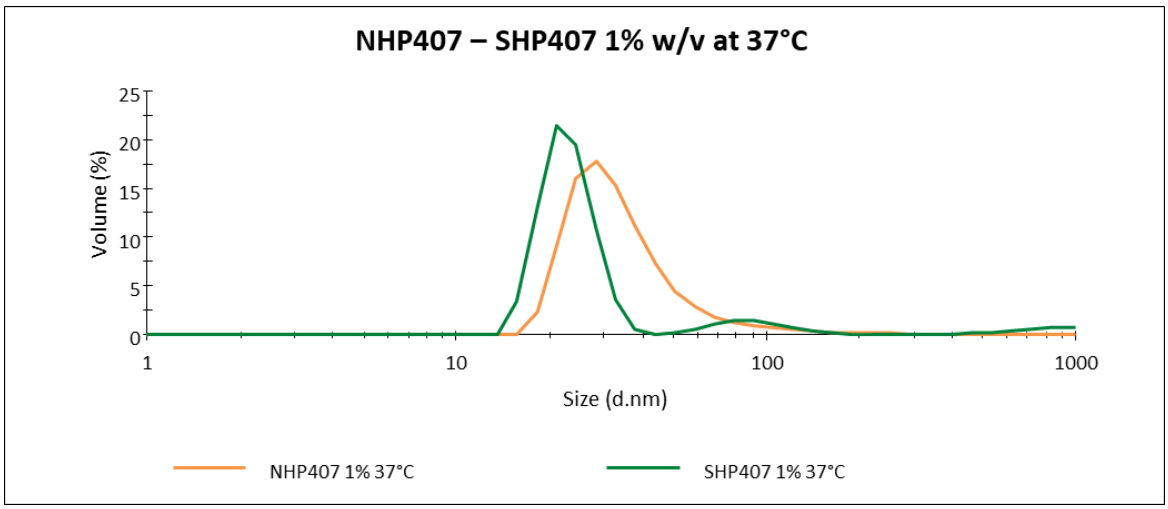

Figure 51: Comparison between NHP407 and SHP407 volumetric distributions at the same concentration (1% w/v)

3.2.2 Critical micellar temperature (CMT)

The critical micellar temperatures were investigated for the polyurethanes NHP407 and SHP407 at the concentrations of 0.1, 0.5- and 1% w/v. The sample were analyzed at UV-vis spectroscopy using DHP as dye, as previously described.

Figure 52 shows as an example the absorption curves obtained for the SHP407 0.1% w/v solution at the temperatures of 20-25-30-40 °C. DHP molecules emit a signal when incorporated into the hydrophobic core of the micelles. At low temperature, the lack of the DHP peak at 356 nm indicates the absence of micelles in the hydrogel solution. The increase of temperature leads to an increase of the DHP peak intensity and this result is related to the formation, increase in number and organization of micelles.

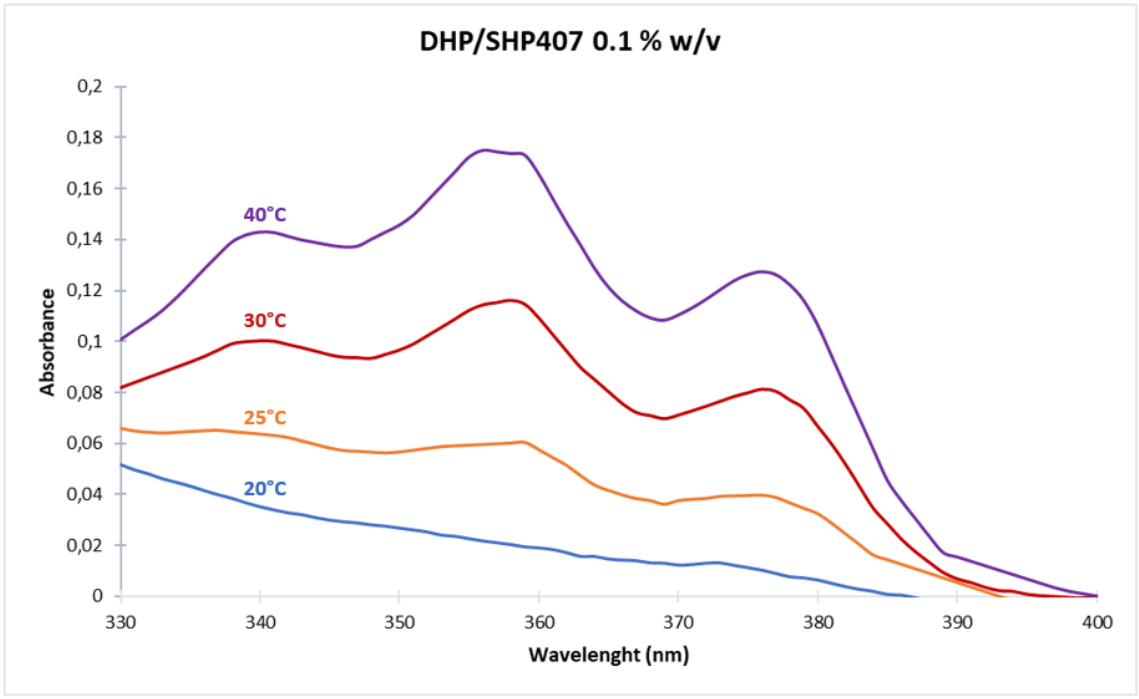

Figure 52: UV−visible absorption spectra of DPH/SHP407 solution (0.1% w/v) at different temperatures.

Figure 53 reports the CMT diagram comparing NHP407 and SHP407 at the same concentration (0.5 % w/v). The CMT value was estimated from the first inflection of the sigmoidal curve of the plot, identified with the moment when micelles start to form in the DHP/PU solutions.

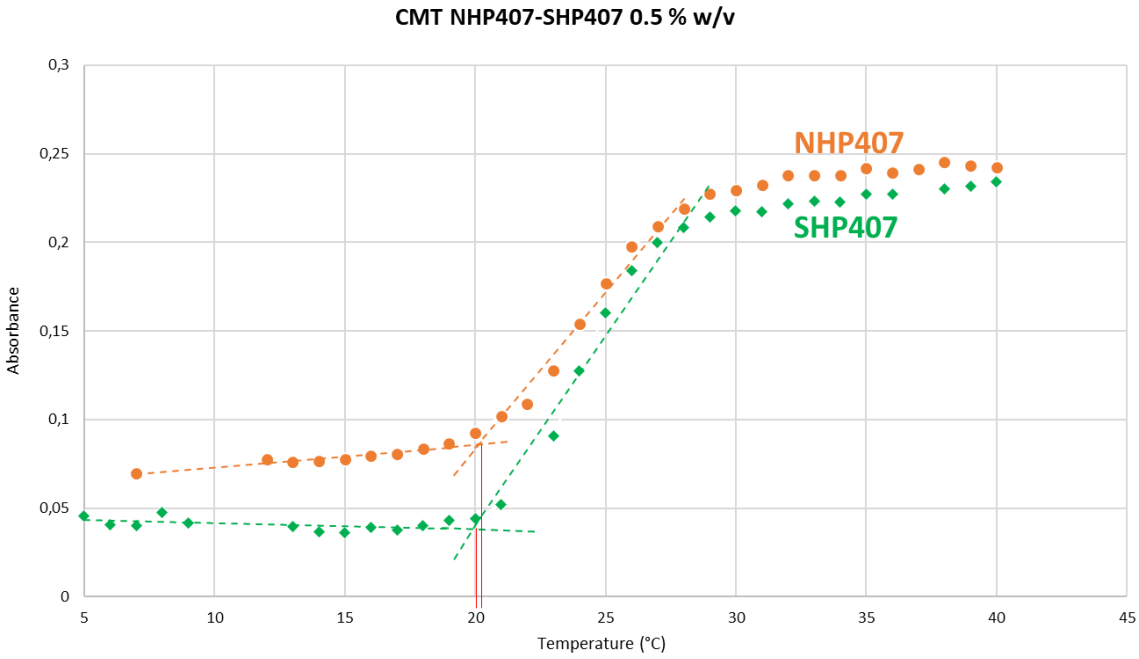

Figure 53: CMT plot of NHP407 and SHP407 at 0.5 % w/v.

Table 8 resumes the critical micellar temperatures (CMT) for both the materials at each tested concentration.

Table 8: CMT values of NHP407 and SHP407 solutions at three different concentrations.

	CMT (°C)	
Concentration (% w/v)	**NHP407**	**SHP407**
0.1	20.6	20.6
0.5	20.1	20
1	19.5	19.4

For both the materials, the increase of concentration leads to a decrease of the CMT value, however the variation between the values is less than 1°C. The presence of deprotected amine did not generate a significant difference in the kinetic of micelle formation, being the CMT values approximately the same for both NHP407 and SHP407.

12.2.3 Tube Inverting Test

The gelation properties of NHP407- and SHP407-based hydrogels were investigated by tube inverting test in the range from 5°C to 46°C and for concentrations between 4 and 15% w/v in PBS. Concentrations over 15% w/v were not tested because for the purpose of designing a blend systems, higher concentrations of polyurethane were not deemed suitable.

The temperatures at which the sol-gel transitions occurred for each sample (lower critical gelation temperature, LCGT) are reported in **Table 9** and shown in **Figure 54**.

Table 9: LCGT values for NHP407 and SHP407-based hydrogels. Error: ± 1°C.

NHP407		**SHP407**	
Concentration (% w/v)	**T (°C)**	**Concentration (% w/v)**	**T (°C)**
4	46	4	-
5	46	5	-
6	43	6	43

7	38	7	38
8	35	8	35
9	34	9	34
10	32	10	32
11	31	11	30
12	29	12	28
13	28	13	27
14	27	14	26
15	26	15	25

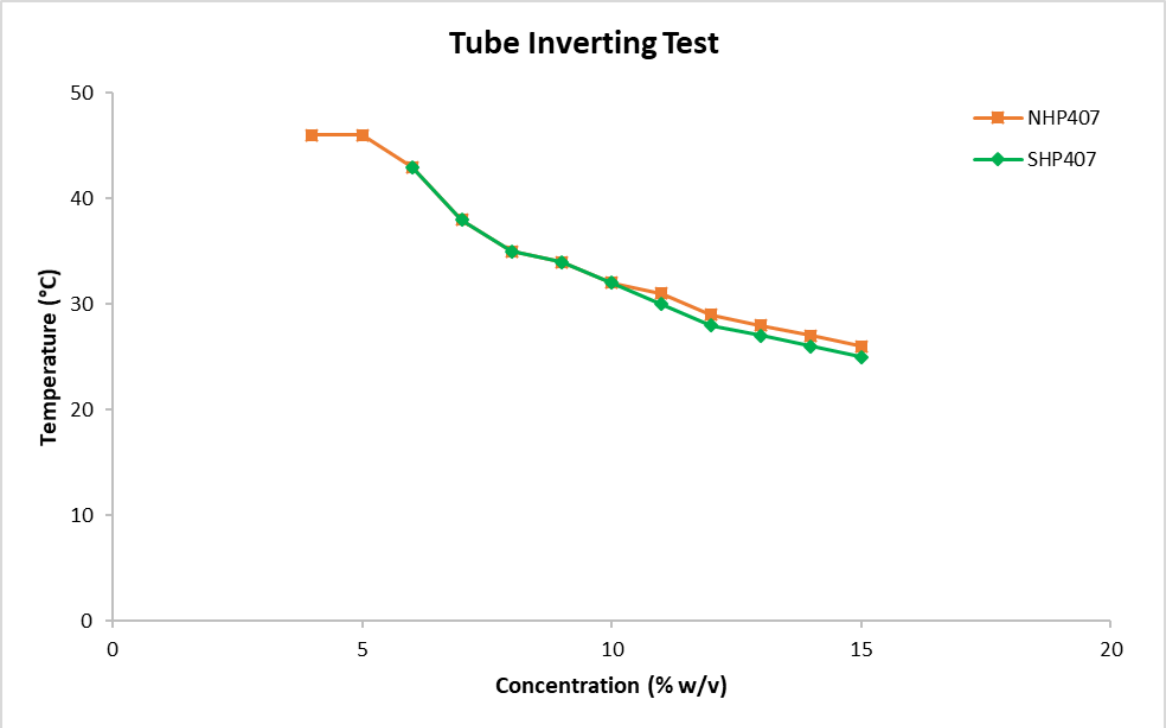

Figure 54: Tube inverting test of NHP407 vs SHP407 shows the similar behaviour of the materials. SHP407 at the concentrations of 4 % w/v and 5 % w/v are not represented because for these samples the sol-gel transition does not occur in the range of temperatures tested (5-46 °C).

It was observed that with the decrease of hydrogel concentrations, higher temperatures are necessary to undergo sol-gel transitions. Considering that the margin of error for this test is ± 1°C, relevant differences between the two material were not found. However, it was also possible to define a critical gelation concentration (CGC), below which the system remains always in a sol state following an increase in temperature: in this case, for SHP407 the value was found to be 6 ± 1%, while for NHP407 was 4 ± 1%.

3.2.4 Gelation time test at 37°C

The time required by NHP407- and SHP407-based hydrogels sol-gel transitions to occur at physiological conditions (37°C) were investigated by gelation time test. The gelation times are reported in the bar chart of **Figure 55**.

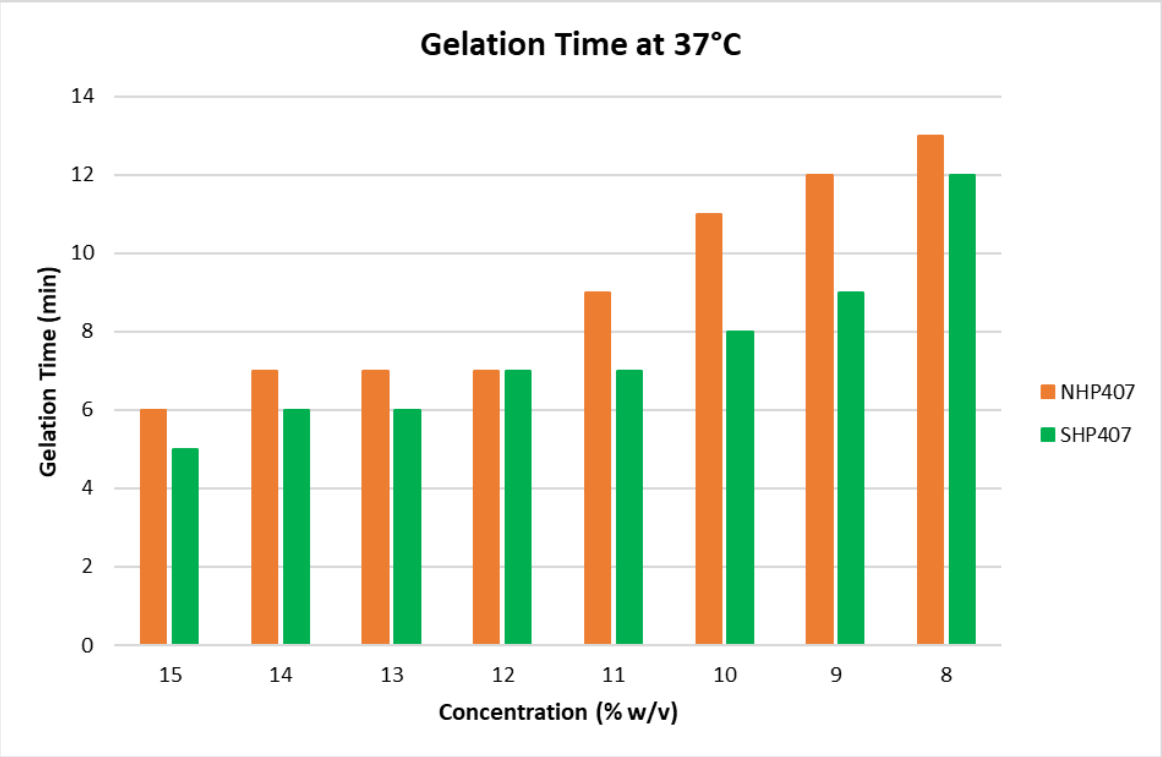

Figure 55: Gelation time at 37°C for NHP407- and SHP407-based hydrogels. Error: ± 1 min.

From these results, it was again observed that the decrease of the hydrogel concentrations leads to an increase of time needed to undergo sol-gel transitions. As for LCGT values, no significant differences were found for the two polyurethanes: it is then confirmed that the amine deprotection did not cause a relevant change in the thermo-sensitive response of the sol-gel systems obtained from these materials.

The results obtained for the PUs thermal characterization were consistent to what was found in a previous work [66] regarding similar systems, in which NHP407 was used at a 12.5% w/v concentration . For this reason, since no relevant differences were detected between the two PUs, in this work it was decided to maintain the same concentration for SHP407. This way, the system respected the requirements for application in the tissue

engineering field, i.e. a gelation temperature within the physiological range (28 ± 1°C) and a suitable gelation time at 37 °C (8 ± 1 min).

3.2 PEGDA Chemical Characterization

3.2.1 Attenuated Total Reflectance Fourier Transform Infrared (ATR-FTIR) spectroscopy

The synthetized Poly (ethylene glycol) Diacrylate (PEGDA) synthesis were characterized by Attenuated Total Reflectance Fourier Transform Infrared (ATR-FTIR) spectroscopy analysis to verify the success of the synthesis. **Figure 56** shows the spectra of PEG 3350 on behalf of all the PEGs at different molecular weights (3350 Da, 4600 Da and 6000 Da), while all the PEGDAs are reported. This representation was chosen because all PEGs spectra were almost identical, while some considerations on PEGDAs spectra comparison can be done. The success of all PEGDA synthesis was confirmed by the comparison of PEG and PEGDAs spectra. The presence of acrylate groups in the material was recognizable by the appearance of characteristic absorption peaks of ester C=O at 1720 cm^{-1} and C=C at 1637 cm^{-1}. The intensity of these peaks revealed a qualitative evidence of acrylation degree, that was further proved with subsequent analysis. The absorption peak in a range 2500 cm^{-1} to 3000 cm^{-1} is characteristic of -OH groups; however, in this case it was probably due to air humidity and presence of water in the material and not to unreacted groups.

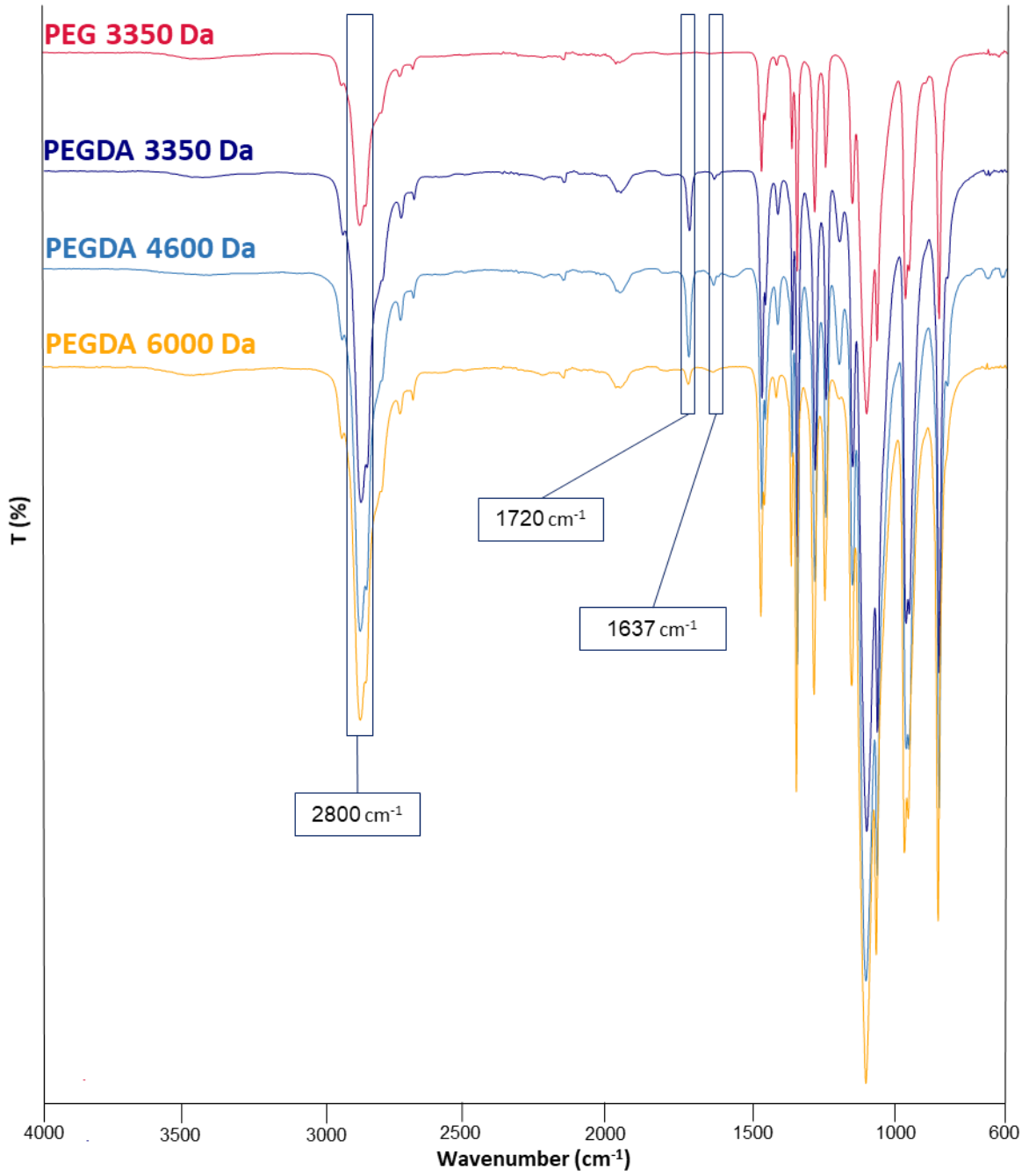

Figure 56: PEG-PEGDA spectra.

3.2.2 Size exclusion chromatography (SEC)

With size exclusion chromatography (SEC), the molecular weights of PEGDAs were measured. The molecular weights of PEGDA 3350, PEGDA 4600 and PEGDA 6000 were compared to originals PEGs and no significant differences were detected. These results proved that the PEGDA synthesis was not a degradative reaction. **Figure 57** shows the synthetized PEGDA 3350 Da as example.

Figure 5714: Synthetized PEGDA.

3.2.3 Proton Nuclear Molecule Resonance Spectroscopy (^{1}H-NMR)

^{1}H-NMR analyses were performed to verify the PEGDA synthesis success and to measure the degree of PEG acrylation comparing the different PEGs and PEGDAs spectra with the same molecular weight. The success of the PEGDA synthesis is indicated by the chemical shift located at 5.9–6.4 ppm, assigned to the protons of vinyl groups as shown in **Figure 58** [71]. In these spectra the area under the characteristic peak is related to the number of protons that are responsible for the specific peak.

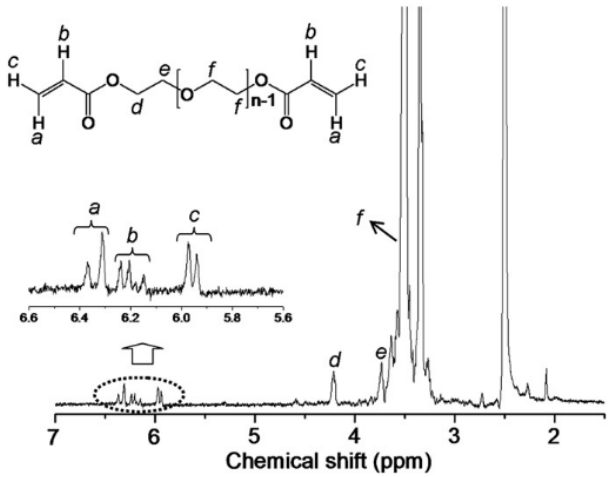

Figure 58: 1H-NMR spectrum of PEGDA in DMSO d6 with peaks relative to vinyl groups.

The area under the peaks of interest was calculated for each PEG-PEGDA pair and the peaks areas ratio were determined and used as a quantification of the acrylation degree. The **Figure 59** shows the full superimposed spectra of PEG and PEGDA (3350 Da as example) and highlights the region of interest (5.9–6.4 ppm) where the acrylate peaks are located. **Figure 60, 61, 62** show the PEG-PEGDA pairs superimposed spectra.

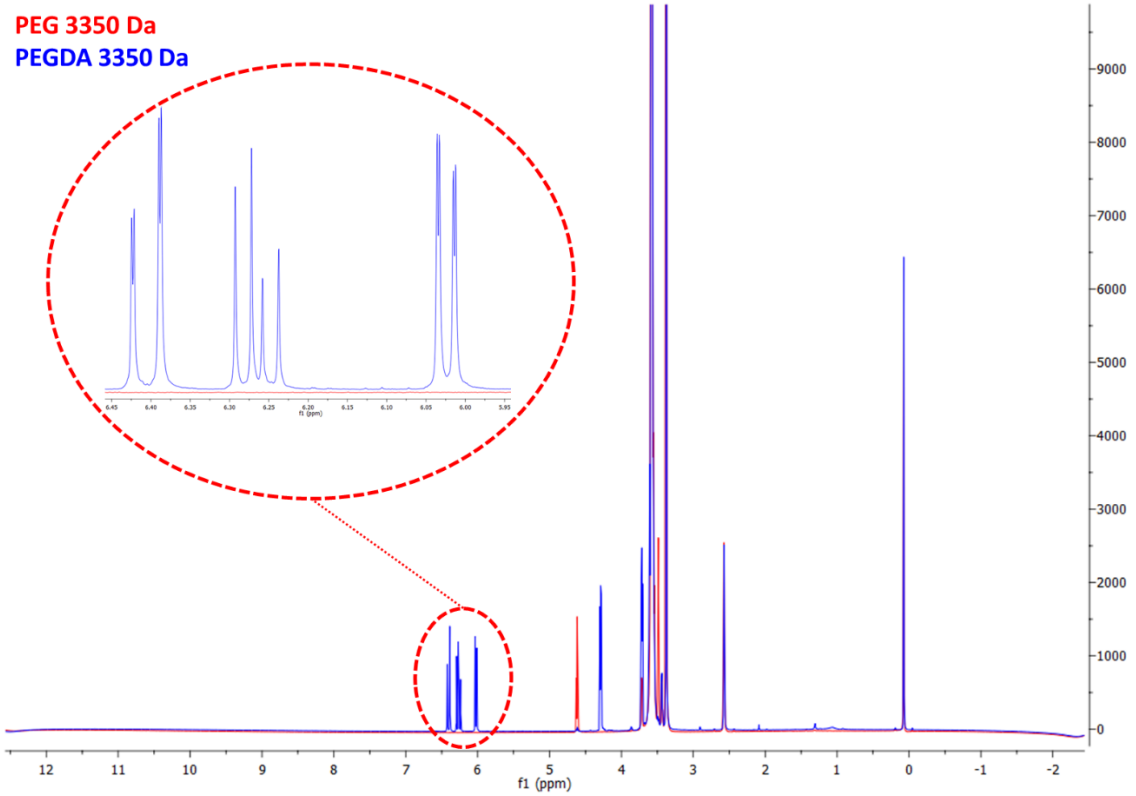

Figure 59: 1H-NMR full spectra of PEGDA and PEGDA (3350 Da as example). The superimposed spectra show that a set of peaks relative to acrylate groups appears after synthesis of Poly (ethylene glycol) Diacrylate. These peaks are located at 5.9-6.4 ppm.

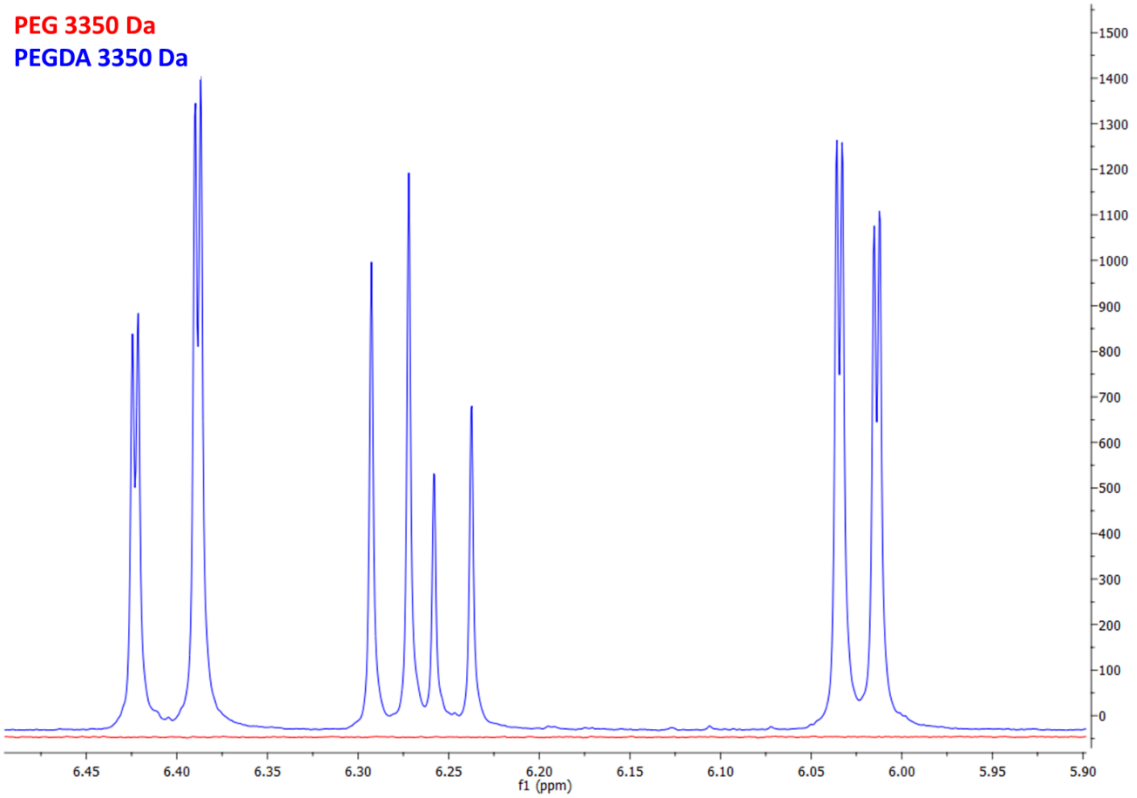

Figure 60: 1H-NMR superimposed spectra of PEG and PEGDA 3350 at 5.9–6.4 ppm.

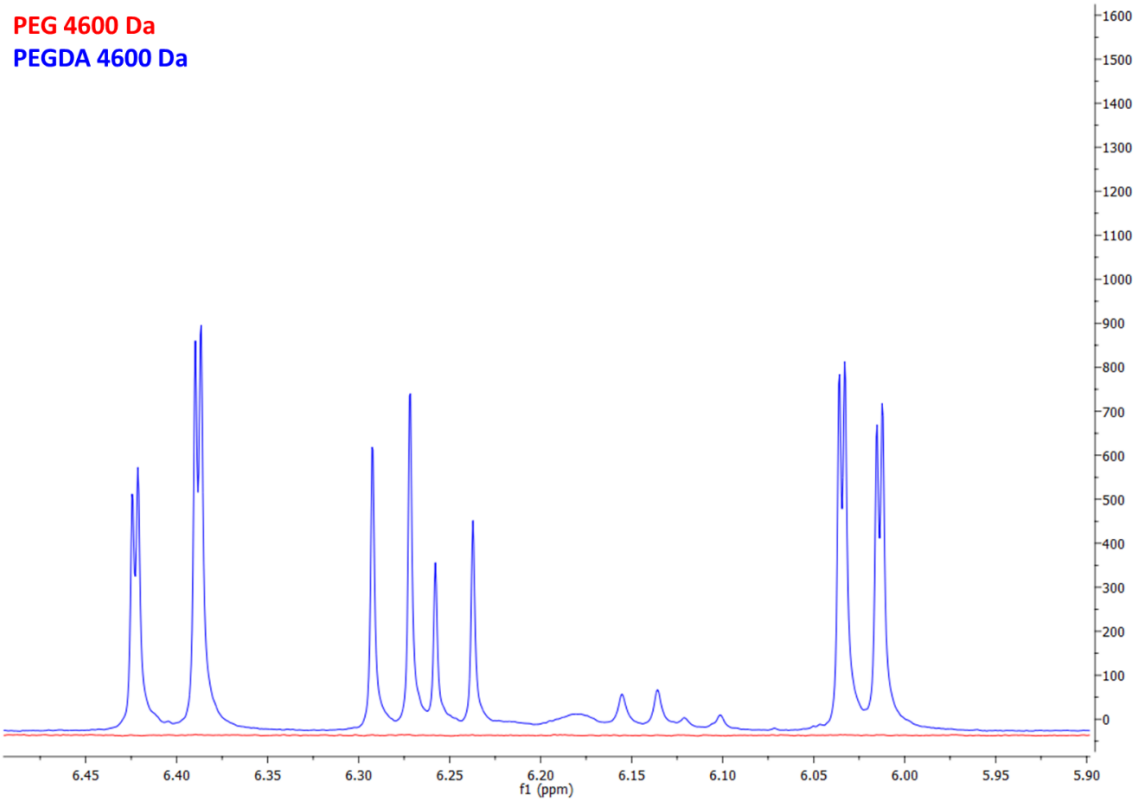

Figure 61: 1H-NMR superimposed spectra of PEG and PEGDA 4600 at 5.9–6.4 ppm.

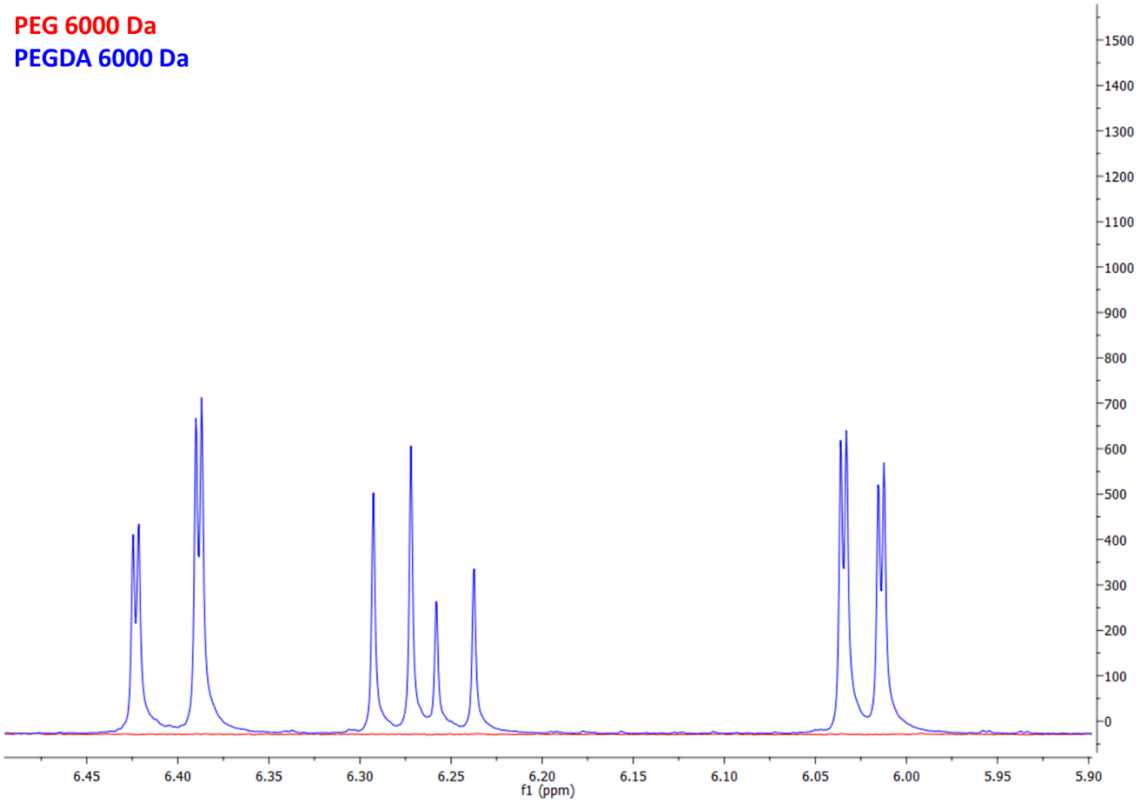

Figure 62: 1H-NMR superimposed spectra of PEG and PEGDA 6000 at 5.9–6.4 ppm.

^{1}H-NMR analyses allowed to know the number of acrylate groups per polymeric PEGDA chain, as resumed in **Table**. This information was used in blend selection to compare PEGDA concentrations with different molecular weights but similar number of acrylate groups (responsible of the photo-crosslinking).

Table 10 reports data results:

Table 10: ^{1}H-NMR PEGDA results.

Molecular Weights	Peaks Areas ratio	Acrylation (%)	Acrylate Groups per polymeric chain
3350 Da	0.8097	81 %	1.6
4600 Da	0.858	86 %	1.7
6000 Da	0.77	77 %	1.54

3.2.4 PEGDA solubility test

The solubility of the three synthetized PEGDAs (3350, 4600 and 6000 Da) in PBS (Phosphate Buffered Saline) was tested to evaluate their suitability to create blends with SHP407. PEGDA 3350 and PEGDA 6000 resulted soluble up to a 20 % w/v concentration, which was considered as the maximum value of solubilization appropriate for the thesis goal. On the other hand, PEGDA 4600 resulted to have a limit of solubilization of 1.5 % w/v and this concentration was considered too low for a photocuring application. For this reason, blend based on PEGDA 4600 have not been produced and only PEGDA 3350 and PEGDA 6000 were used.

The limit of solubilization of PEGDA 4600 is probably due to the high amount of acrylate groups present in the material: indeed, between the three tested PEGDA, the degree of substitution found for PEGDA 4600 was the highest (86%). The higher number of acrylate groups impacts on the hydrophobicity of the material, resulting in lower limit of solubility.

3.5 PU-PEGDA blends

3.5.1 Micelle size analysis - Dynamic Light Scattering (DLS)

Dynamic Light Scattering (DLS) analysis were performed on SHP407-PEGDA blends to investigate how the addition, in terms of concentration and molecular weights, of PEGDA to SHP407 influenced the mechanism of polymeric structures formation and the micelles sizes. The tests were performed at 25°C, 30°C, 37°C following the same protocol applied for sole SHP407 and described before.

To better highlight the effect of the addition of PEGDA to the polyurethane, the formulations with highest concentrations of PEGDA were selected for the following figures. Results for EDA3350_0.8% at 25, 37 and 45°C are reported in **Figure 63** as representative of all the blends that contain PEGDA 3350 Da, since the behavior of the other two formulations (EDA3350_0.24% and EDA3350_0.44%) is similar. PEGDA chains interacted with the SHP407 micelles, but because of the relatively low molecular weight of PEGDA 3350, they have small influence on their shape and dimension. In this case, the addition of

PEGDA to the system is not very appreciable. The comparable behavior of EDA3350 at different concentrations is in line with the sol-gel transition studies (tube inverting test and gelation time test), which results were similar for all the EDA3350 formulations.

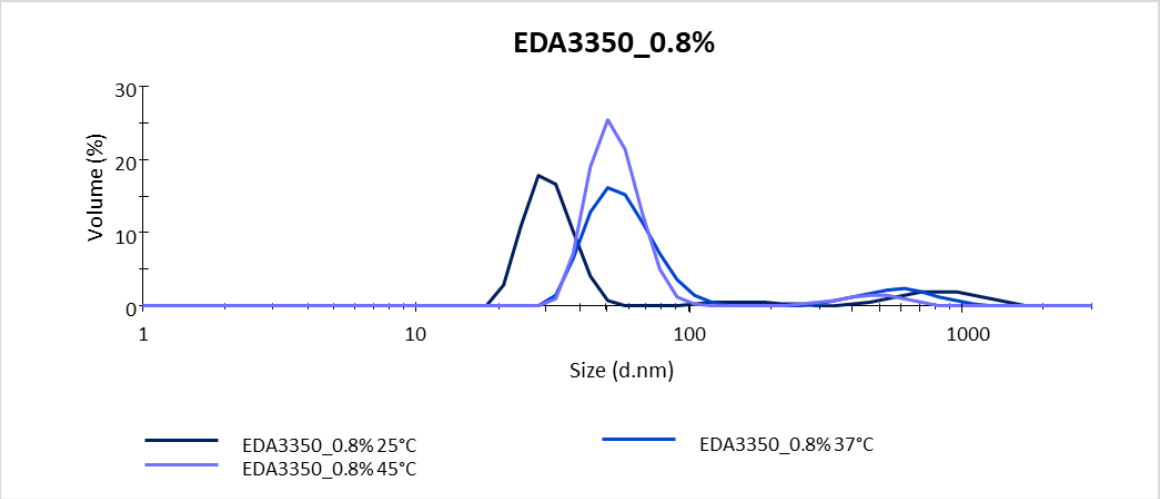

Figure 63: EDA3350_0.8% volumetric distributions at 25, 37 and 45°C.

The values of the main diameter sizes represented in **Figure 63**, representative of EDA3350 behaviour, are reported in **Table 11**.

***Table 11**: Diameter size peaks relative to **Figure 63**.*

EDA3350_0.8%	
Temperature (°C)	**Diameter size (nm)**
25	36.2
37	63.31
45	57.27

Figure 64 shows the DLS results of EDA6000_1.44%, selected as representative of all the blends based on PEGDA 6000.

In this case, the volumetric distribution is very similar for all the temperatures considered (25, 37, 45°C). PEGDA 6000 chains are considerably longer (almost double in length) than PEGDA 3350, so they have a more marked effect on the signal. In particular, it can be speculated that PEGDA 6000 caused the formation of less spherical aggregates by interacting with SHP407-formed micelles, thus resulting in higher values of hydrodynamic

diameter registered by the instrument. The systems formed is also less stable, as evidenced by the presence of a multimodal distribution.

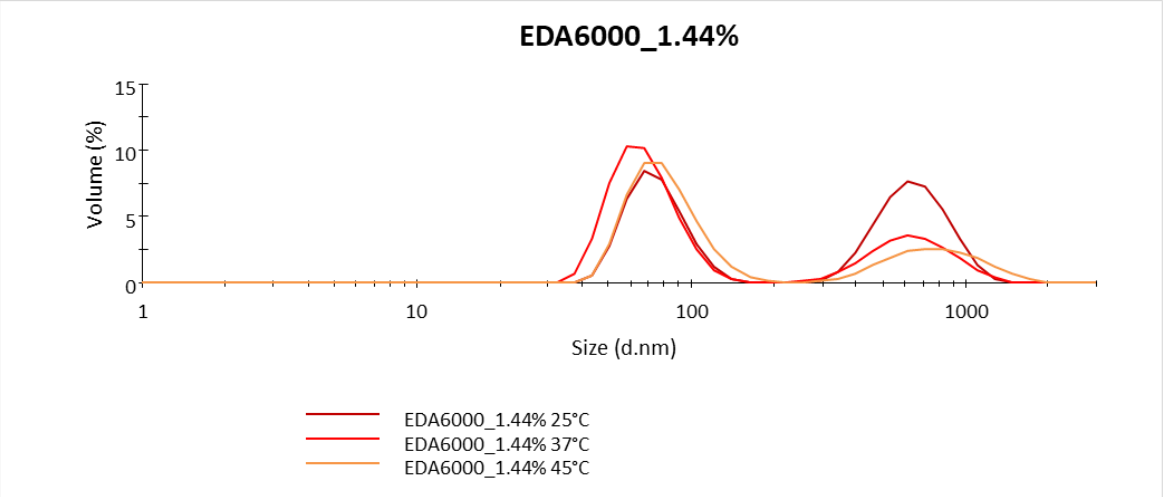

Figure 64: EDA6000_4.4% volumetric distributions at different temperatures (25, 37, 45°C).

Table 12 reports the values of the main peaks formed by the EDA6000 blend shown in **Figure 64**.

Table 12: EDA6000_1.44 diameter sizes values at different temperatures.

EDA6000_1.44%	
Temperature (°C)	**Diameter size (nm)**
25	93.23
37	85.41
45	84.01

Figure 65 compares the spectra of the two set of blends (EDA3350 and EDA6000) to the sole polyurethane component (SHP407) at 37°C.

EDA3350_0.8% and EDA6000_1.44% were again selected as representative of blends based on PEGDA 3350 and PEGDA 6000, respectively. All the measurements were performed at 37°C. It is evident in this case that the addiction of PEGDA 3350 had a scarcely significant effect on the volumetric distribution compared to the control (SHP407 1% w/v), only leading to a small shift in the main peak. On the other hand, for PEGDA 6000-based blend the effect was more relevant and as previously explained due to a greater interaction with SHP407 micelles, leading to the formation of less stable non-spherical aggregates.

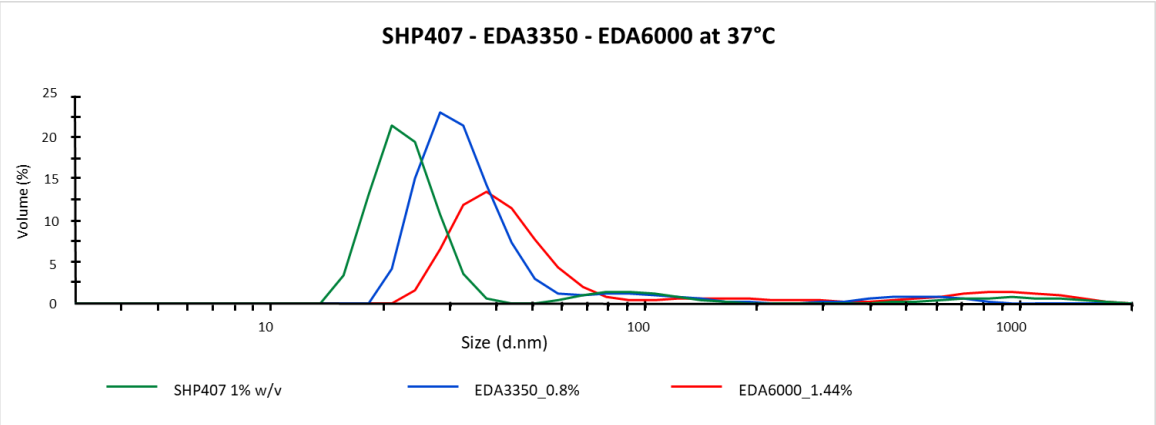

Figure 65: Comparison of volumetric distribution at 37°C of SHP407 1% w/v, EDA3350_0.8% and EDA6000_1.44%.

3.5.2 Critical micellar temperature (CMT)

The critical micellar temperature of each blend was investigated, in order to underline the effect of the PEGDA presence on the gelation kinetic. **Table 13** reports the CMT of all the formulations.

Table 13: *Critical Micellar Temperatures of SHP407 at 1% w/v and SHP407-PEGDA blends.*

Sample	CMT (°C)
SHP407 1% w/v	19.4
EDA3350_0.24	20.6
EDA3350_0.44	20.5
EDA3350_0.8	20.6
EDA6000_0.44	19.1
EDA6000_0.8	20.9
EDA6000_1.44	20.4

Based on these results, it was observed that all the formulations have approximately the same behavior, with a CMT temperature ranging around 20°C. **Figure 66** reports the curve obtained for EDA6000_0.44 as an example compared to sole SHP407 at 1 % w/v.

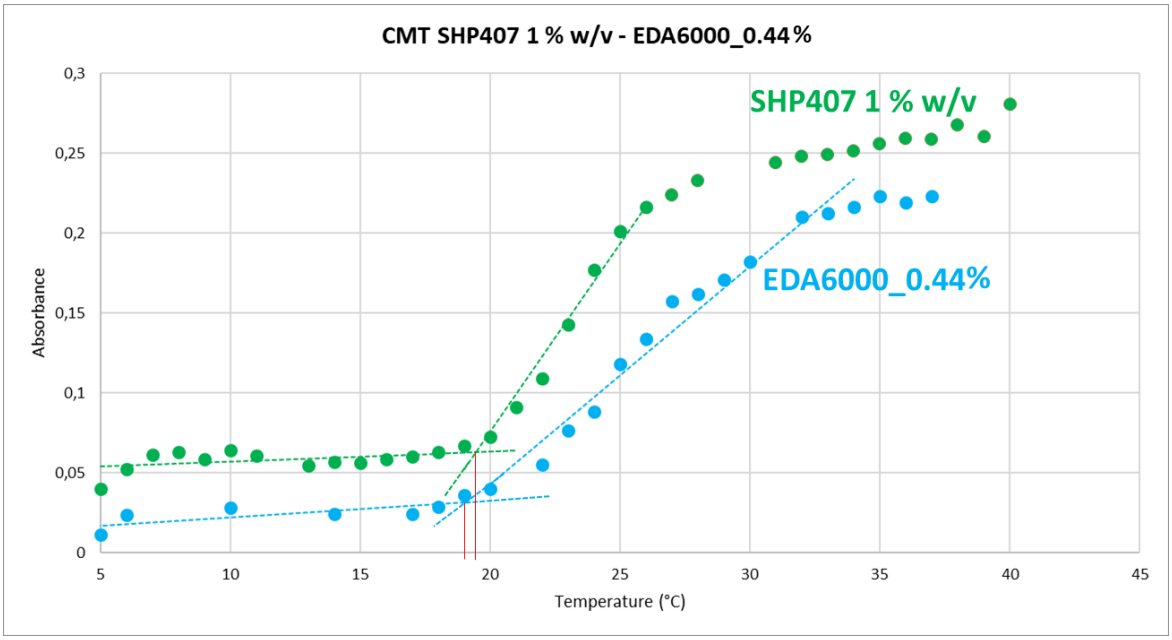

Figure 66: Absorbance at 356 nm vs temperature for SHP407 1% w/v and EDA6000_0.44%. The addition of PEGDA to SHP407 does not influence the CMT in a relevant way.

Furthermore, comparing the results of sole SHP407 and blends, it was confirmed that the addition of PEGDA to SHP407 doesn't lead to a relevant influence in the formation of the first micelles, being the CMT values found approximately the same. This effect was expected considering the non thermo-sensitive nature of PEGDA.

3.6 Blends-based sol-gel systems characterization

3.6.1 Tube Inverting test

The tube inverting test was performed also on the blend formulations to investigate the influence of PEGDA on the LCGT. The protocol is the same followed before. The control formulation is represented by SHP407 12.5%. **Table 14** resumes the results found for each formulation.

Table *14: Gelation temperatures of blend formulations.*

PEGDA 3350 Da	Temperature (°C)	PEGDA 6000 Da	Temperature (°C)
EDA3350_3	28	EDA6000_5.5	27
EDA3350_5.5	28	EDA6000_10	22
EDA3350_10	28	EDA6000_18	15
	CTRL	28	

All the blends based on PEGDA 3350 presented the same behavior, independently from the concentration. For all of them, indeed, the sol-gel transition occurred at 28°C, as for the control sample. In the case of PEGDA 6000 blend, however, the increase of concentration lead to a relevant decrease of the LCGT, especially for EDA6000_10% (LCGT=22°C) and EDA6000_18% (LCGT=15°C).

From these results, it was deduced that the PEGDA molecular weight influences the gelation behavior. The interaction of the polymeric chains of PEGDA 3350 Da with SHP407 is generally not relevant, probably because of their limited length. On the other hand, the PEGDA 6000-SHP407 interaction is more evident, supposedly because the chains are longer and their steric hindrance helps the micelle packing, favoring the sol-gel transition.

The results of this qualitative test were then further verified through rheological characterization.

13.4.4 Gelation time test in physiological conditions

The gelation time of the blend formulations were investigated as previously mentioned. Results are reported in **Table 15.**

Table 15: Gelation time test results of SHP407-PEGDA blend formulations.

PEGDA 3350 Da	Gelation time (min)	PEGDA 6000 Da	Gelation time (min)
EDA3350_3%	7	EDA6000_5.5%	5
EDA3350_5.5%	6	EDA6000_10%	4
EDA3350_10%	5	EDA6000_18%	3
	CTRL	8	

For both PEGDA 3350- and PEGDA 6000-based blends, the increase of concentration lead to a decrease of the time required for the sol-gel transition to occur. The effect is again more evident for the formulation with higher concentrations of PEGDA 6000, consistently to what was found during tube inverting test.

It can also be noted that the thermic response of the blends is not influenced solely by the PEGDA molecular weight, but also by the system final concentration. For EDA6000_18%, in particular, the final concentration of the hydrogel (considering both SHP407 and PEGDA

contribution) was over 30% w/v, resulting in a density of the system that was noticeably higher than the other blends even in the sol state. **Figure 67** shows the sol-gel transition of EDA6000_18%, as example

Figure 6715: Sol-gel transition of EDA6000_18%, as example.

3.7 Rheological characterization

3.7.1 Strain sweep tests

The frequency sweep tests were performed for all the hydrogels blends compositions to define the linear viscoelastic region (LVE) of the materials at 37°C at constant frequency (10 Hz) and different strains. **Figure 68** and **Figure 69** show the trend of storage modulus (G', relative to elastic properties) and loss modulus (G'', relative to viscous properties) over strain within the range 0.1-500% relative to the hydrogels based on PEGDA 3350 and EDA6000_5.5% and EDA6000_10%, respectively. For all the blends, in the first phase of the graphs both the moduli maintained constant values, the elastic component of the material compensated the force applied by the instrument to cause the deformation. Then, G' decreased and assumed lower values than G''. The value of deformation that corresponds to the initial decrease of G' represents the breaking of the gel (LVE value). Furthermore, the distance between G' and G'' in the constant region indicates the mechanical resistance of the gel.

Comparing the three compositions of blends based on PEGDA 3350, no relevant differences were observed in terms of viscoelastic properties and resistance to applied strain (LVE: γ = 11.6 % for all three blends). In terms of rigidity, the increase of PEGDA concentration lead to stiffer gel and this property is observed by the increasing of distance between G' and G'' in the first region of constant values (LVE region).

In the case of blends based on PEGDA 6000, the increase of PEGDA concentration lead to a reduction of LVE region and then to a more rigid and fragile gel. EDA60000_5.5% resulted more resistant (LVE: γ = 1 %) than EDA6000_10% (LVE: γ = 0.7 %). EDA6000_18% resulted to be the more rigid formulation, breaking with very low strain values (γ < 0.01%) to have appreciable results. For this reason, it was not possible to define the LVE region. Therefore, all the further rheological test could not be performed, since they need to be conducted in the linearity region to be consistent.

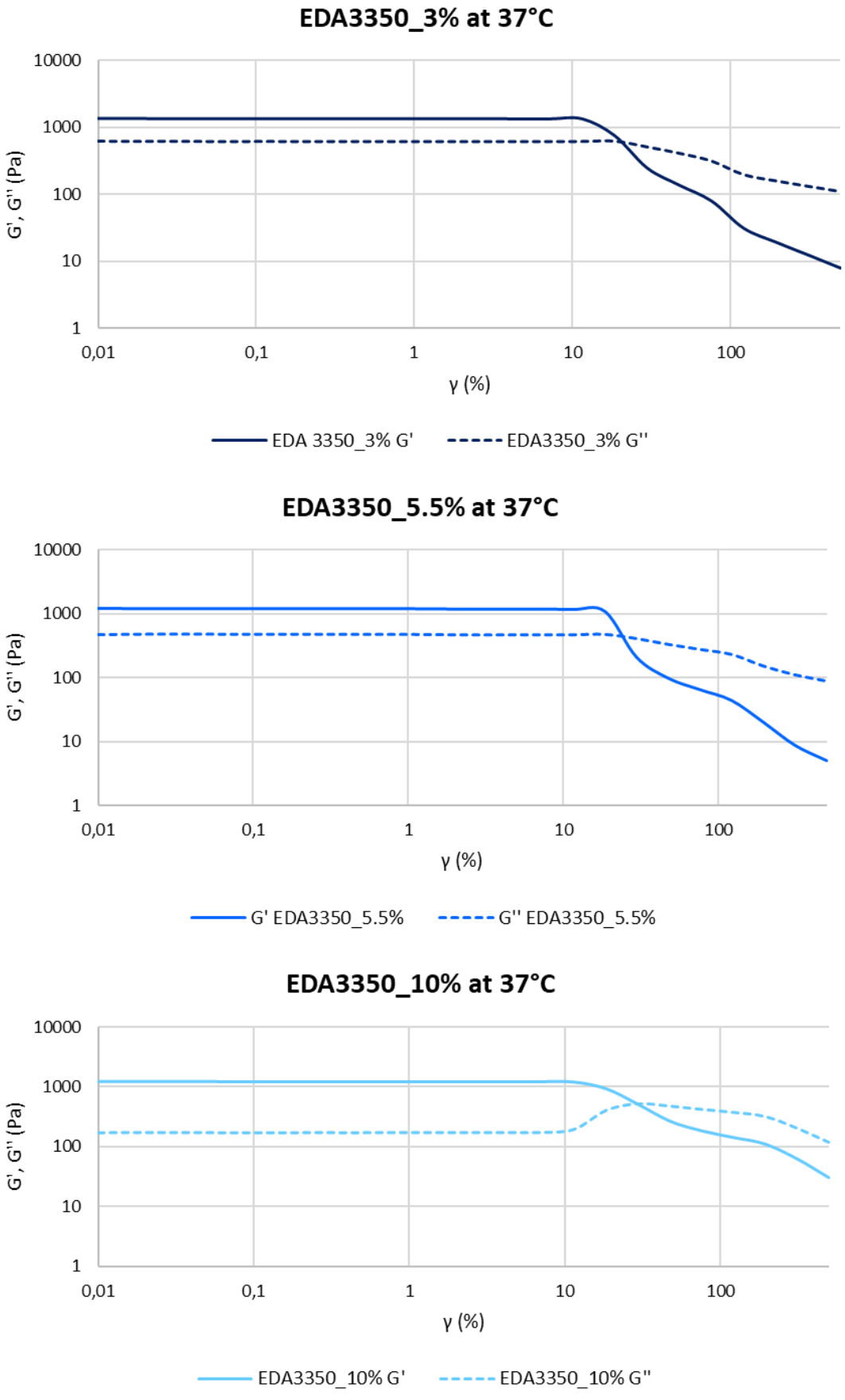

Figure 68: Strain sweep test results relative to EDA3350 blends.

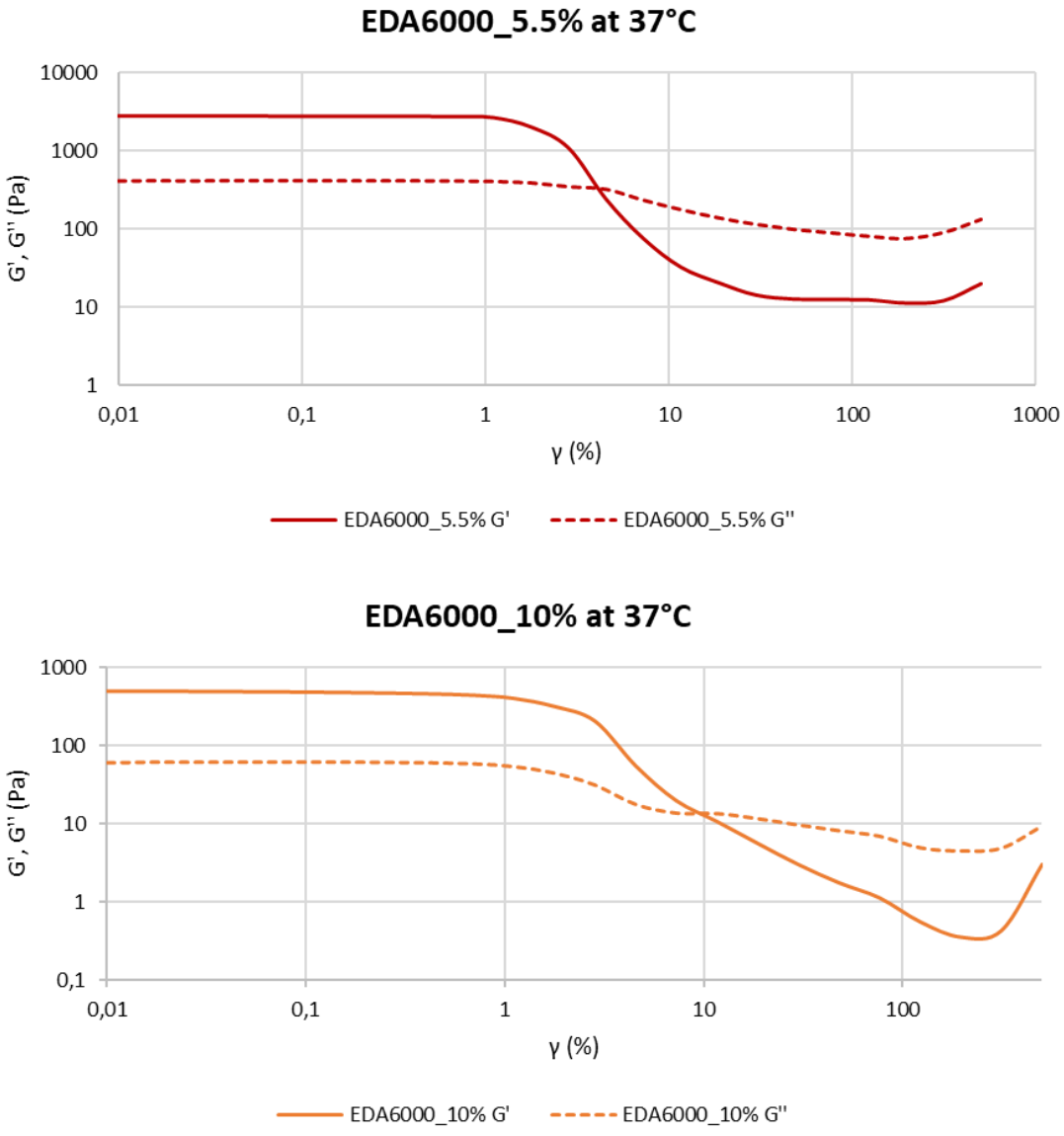

Figure 69: Strain sweep test results relative to EDA6000 blends.

3.7.2 Frequency sweep tests

In order to investigate the kinetic of sol-gel transition that lead to gel formation and development, the frequency sweep test was performed for all the blend compositions except EDA6000_18% as previously explained. The test was performed applying a frequency in the range 0.1-100 rad/s and maintaining the strain constant. The test was repeated at different temperatures (25, 30 and 37°C) and the storage modulus (G') and loss modulus (G'') were studied. The measures were performed in the Linear Viscoelastic Region (LVE) of each material.

Figure 70, 71, 72, 73, 74 show the results obtained. The G'/G'' crossover (in which G' becomes lower than G'') identifies the sol-to-gel transition and it is expected at lower values of angular frequency (rad/s) at the increasing of temperature. **Table 16** reports the crossover frequencies calculated for the blends.

Table 16 : Frequency (rad/s) of the crossover between G' and G'' for the blends based on PEGDA 3350 and PEGDA 6000 at three different temperatures (25, 30, 37°C).

	ω (rad/s)		
Sample	**25°C**	**30°C**	**37°C**
EDA3350_3%	32.975	2.1311	-
EDA3350_5,5%	16.9505	1.2498	-
EDA3350_10%	4.8676	0.3784	-
EDA6000_5,5%	9.1978	0.69567	-
EDA6000_10%	1.3222	0.1	-

The blends based on PEGDA 3350 have a similar behavior, with a progressive shift of the crossover on lower frequency by increasing temperature and PEGDA content. All the compositions resulted to have a fully developed gel behavior at 37°C, because the G' curve became independent on the frequency, assuming an almost constant value, and the difference between G' and G'' values at 100 rad/s was more than an order of magnitude. As already evidenced by gelation time test at 37°C, the increase of PEGDA in the blends accelerates the sol-to-gel transition kinetic.

For the blends based on PEGDA 6000, the considerations are similar. Also in this case, all the formulations were fully developed gels at physiological temperature and an increase of temperature and PEGDA concentration induced a shift of the crossover point to lower frequency. Generally, PEGDA 6000 had a more marked effect on the gelation kinetic, as already observed with tube inverting test, resulting in a wider shift of the crossover values.

These characteristics enable these materials to be used in tissue engineering applications: all the hydrogel blends are fully developed at physiological temperature so they are more stable and able to better retain the given form.

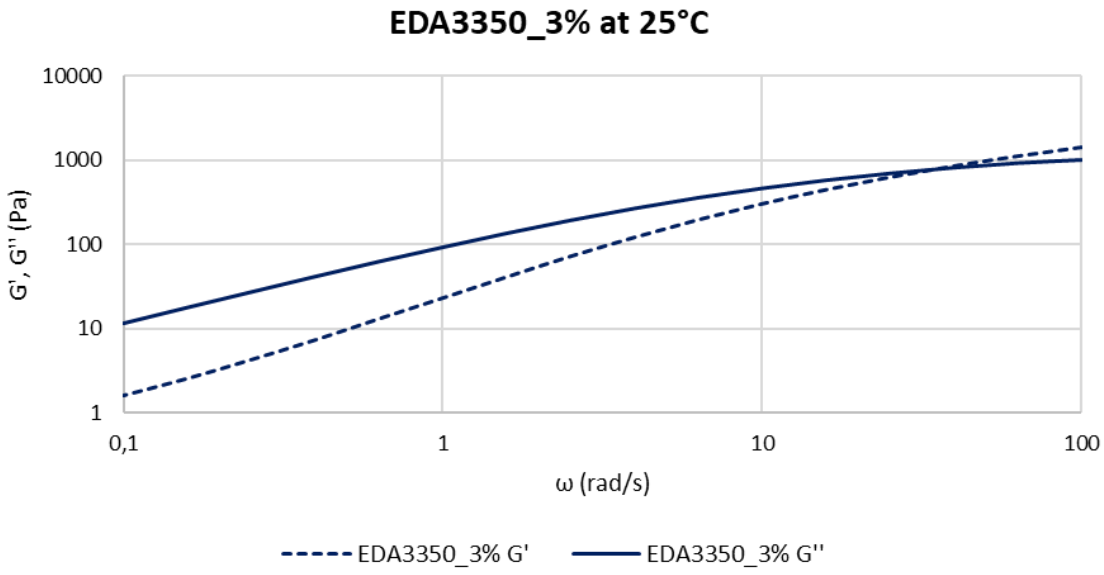

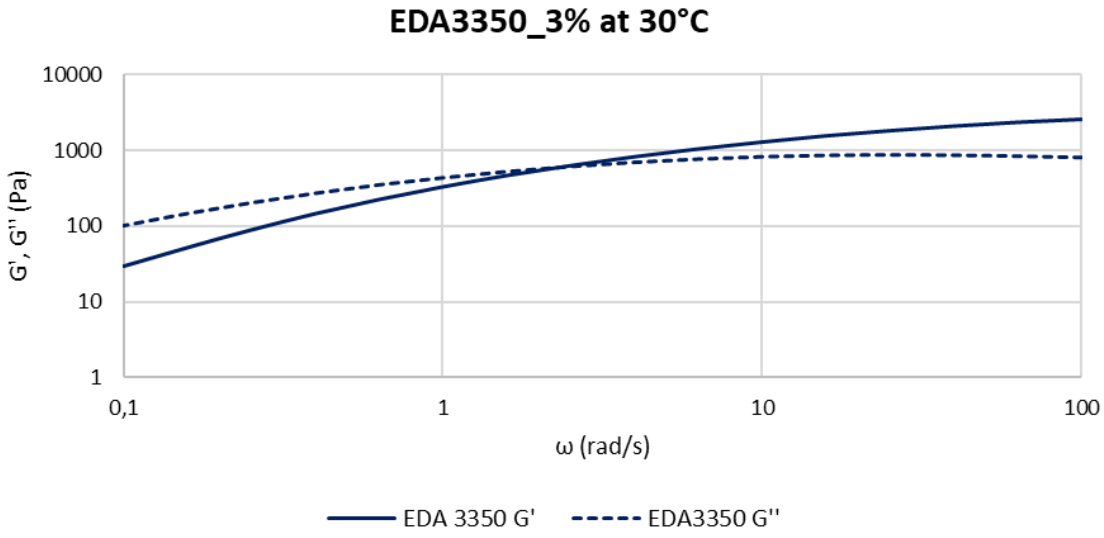

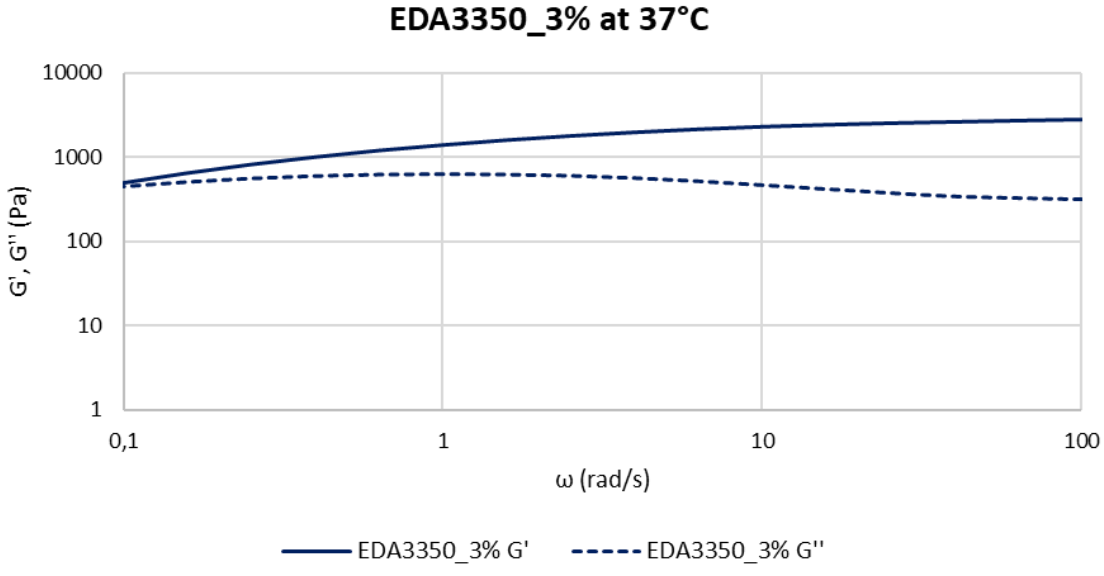

Figure 70: Frequency sweep test results for EDA3350_3% at three different temperatures (25, 30, 37°C).

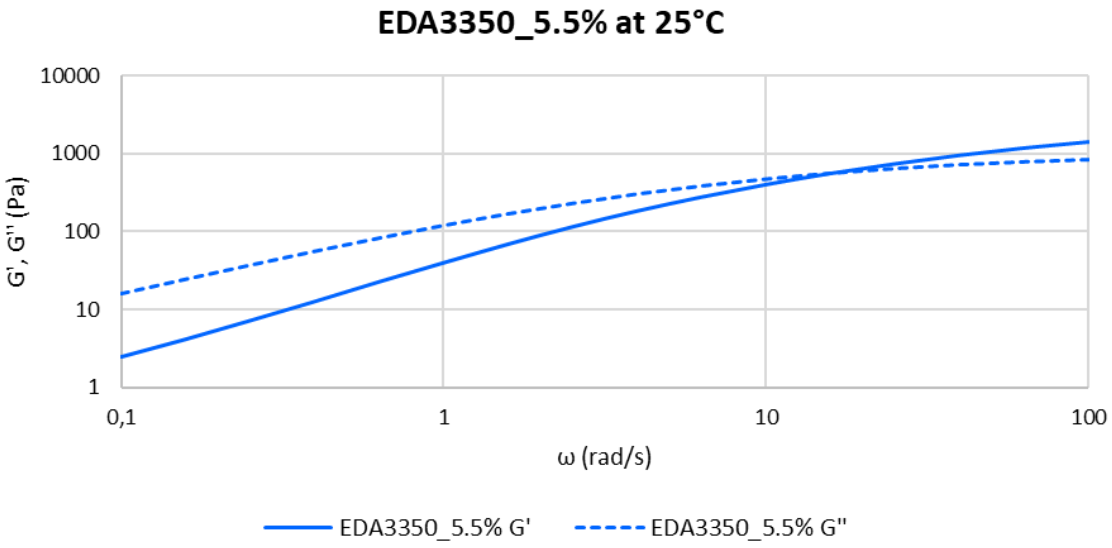

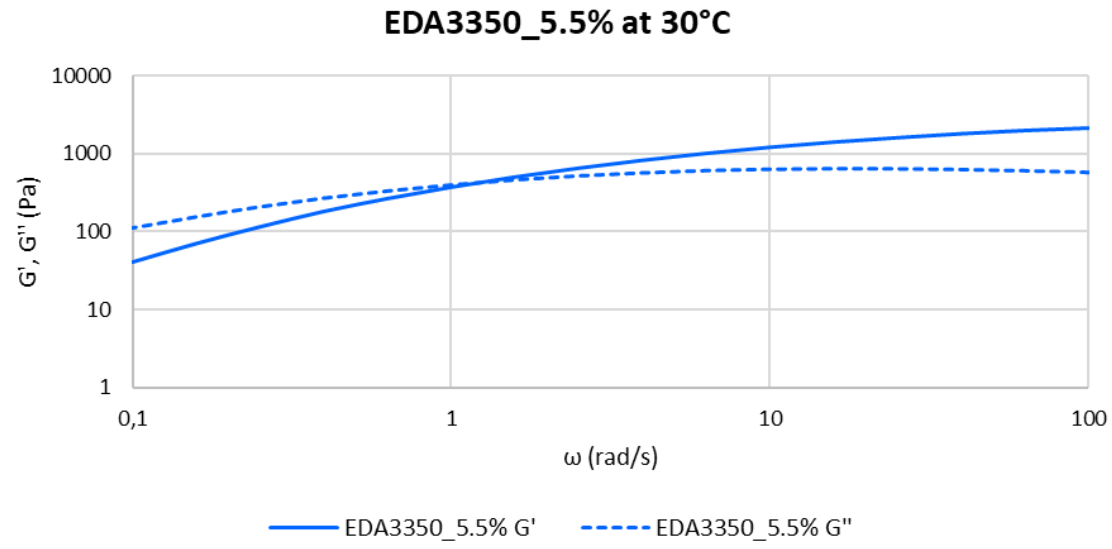

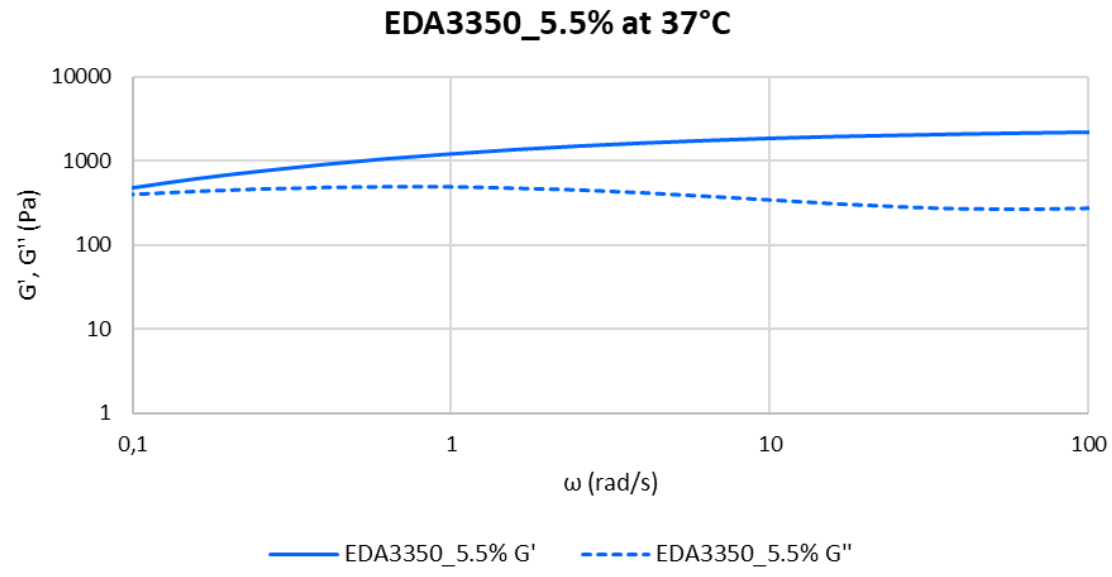

Figure 71: Frequency sweep test results for EDA3350_5.5% at three different temperatures (25, 30, 37°C).

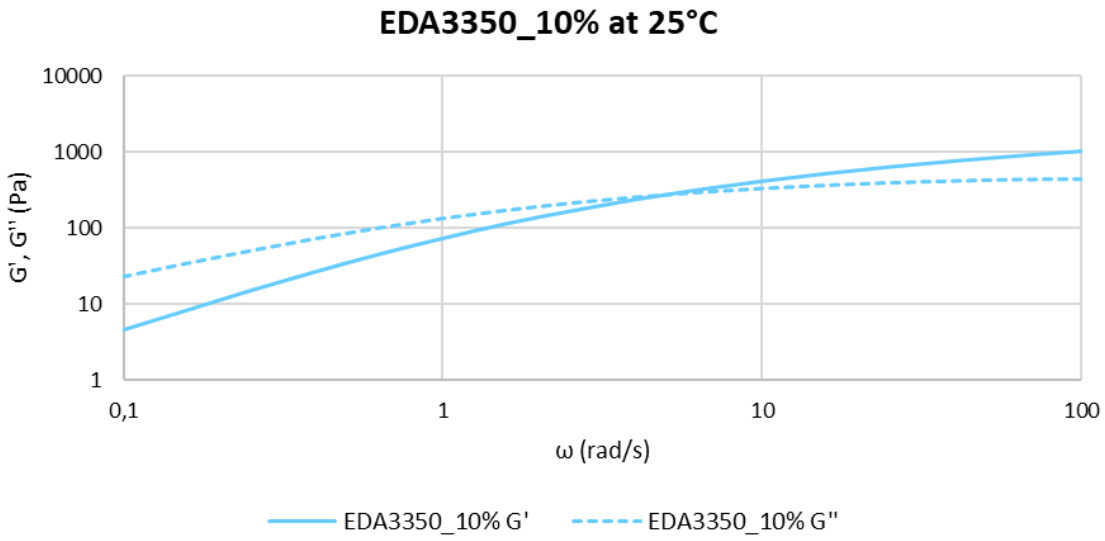

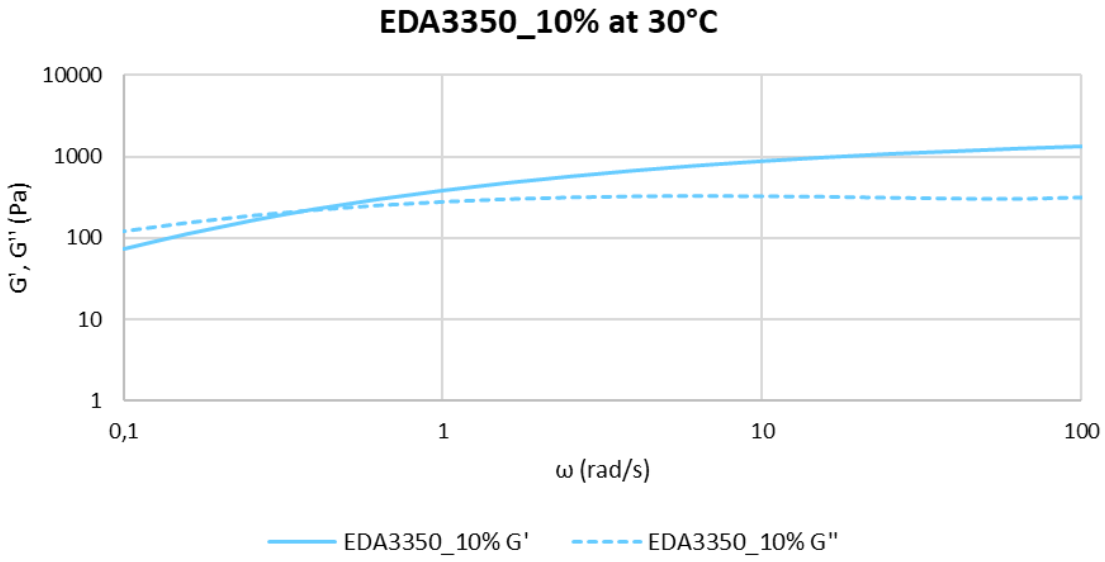

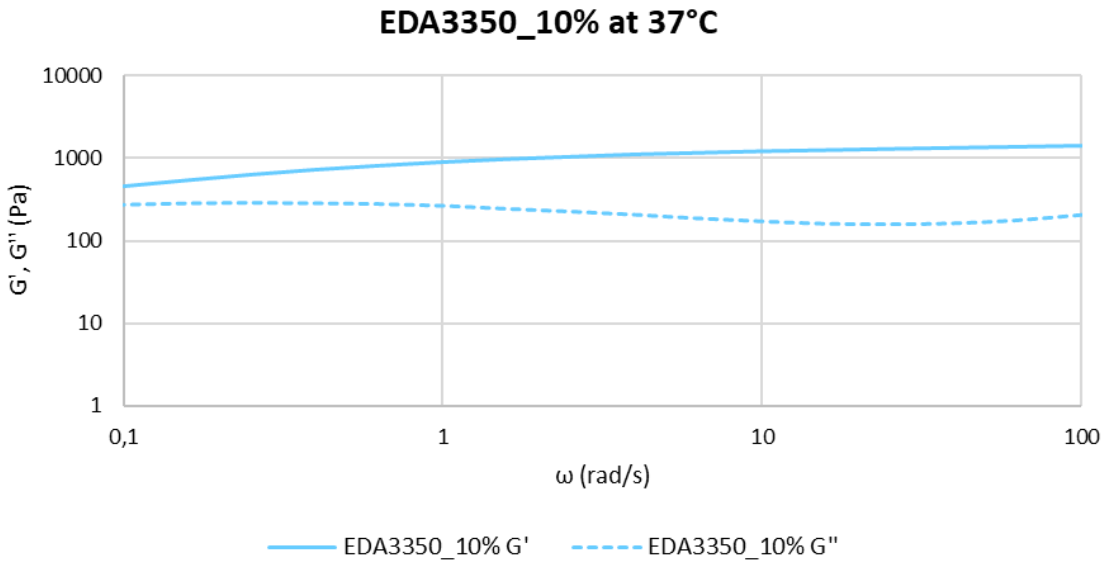

Figure 72: Frequency sweep test results for EDA3350_10% at three different temperatures (25, 30, 37°C).

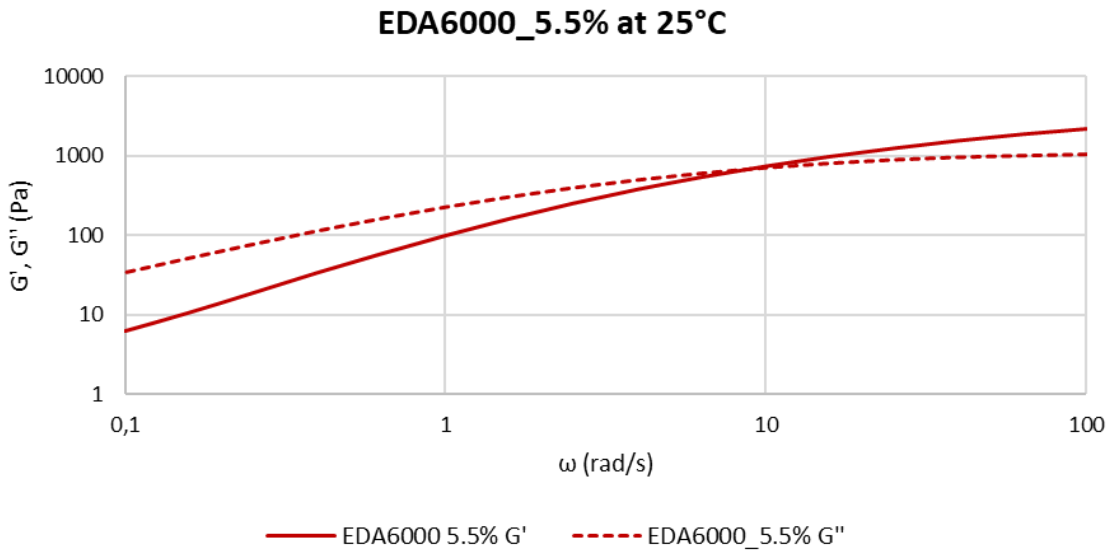

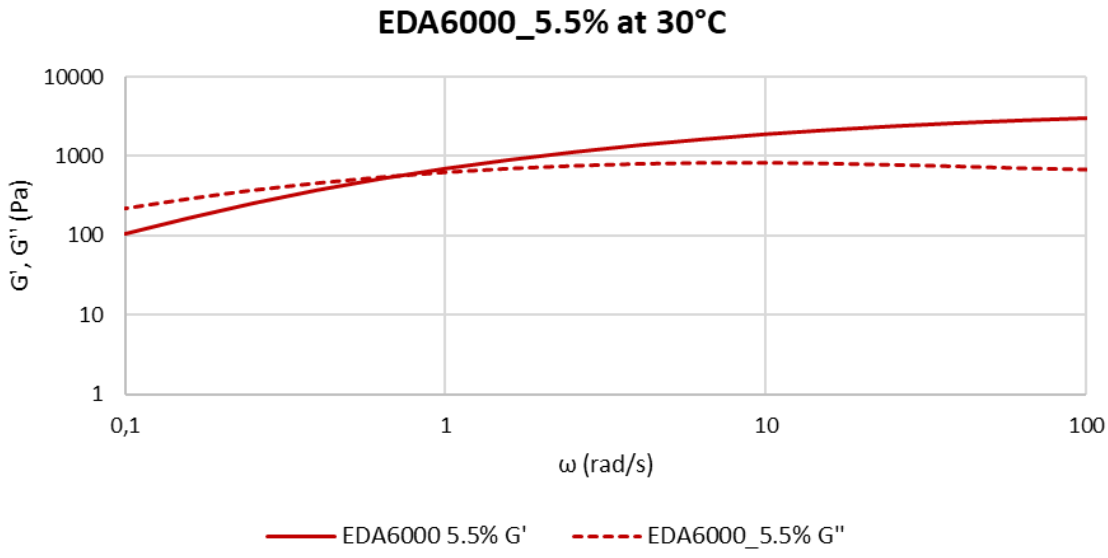

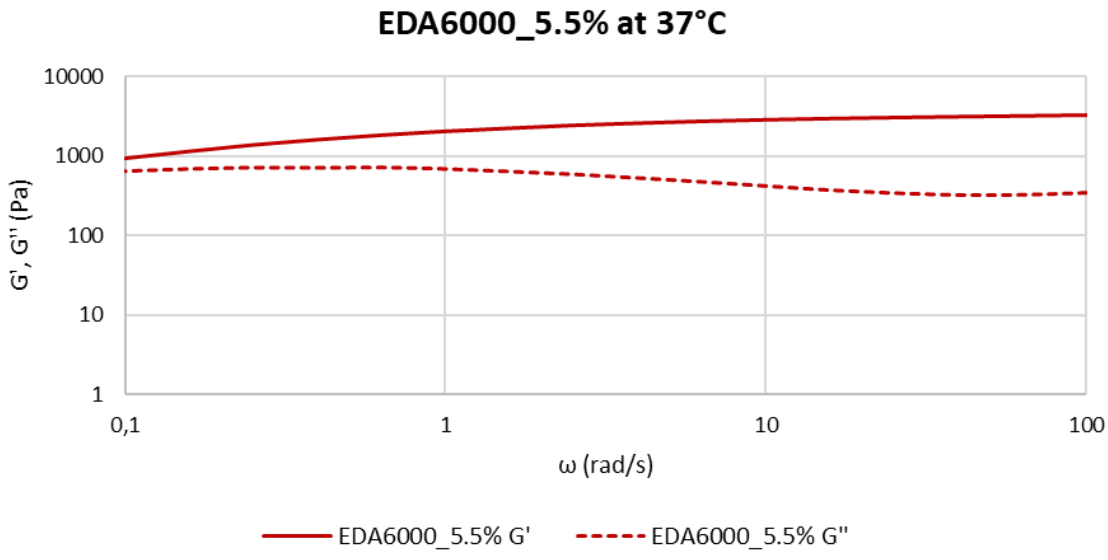

Figure 73: Frequency sweep test results for EDA6000_5.5% at three different temperatures (25, 30, 37°C).

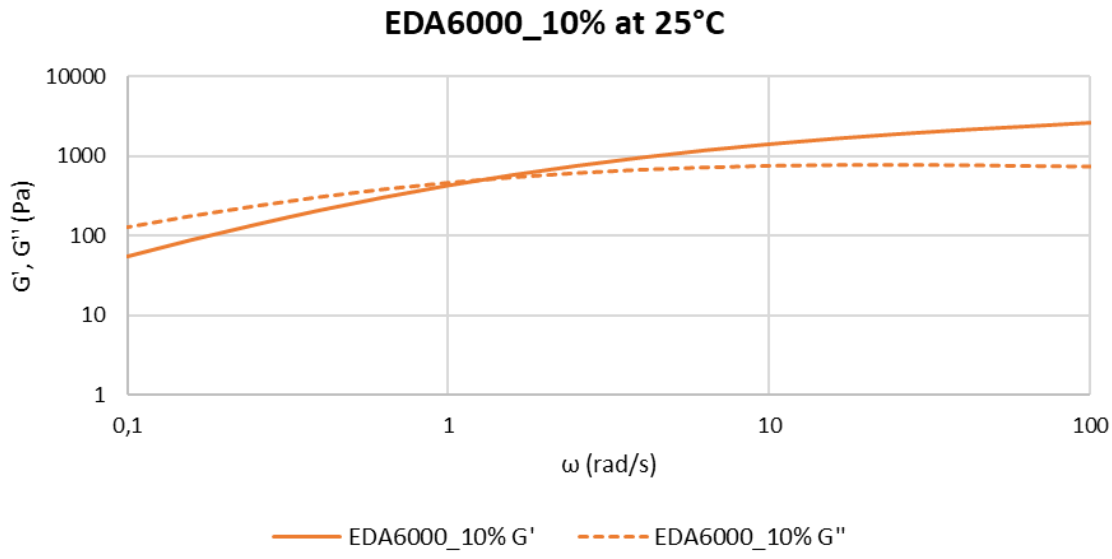

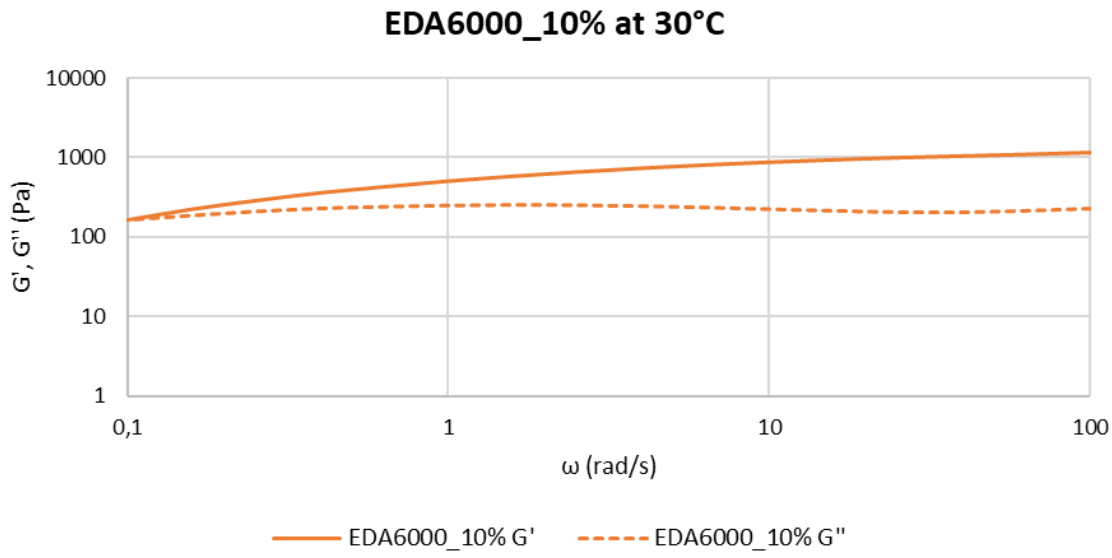

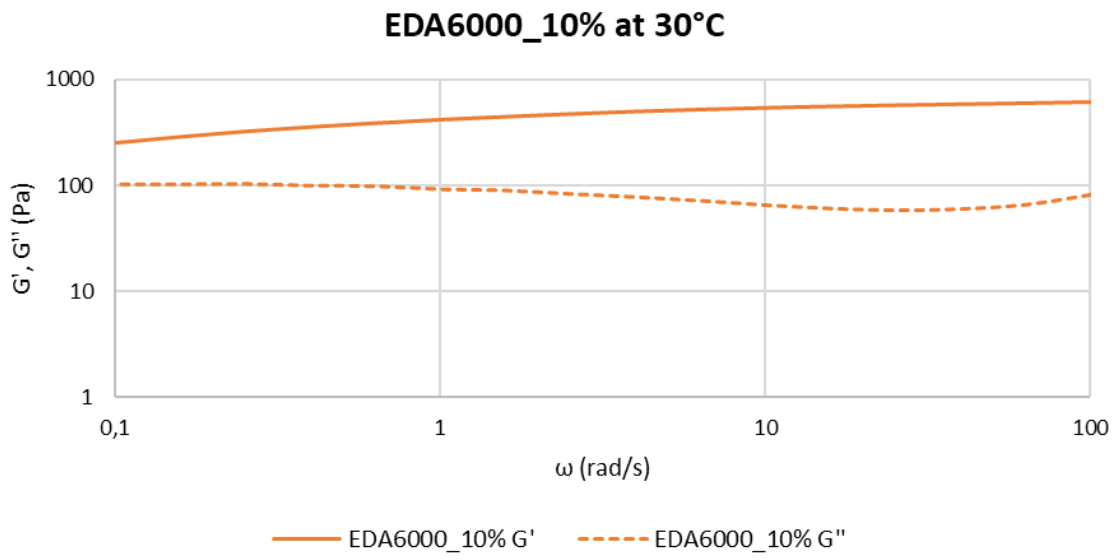

Figure 74: Frequency sweep test results for EDA6000_10% at three different temperatures (25, 30, 37°C).

3.7.3 Temperature ramp tests

The temperature-dependence of the sol-to-gel transition of the hydrogels was investigated through temperature ramp tests. This test is performed at constant frequency and allows to study the trend of viscosity as function of temperature. The measures were applied in the range 0-40°C and all the blends could be tested in this case. **Figure 75, 76** reports the temperature ramps obtained for blends based on PEGDA 3350 and PEGDA 6000, respectively.

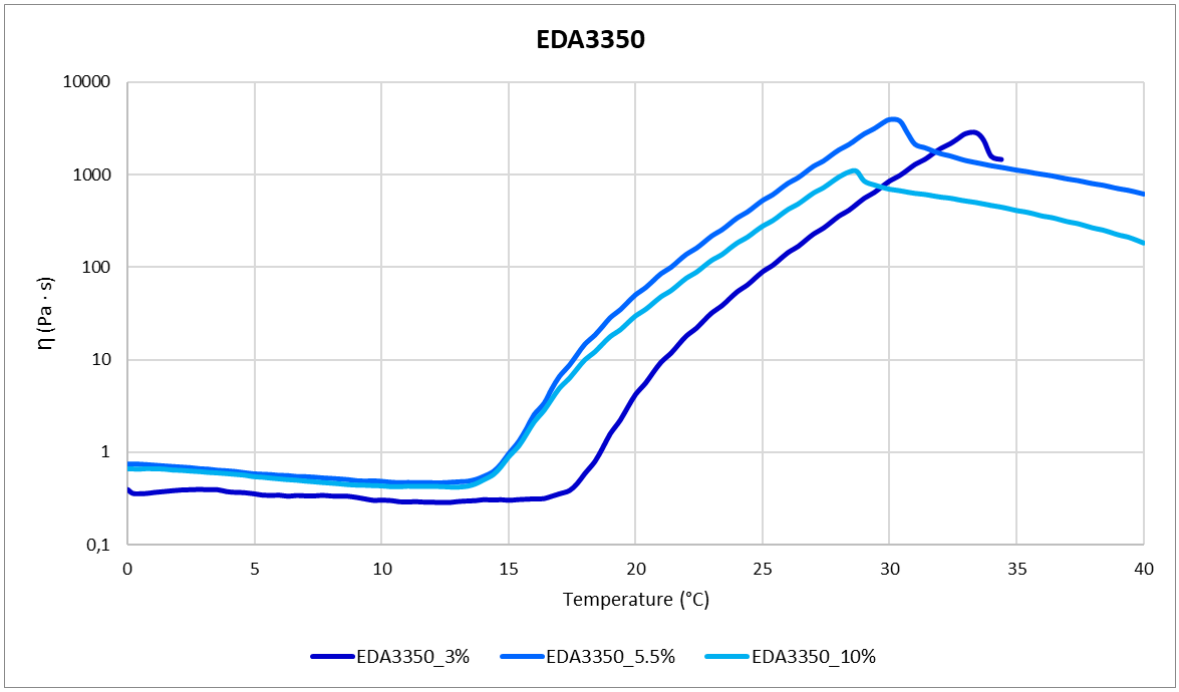

Figure 7516: Temperature ramp results in the temperature range between 0 and 40°C for the three PEGDA 3350 Da-based hydrogels.

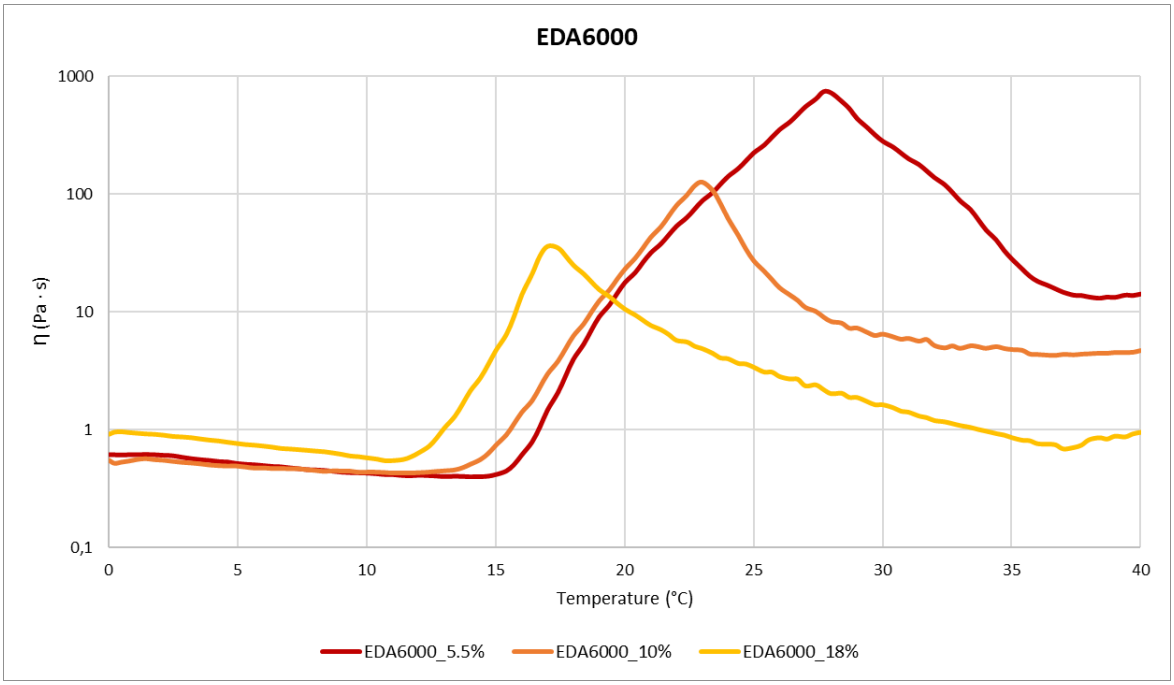

Figure 76: Temperature ramp results in the temperature range between 0 and 40°C for the three PEGDA 6000 Da-based hydrogels.

Both the blend sets have a similar behavior. From the starting value of viscosity at 0°C, the increase of temperature lead to a decrease of viscosity (physical behavior characteristic of fluids) until a minimum value is reached. Then, the viscosity increases to a maximum value. A phase of decrease follows the maximum value of viscosity and this means that the melt fracture phenomena occurred. In both the blend sets the increasing of concentration of PEGDA lead to an increasing of the initial value of storage modulus. This phenomenon is more emphasized at low concentration and it is supposed to concern the plasticizer effect of PEG that is often used as a plasticizer and has a known effect in decreasing the viscosity of polymeric solutions, such as PLA ([72], [73], [74]). The high hydrophilicity of PEG allows to rake a large amount of water molecules through the polymeric chains decreasing the friction phenomenon and then decreasing viscosity. This hypothesis was then confirmed by the study of the complex viscosity at 37°C.

The minimum value of viscosity identifies a characteristic temperature (T_{onset}) that define the starting point of sol-gel transition. The T_{onset} values of each blend formulation are reported in **Table 17**.

Table 17: T_{onset} of the blends.

	T_{onset} (°C)
EDA3350_3%	12.55
EDA3350_5.5%	12.2
EDA3350_10%	13
EDA6000_5.5%	14
EDA6000_10%	11
EDA6000_18%	10.7

From these results, it was observed that the increase of PEGDA concentration at both the molecular weights lead to a decrease of the T_{onset} value. This meant that the sol-gel transition starts earlier and this results are consisted to what was demonstrated in the previously illustrated tests. PEGDA 3350-based blends have T_{onset} values comprised in the same range (12-13 °C), as confirmed also by their similar gelation temperature. On the other hand, PEGDA 6000-based blends presented T_{onset} values more variable between the compositions. This is again representative of the different physical behavior of the three compositions, because as observed empirically the gelation process of these systems, especially EDA6000_10% and EDA6000_18%, were faster and occurred at lower temperature than the PEGDA 3350_based hydrogels.

12.10 Blend-based hydrogels photo-polymerization

Swelling and stability tests were performed on circular shaped photocured hydrogel disks (**Figure 77**) produced using a mold, as previously described. **Table** reposts the photocuring parameters.

Figure 77: Hydrogel disk sample.

Table 18: Photo-crosslinking parameters.

Photo-crosslinking Parameters	
Wavelength	365 nm
Intensity	10 mW/cm^2
Irradiation time	3 min
LAP	0.05 % w/v

In all the blend compositions that were investigated, a reaction of the hydrogel to the UV light exposure was empirically observed. The PEGDA chains dispersed in the polyurethane component (SHP407), in response to the UV light irradiation, bound together forming a PEG mesh that give to the hydrogel a higher stiffness valuable at the touch. The stiffness that the material gains depends on the PEGDA concentration and on the PEGDA molecular weight.

In both EDA3350 and EDA6000 a gradient of rigidity and compactness was observed at the increasing of the PEG concentration. This behaviour was theoretically justified by the increase of density of the PEGDA mesh that is formed thanks to UV irradiation, due to higher amount of PEGDA. In details, EDA3350_3% disks resulted to be very difficult to detach from the metallic mould without damage it because the material was too sticky and fragments of it remained adherent to the mould. EDA3350_5.5% hydrogel disks had quite similar behaviour to EDA3350_3%, because of the small difference in PEGDA concentration. EDA3350_10% hydrogel disks gave less problem during the detach phase from the mould and resulted to be the most rigid sample of this set.

The three EDA3350 blends hydrogel photocured disks results to be softer and more sticky compared to EDA6000 ones. The production of EDA6000 hydrogel samples resulted easier because the photocured material was less sticky and more compact and then easier to remove from the metallic mould. For EDA6000 hydrogel disks, a gradient in rigidity in function of PEGDA concentration was also observed. EDA6000_5.5% samples resulted to have a rigidity quite similar compared to EDA3350_10%. EDA6000_10% and EDA6000_18% photocured disks detached easily from the metallic mould, also without the use of a syringe

needle but only pushing them out through the circular mould. EDA6000_18% was the most rigid sample compared to all the others.

It is possible to state, in conclusion, that a higher PEGDA concentration and PEGDA molecule weigh lead to a higher stiffness of the material.

3.8 Photo-rheological characterization

The kinetics of gel photopolymerization for the blend formulations following the exposure at UV light was evaluated with photo-rheological analyses. The graphs in **Figure 78** and **Figure 79** report the trend of storage modulus as function of time for blends based on PEGDA 3350 and PEGDA 6000, respectively. All the sample underwent an initial phase of equilibration at 37°C for 60 seconds, then UV light irradiation for 90 seconds and then storage modulus (G') values were recorded for 60 seconds after the irradiation was stopped.

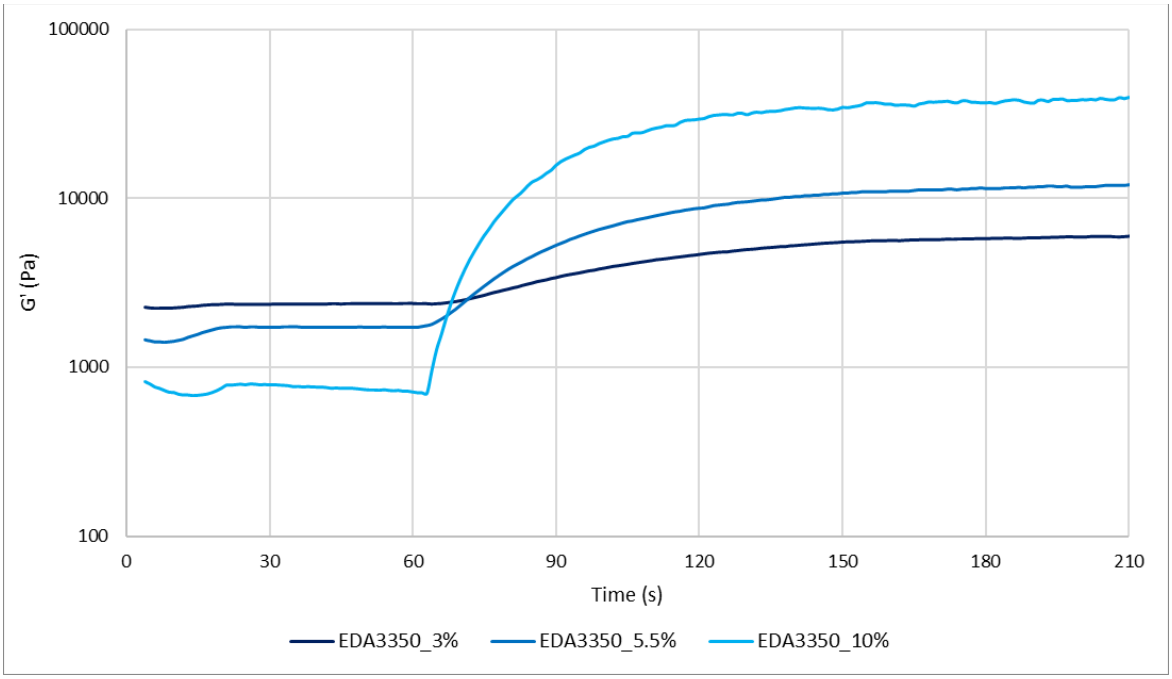

Figure 78: Storage moduli (G') over time for PEGDA3350-based blend sol-gel systems.

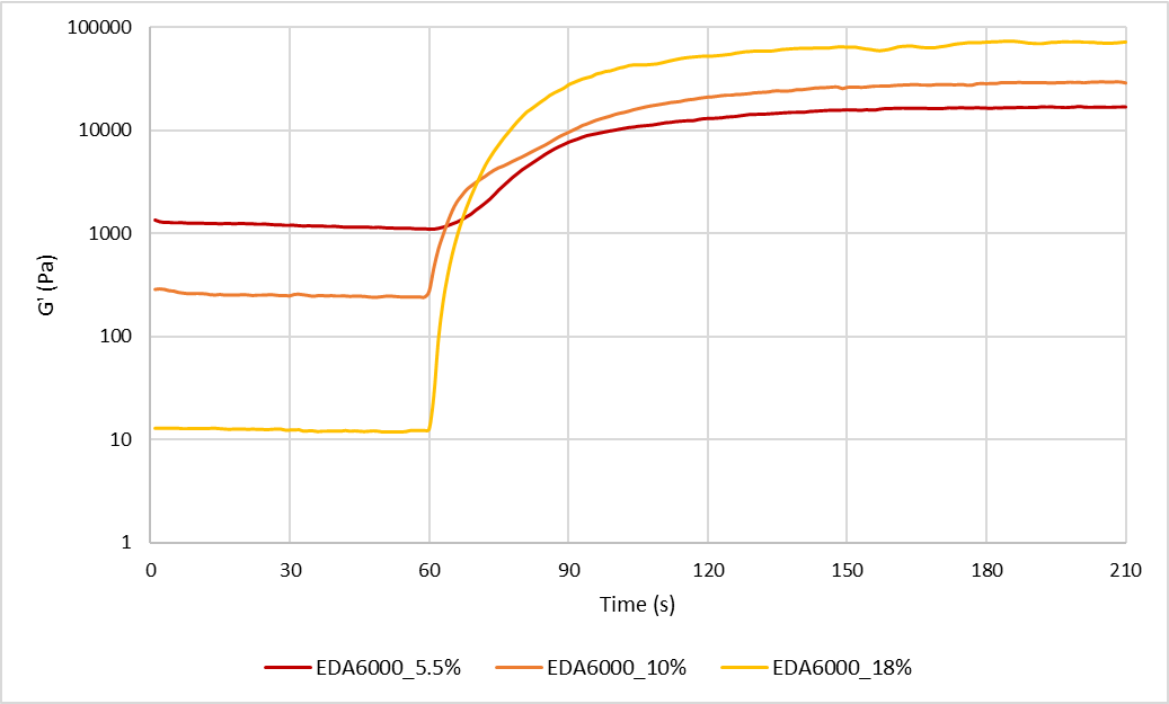

Figure 7917: Storage moduli (G') over time for PEGDA6000-based blend sol-gel systems.

Both of the blend sets have similar behavior, with some differences in the efficiency and speed of the photocuring process and in the final G' value consequent to crosslinking. In the first phase, G' has an approximately constant value, indicating the quiescent state of the sample that was not undergoing a transition. After the UV lamp is switched on (60s), it is noticeable a sudden increase of G' value, denoting that the cross-linking was taking place. Finally, the values of the storage moduli remained constant after switching off the UV lamp (150s), setting a plateau that defined the final value of G' after photocuring. It is possible to observe that EDA3350_10% and EDA6000_18% reached the maximum G' value before the end of the irradiation process, indicating that their crosslinking process is completed in a shorter time than what was set for the test. Indeed, the slope of the curves relative to these two samples is noticeably sharper than what found for the other systems.

ΔG' were also calculated for each blend formulation, as the difference of the G' value at the end (150 s) and at the beginning (60 s) of the photocuring process, respectively. The results are reported in **Table 19**.

Table 19: ΔG' of each blend formulation.

	ΔG' (kPa)
EDA3350_3%	3.13
EDA3350_5.5%	9.16
EDA3350_10%	16.68
EDA6000_5.5%	14.79
EDA6000_10%	16.68
EDA6000_18%	69.01

From the ΔG' values, it was generally observed that raising the PEGDA concentration lead to a more efficient process of photo-crosslinking, with an increase in the G' values significantly higher for the two more concentrated systems. ΔG' values are indeed related to the efficiency of the photocuring process, since the reaction of the acrylate moieties responsible of the cross-linking creates a stiffer structure and results in an increase in the storage modulus values.

To better explain what was observed, **Table 20** reports the values of G' before and after photocuring.

Table 20: Storage modulus of blends formulations before and after photocuring.

	G' Before photocuring (Pa)	G' After photocuring (Pa)
EDA3350_3%	2380	5970
EDA3350_5.5%	1720	12000
EDA3350_10%	750	38300
EDA6000_5.5%	1130	16900
EDA6000_10%	53	28900
EDA6000_18%	12	72500

From the curves reported in **Figure 78** and **Figure 79**, the G' values before the photocuring process are lower the higher the concentration of PEGDA, regardless of its molecular weight. However, after photocuring process this order is inverted and the higher G' values are generally obtained for the more concentrated systems. This can be explained considering that before photocuring the plasticizer effect of PEGDA is prevalent, resulting

in lower viscosity values (although the gels appeared visually denser). After photocuring, the PEGDA chains are permanently cross-linked and the efficiency of this process is strongly dependent on the probability that the acrylate groups at the end of the chains meet and react. Evidently, the probability is higher when the amount of chains is higher, so that a more concentrated system should crosslink more. Moreover, for systems with the same concentration, the presence of a PEGDA with a lower molecular weight was expected to present a higher grade of crosslinking, because the amount of chains is higher (i.e., for PEGDA 3350- and PEGDA 6000-based systems at the same concentration, the former has almost a 2-fold number of chains). The number of chains is indeed directly correlated to the number of acrylate groups, since it was demonstrated that the degree of substitution was approximately the same for the two PEGDAs and therefore should be a valid indication of the capability of the systems to create a crosslinked mesh.

However, the effect observed in this case appears to be opposite. A possible explanation could be found in the presence of the polyurethane micelles. As a matter of fact, the photo-crosslinking process occurred when these systems were already in a gel or semi-gel state, with micelles already formed and, in some case, packed. For this reason, despite being present in a higher amount, the shorter PEGDA 3350 chains have a lower probability to be in the right conformation to permit a bond, so that the mesh formed is less homogeneous than PEGDA 6000 and presents some defects, resulting in lower mechanical strength (e.g. lower G' values) and lower cross-linking efficiency (e.g. lower ΔG' values).

Contrary to what was previously said, from **Table 21**, the G' value for EDA3350_10% after photopolymerization (38,3 KPa) is higher than the one observed for EDA6000_10% (28,9 KPa). Munoz-Pinto and colleagues observed a similar behavior with PEGDA gels at the same concentration and different molecular weights. However, they explained that the trend followed by the modulus-mesh size (correlated to concentration) curves for PEGDA at different molecular weight (i.e. 3.4 KDa and 6 KDa) follow a common trendline and are not statistically distinguishable [75]. It is also possible that in this case the PEGDA concentration is sufficiently high for PEGDA 3350 chains to form a more regular mesh and therefore create a stronger gel than in the other cases. This behavior was also observed in another literature work, in which no significant difference in gel stiffness was found for PEGDA at comparable

molecular weights to those analyzed in this work (3000 and 5000 Da) at a 10% w/v concentration [76].

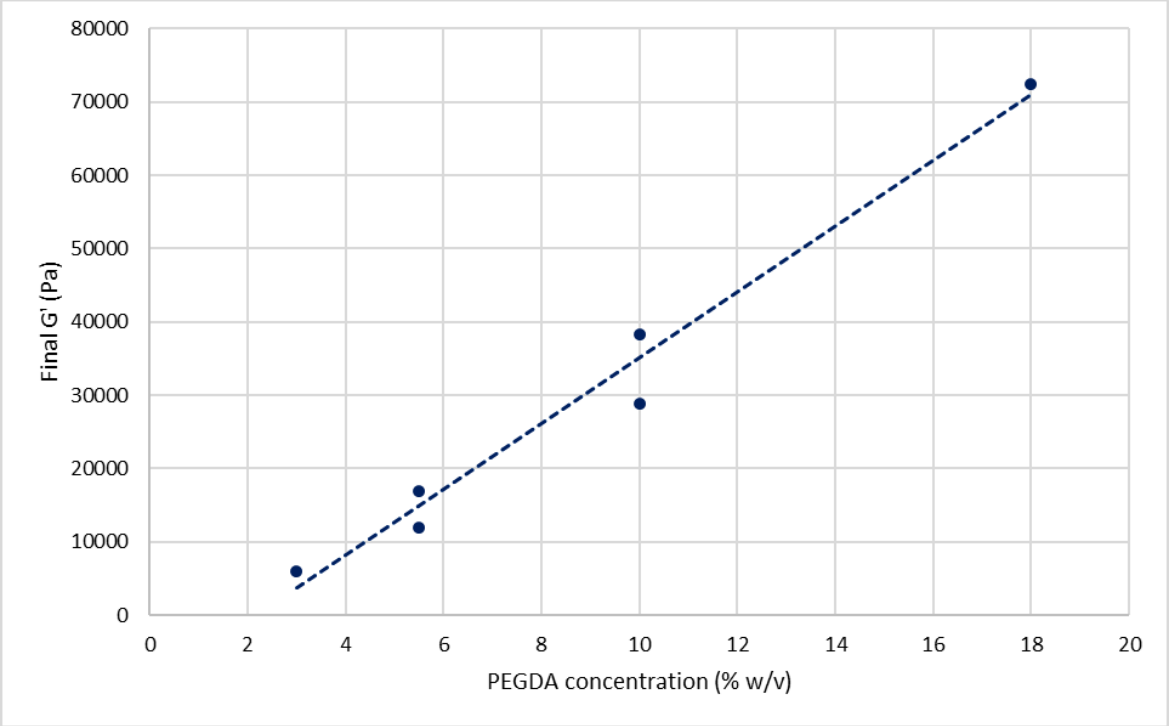

Figure 8018: Storage modulus after photocuring in function of PEGDA concentration for all the blends.

3.9 Swelling and stability in physiological conditions

Swelling and stability tests were performed on the circular shaped samples prepared as previously described. These tests were performed to evaluate their behavior in terms of stability in aqueous environment and their ability to absorb the surrounding medium (i.e. PBS, pH 7.4). In this case, the aim was to assess the effect of the network formed by PEGDAs at different molecular weights on the ability of the hydrogels to swell and remain stable for relatively long period of times.

The results relative to the swelling behavior in terms of PBS absorption of all the tested blends are reported in **Figure 81** and **Figure 82**. In addition, the swelling ratio was calculated for all the formulation (**Table 22**), as explained before.

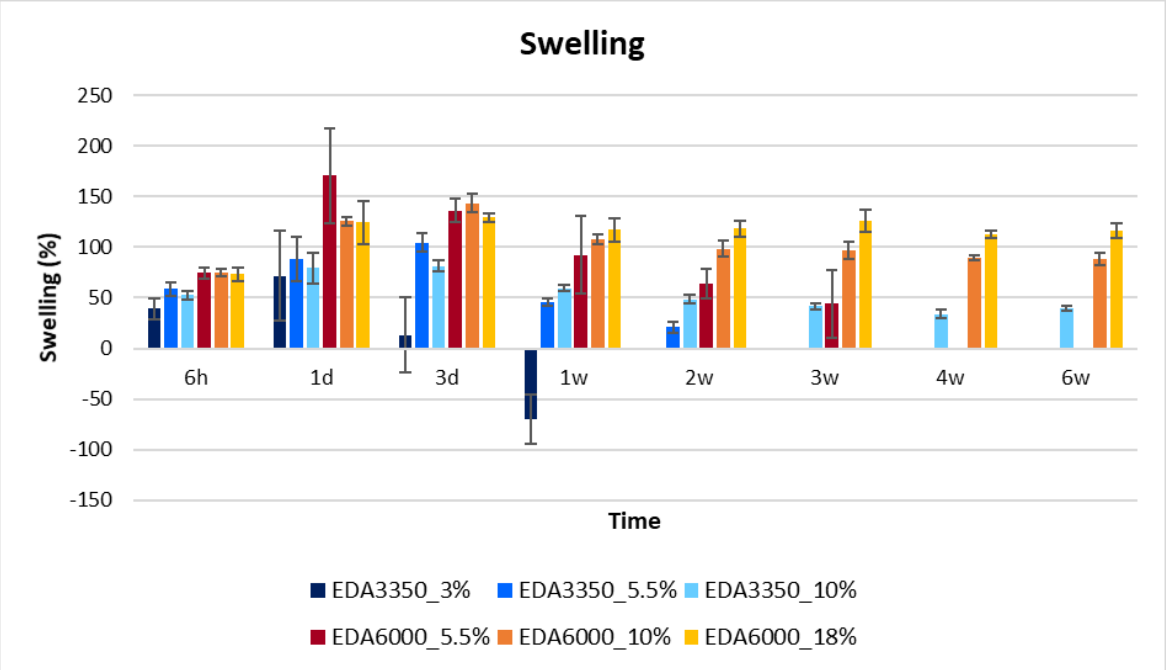

Figure 81: Results of swelling tests for all the blends at different time steps from 6h to 6 weeks.

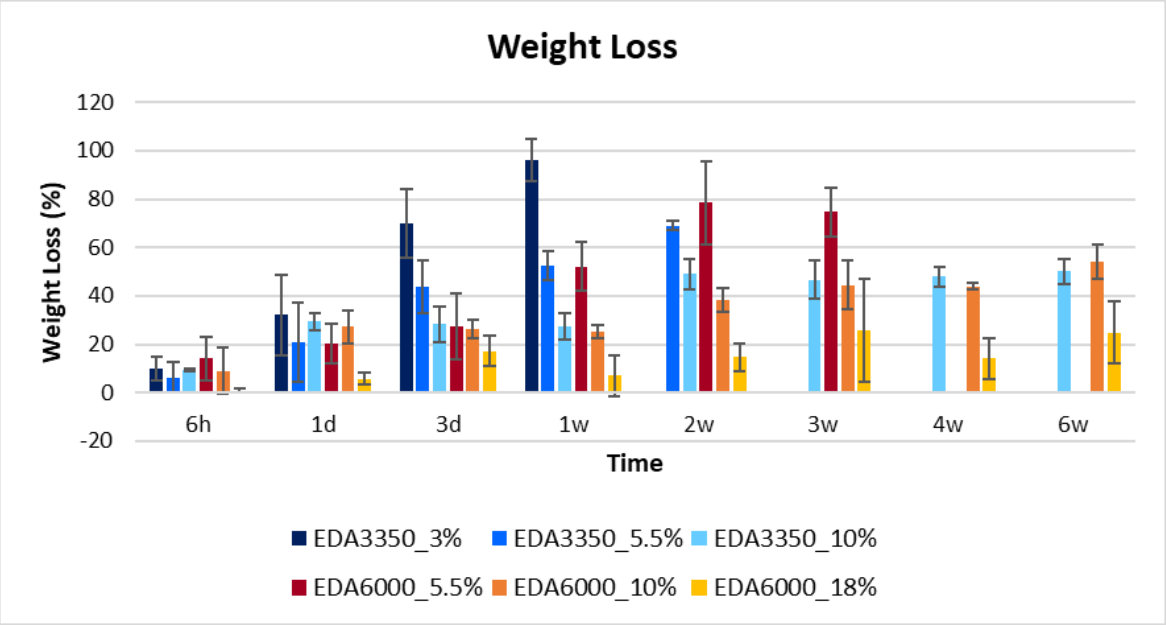

Figure 82: Results of weight loss tests for all the blends at different time steps from 6h to 6 weeks.

In the first 6 hours after the addiction of the PBS solutions above the hydrogels, the systems based on PEGDA 3350 Da presented an increase in volume in the range 40-60%. In the next 24h time step, the dissolution phase started to be prevalent, while for EDA6000 systems the swelling continued to rise. After 3 days, the dissolution phenomena started to prevail on the swelling for all the formulations and the rate was generally faster for EDA3350

blends. For EDA3350_3%, negative swelling values are reached between 3 days and 1 week, after which its dissolution into the PBS solution is completed. A similar behaviour, but shifted in time, is observed for the other systems (EDA3350_5.5% and EDA6000_5.5%).

The blends based on PEGDA 6000 presented higher swelling values in the first hours compared to PEGDA 3350 (around 75%). Although the behaviour is similar to what observed for PEGDA 3350, PEGDA6000-based systems generally presented a slower dissolution rate. Indeed, while only EDA3350_10% samples were still present after 6 weeks of incubation, two formulations containing PEGDA 6000 (EDA6000_10% and EDA6000_18%) resulted almost intact at this final time point (**Figure 83**) It was then assumed that these three systems are stable over 6 weeks.

Figure 83: From left to right, EDA3350_10%, EDA6000_10%, EDA6000_18% hydrogel disk at the end of the 6 weeks time step.

Thus, it was generally observed that the systems based on PEGDA 6000 are characterized by longer stability than PEGDA 3350 ones. These results are contrary to what was expected, since it was initially believed that using a PEGDA with higher molecular weight would have produced a network with a larger mesh size, leading to a faster release of the polyurethane component and therefore a quicker dissolution of the sample. In the following paragraphs, an explanation of these results will be suggested, based on the comparison between the blends previously explained.

13.9.1 Comparison based on the same PEGDA molecular weight

The following figures report the results of swelling (**Figures 84**, **85)**, and weight loss **(Figure 86, 87**), comparing the formulations that contain PEGDA with the same molecular weight (3350 or 6000 Da) but with different PEGDA concentrations.

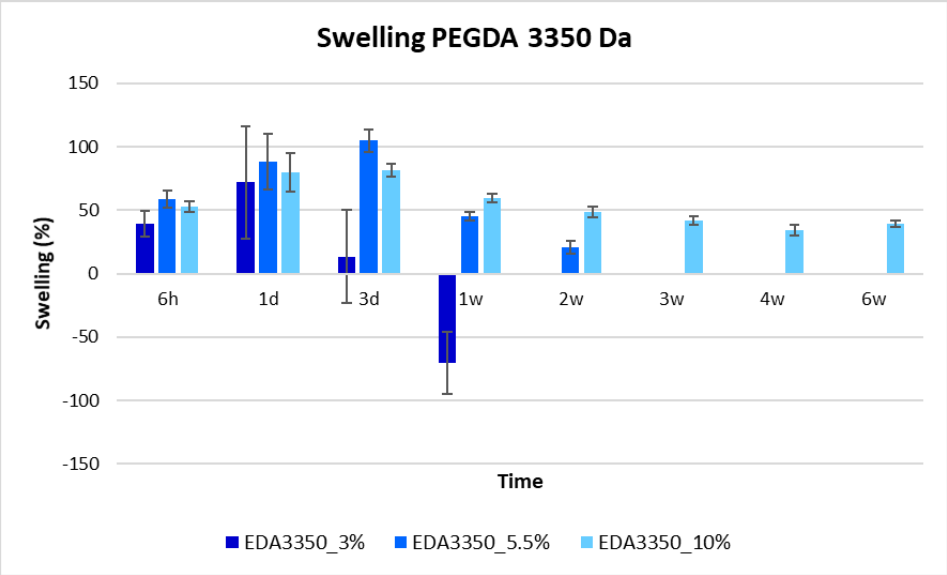

Figure 84: Swelling results relative to the blends based on PEGDA 3350 Da.

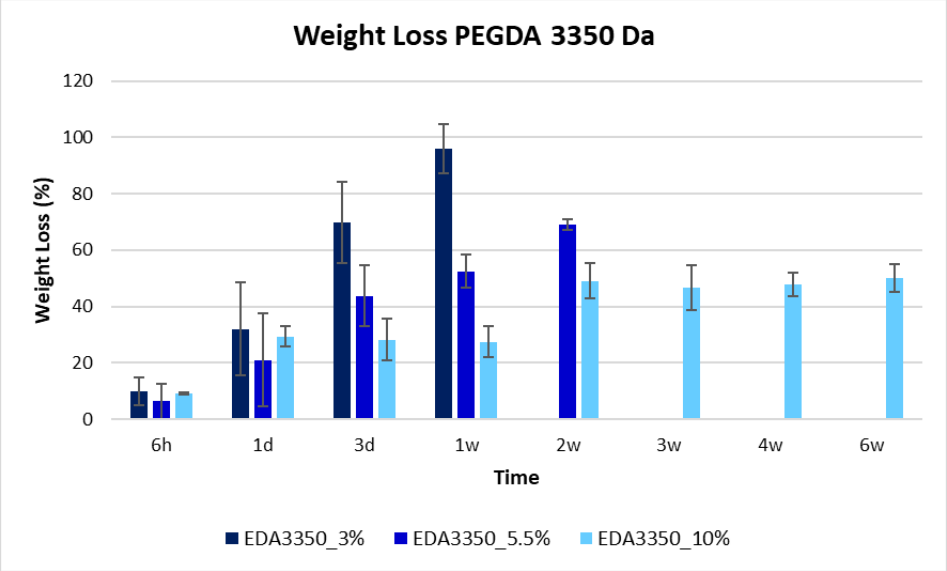

Figure 8519: Weight loss results relative to the blends based on PEGDA 3350 Da.

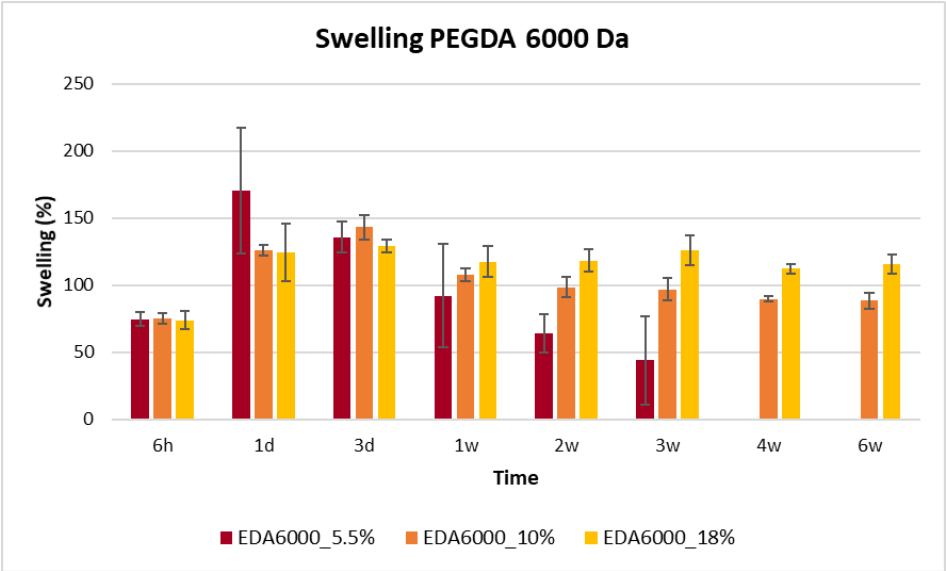

Figure 86: Swelling results relative to the blends based on PEGDA 6000 Da.

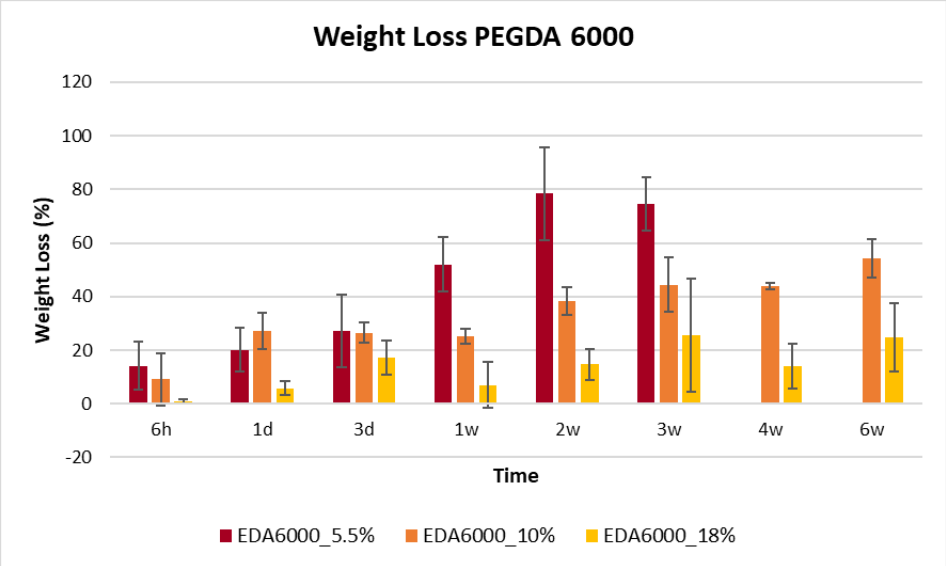

Figure 87: Weight loss results relative to the blends based on PEGDA 6000 Da.

As previously observed, for both EDA3350 and EDA6000 systems an increase of PEGDA concentration lead to better stability, with longer residence time the higher the PEGDA concentration. A possible explanation of this fact is that a higher density of PEGDA chains caused the formation of a more entangled mesh, with a higher amount of cross-linking points. As a consequence, the ability to absorb the surrounding fluids should be reduced for the more concentrated systems. Although not apparently evident from the swelling results, this is confirmed when the swelling ratio is calculated as previously noted (**Table 22**). The swelling ratio, calculated at the 24h time point as a comparison between all the systems, decreased for both PEGDA 3350 and PEGDA 6000 when the concentration was

increased, confirming the results found in other literature works ([45], [77]). This hypothesis of a higher crosslinking density is also consistent to what was found in the photo-rheological characterization. Indeed, a more pronounced increase in the storage modulus (G') was observed after photocuring for the more concentrated formulations.

Table 22: Swelling ratio of blend formulations

PEGDA Molecular Weight	Concentration (% w/v)	Swelling Ratio
3350 Da	3	14.59
	5.5	14.00
	10	9.97
6000 Da	5.5	18.21
	10	12.64
	18	8.79

3.9.2 Comparison based on the same PU-PEGDA molar ratio

For this comparison, the blend systems were coupled as follows: EDA3350_3% and EDA6000_5.5%, EDA3350_5.5% and EDA6000_10%; EDA3350_10% and EDA6000_18%.

Figures 88, **89** and **90**, **91** and **92, 93** reports the results of swelling and weight loss, comparing the blends divided as previously mentioned.

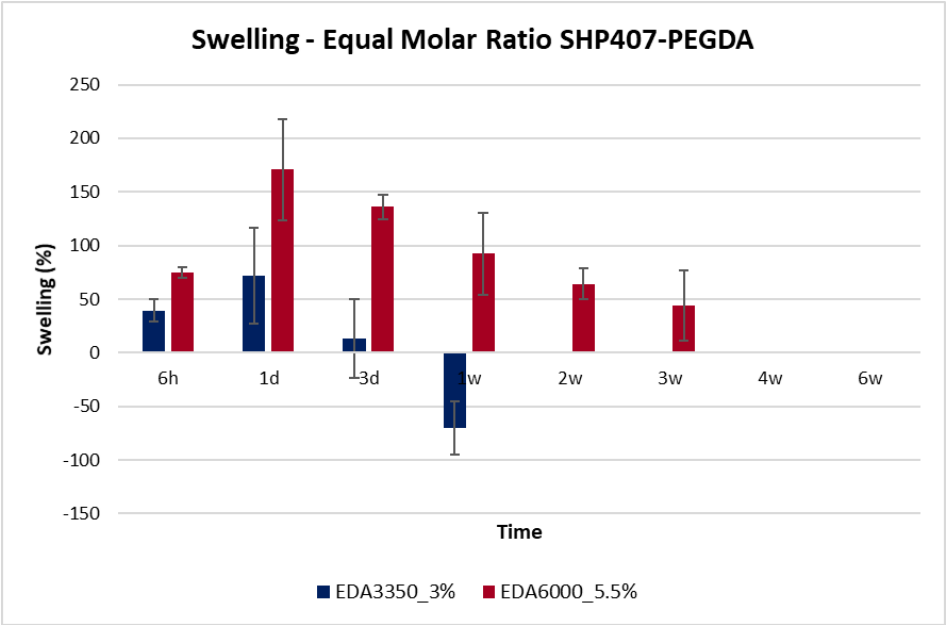

Figure 88: Swelling relative to equal molar ratio comparison.

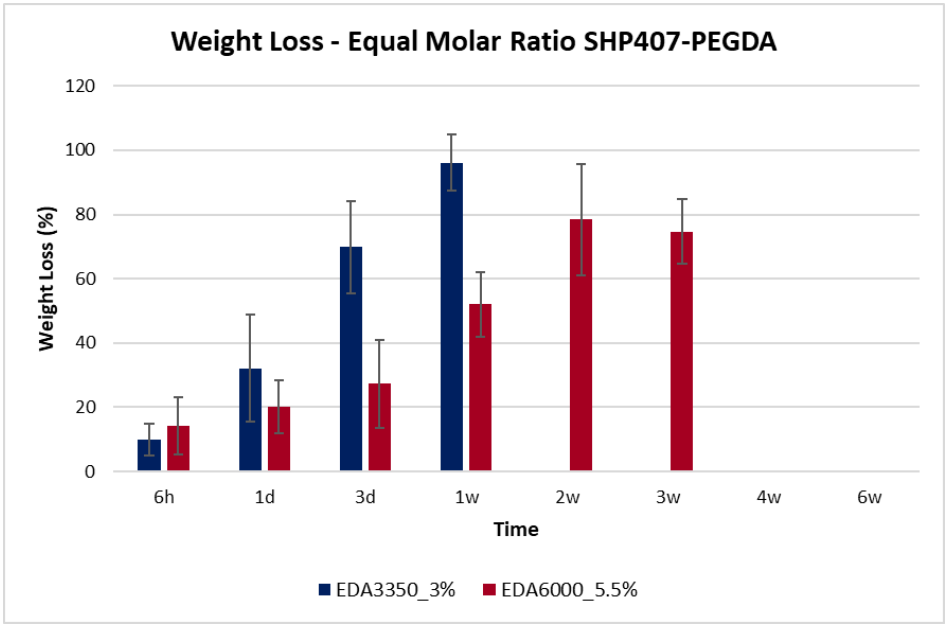

Figure 89: Weight loss relative to equal molar ratio comparison.

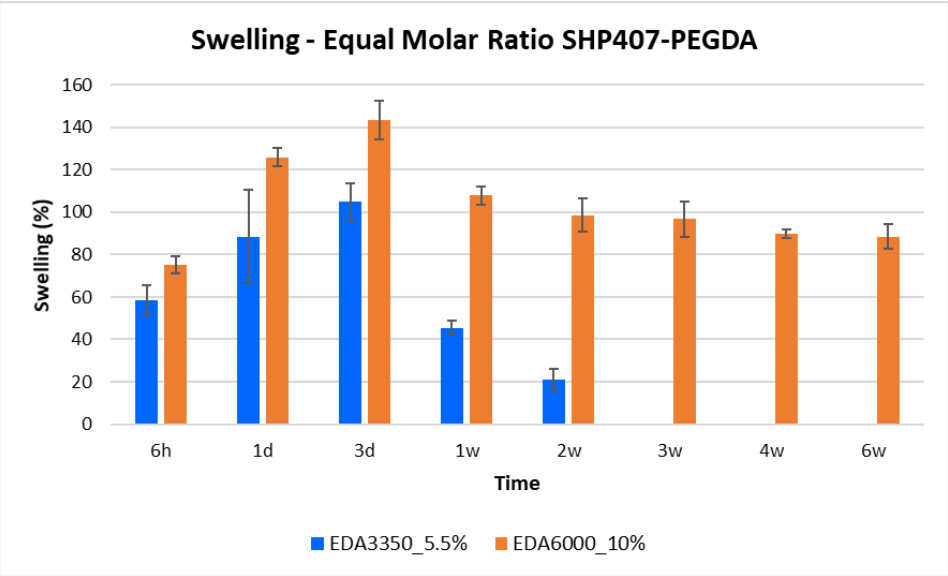

Figure 90: Swelling relative to equal molar ratio comparison.

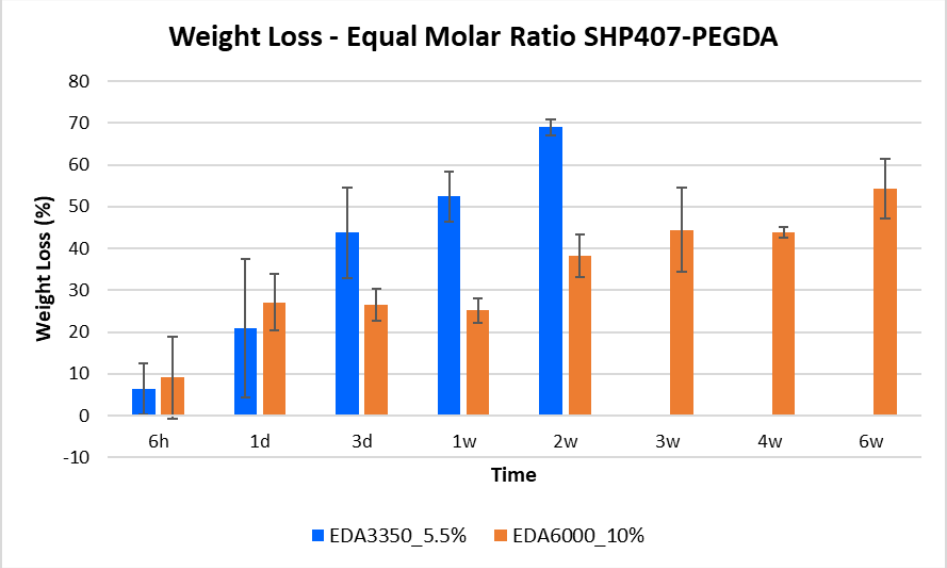

Figure 9120: Weight loss relative to equal molar ratio comparison.

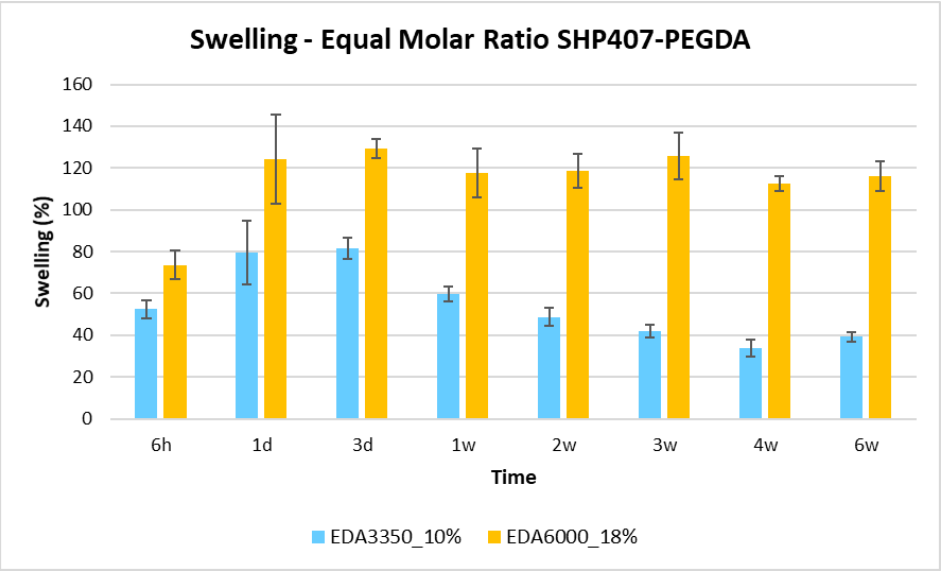

Figure 92: Swelling relative to equal molar ratio comparison.

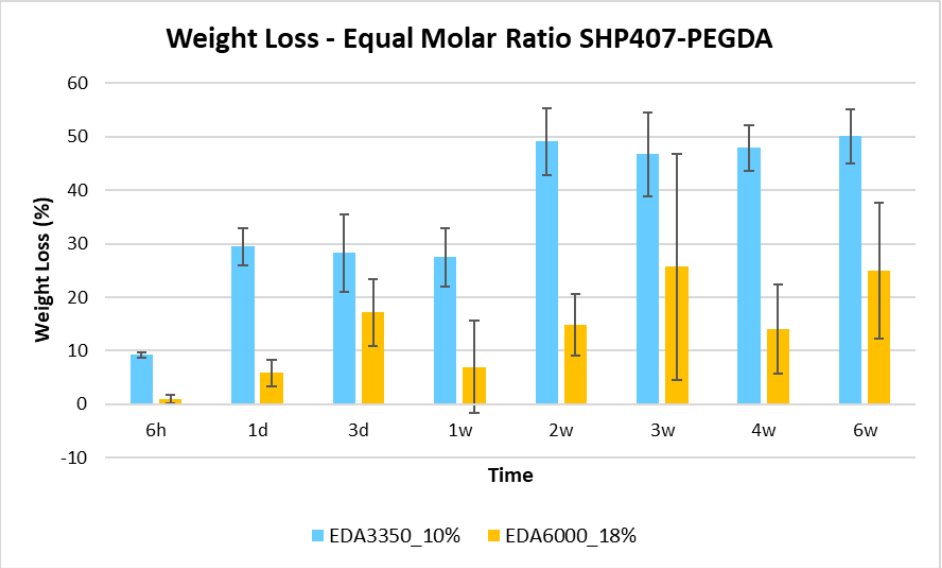

Figure 93: Weight loss relative to equal molar ratio comparison.

From these representations, it appeared evident that, contrary to what was expected from literature [45], the higher PEGDA molecular weight did not involve a faster dissolution rate. A faster dissolution rate for PEGDA 6000-based systems was suggested because of the presence of longer PEG chains, that should have led to higher water absorption and a consequent faster release and dissolutions of the PU component, linked to the larger mesh size. However, for all the samples the opposite was observed.

A possible justification of this behaviour can be found in the different efficiency of the photo-crosslinking process. As already explained for the behaviour observed during the

photo-rheological characterization, the presence of the micelles formed by SHP407 creates an obstacle for the formation of the PEGDA network. PEGDA 6000 chains, however, are longer enough to better overcome this hindrance, forming a more homogenous network, while PEGDA 3350 forms a reticule that presents more defects. As a consequence, the PU component is facilitated in being expelled from the PEGDA 3350 network, affecting the residence time of the samples. After all the polyurethane is expelled, the structure is not strong enough to resist and tends to collapse, resulting in the dissolution of the sample. In case of EDA3350_10%, however, it is possible that the effect of the PEGDA concentration previously mentioned starts to be prevalent and therefore this formulation showed a residence time comparable to the more stable PEGDA 6000 systems.

Figure 94 schematically represents the differences in the network formed by PEGDA 3350 and PEGDA 6000.

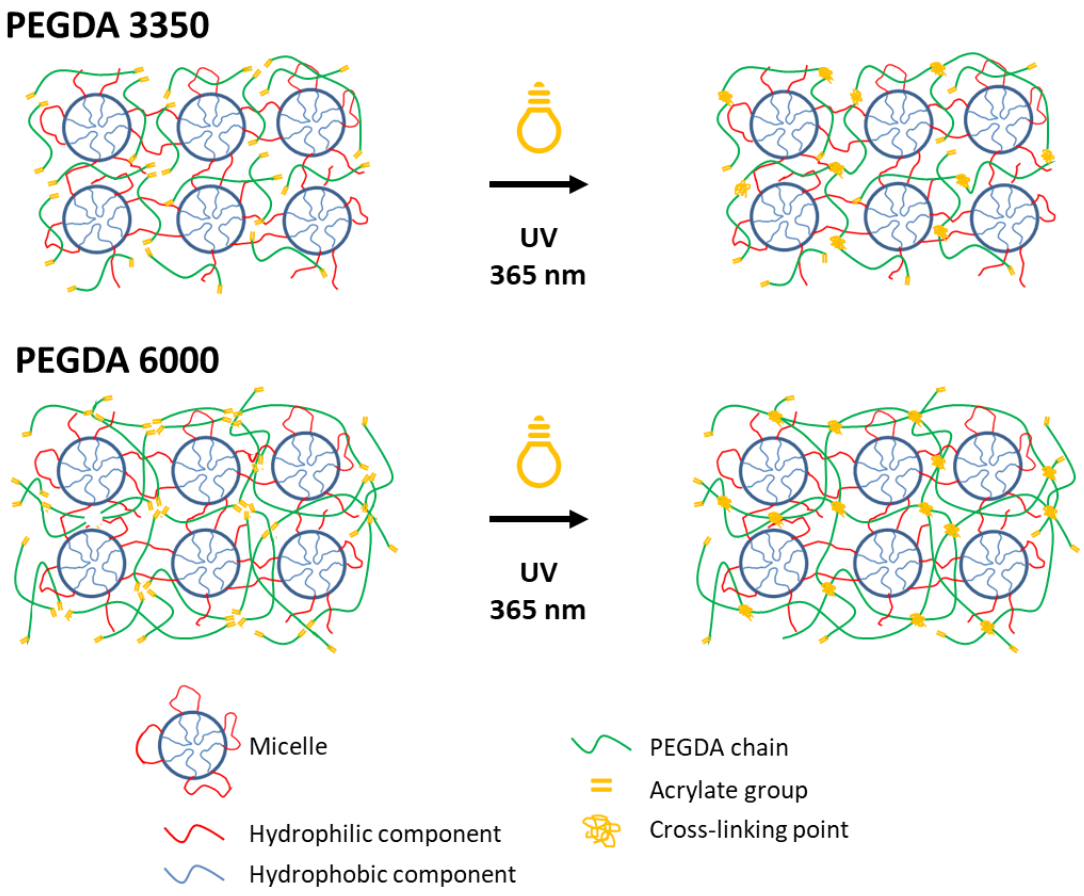

Figure 94: Different behaviour in the PEGDA network formation as a result of UV irradiation for PEGDA 3350 Da and PEGDA 6000 Da (credit: Arianna Grivet Brancot).

3.9.3 Comparison based on the same PEGDA concentration

The comparison between the systems that present the same PEGDA concentration but with different molecular weight confirmed the observation presented before (**Figure 95**, **96** and **97**, **98)**.

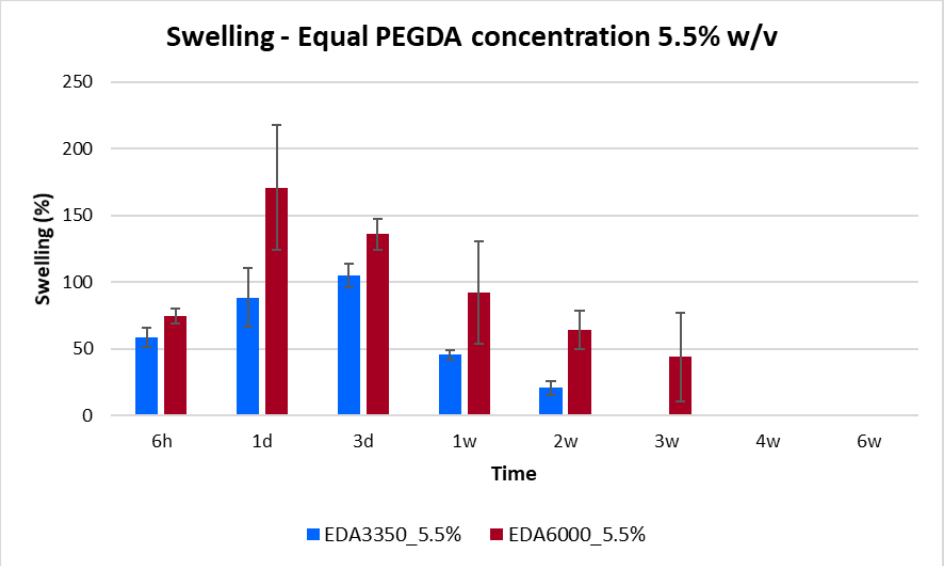

Figure 95:

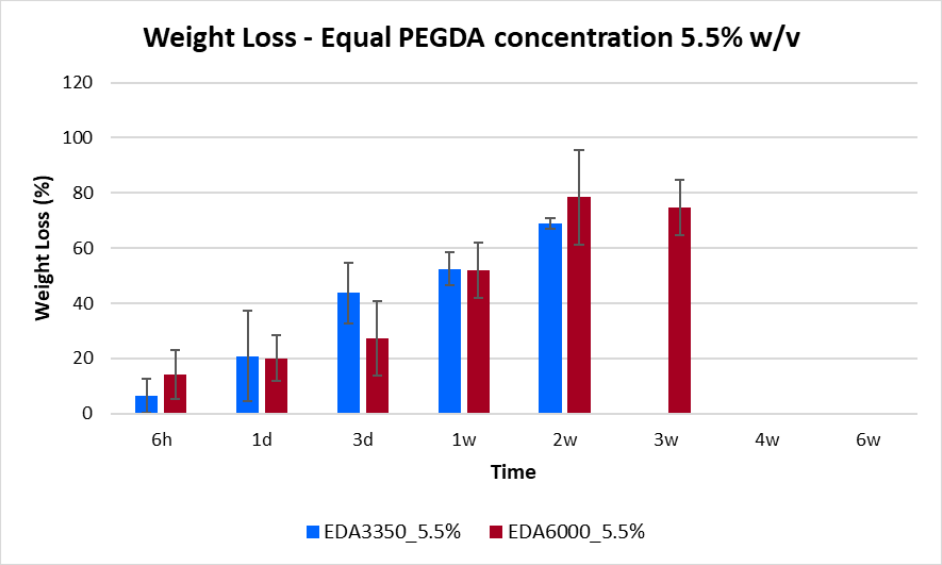

Figure 9621:

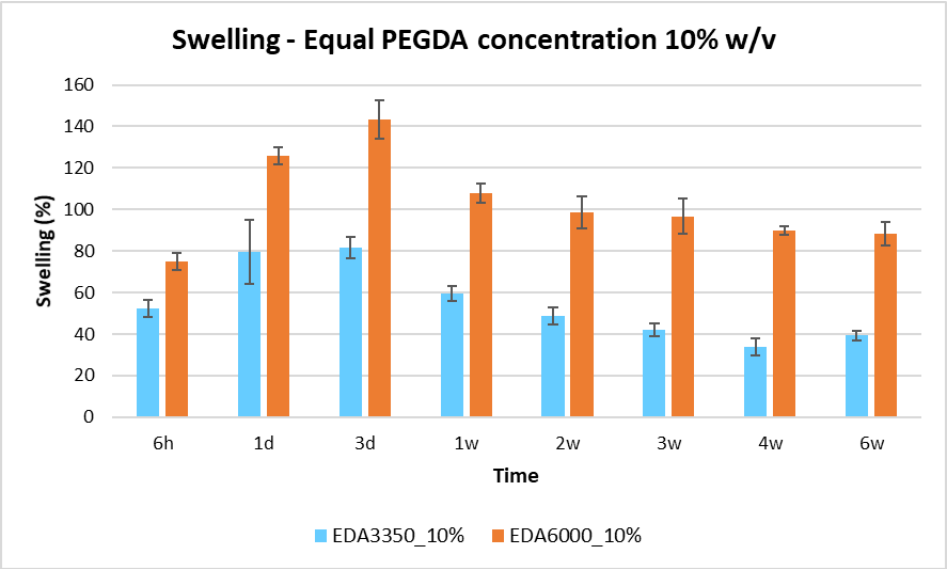

Figure 97:

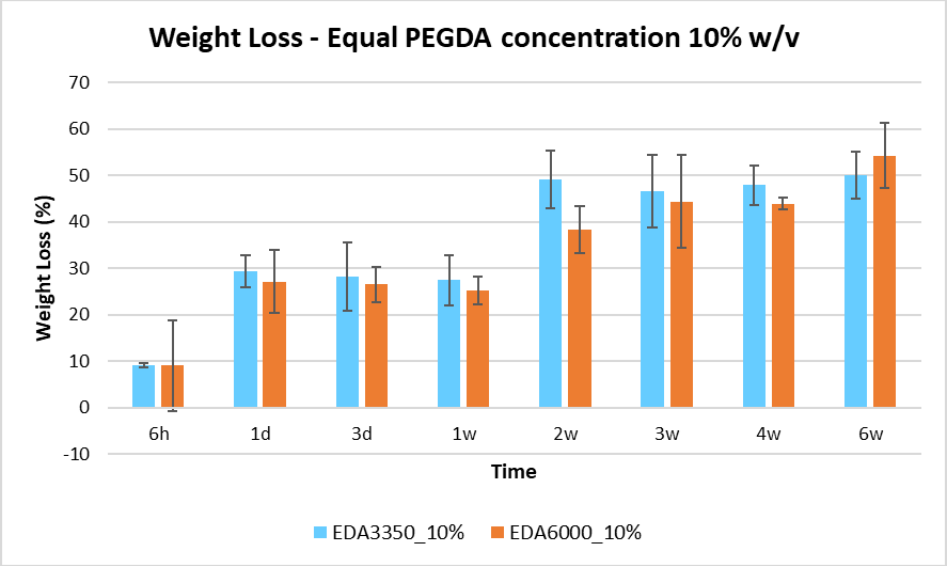

Figure 98:

In brief, considering all the comparisons previously done, it was deduced that:

- The increase of PEGDA concentration at the same molecular weight leads to a decrease of the mesh size and swelling ratio and to an increase of the crosslinking density and therefore of the stability;
- PEGDA 6000 origins a more homogeneous network than PEGDA 3350, because the terminal acrylate groups of longer chains have a better probability to react even in the presence of the steric hindrance of the SHP407 micelles;

- The dissolution of the sample are governed by a kinetic that includes a phase of dissolution and release of the polyurethane component, followed by the collapse of the PEGDA network;
- The dissolution kinetics are strongly influenced by the quality of the PEGDA network formed, and to a lesser extent by the mesh dimension. For this reason, contrary to what was initially expected, PEGDA 6000-based systems were generally more stable than PEGDA 3350-based ones.

3.10 Permeability test

The permeability and consequently the ability to absorb nutrients from the surrounding environment was tested on the same hydrogel photocured samples used for the other tests. FD4 (Fluorescein isothiocyanate-dextran) was used as a model biomolecule.

The results are reported in **Figure 99**.

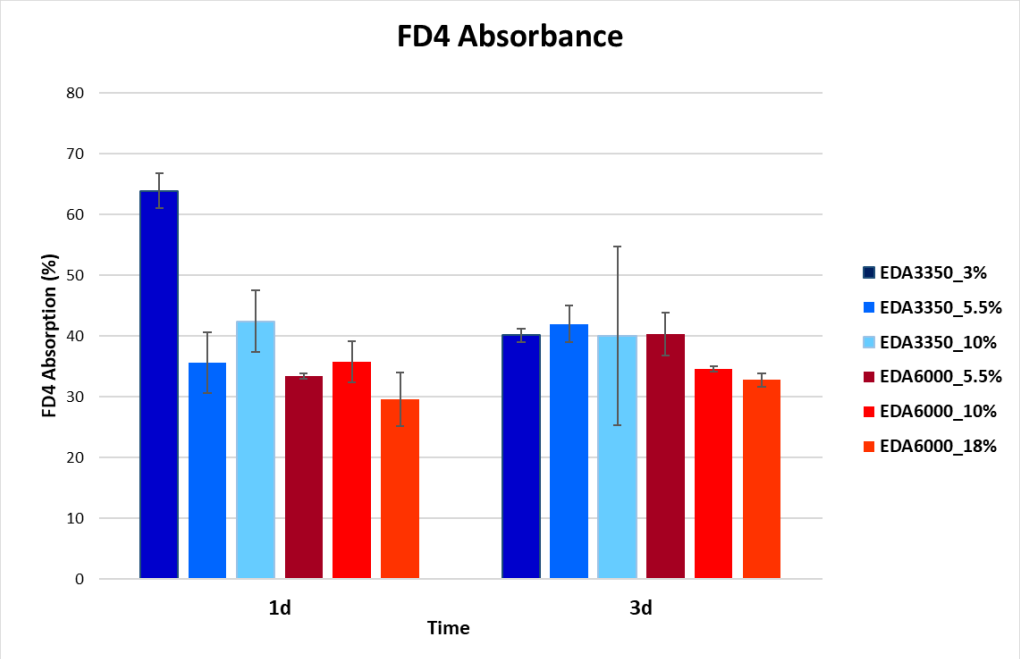

Figure 9922: Percentage of FD4 absorbed by the six different SHP407-PEGDA based blend hydrogels over time.

Generally, the percentage of FD4 absorbed by the samples is similar for all the blends and ranges between 30 and 40%, remaining stable between 1 and 3 days. These results are in accordance with what was observed during swelling and stability tests. However, EDA3350_3% after 1 day of incubation absorbed a significantly higher amount of FD4 (64±14.7 %) with respect to the other formulations, while after 3 days the values were

comparable. This behavior can be explained by the scarce stability of EDA3350_3%, as evidenced by stability tests. Indeed, these hydrogels presented a relevant swelling behavior on the first day of incubation, but dissolution phenomena started to be prevalent after 3 days. In this case, this resulted in a lower percentage of absorbed FD4 after 3 days with respect to 1 day, because due to dissolution the hydrogels released part of the molecule previously absorbed. **Figure 100** reports the visual evidence of the FD4 absorption after 1 day for these systems as an example: the samples, which were clear at the beginning of the test, assumed a bright yellow color due to the molecule present inside.

The high standard deviation found for EDA3350_10% is probably due to inherent difficulties in the hydrogel production process and test conditions, which are very operator-dependent. Indeed, in this case the system has been found to be stable in the time frame considered and swelling and dissolution phenomena are not able to explain the variability found in the results.

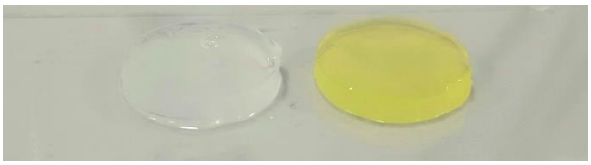

Figure 100: EDA3350_3% hydrogel sample control (Left) and after 1d of FD4 absorption (Right).

3.11 Hydrogel release – FD4

FD4 was used as a model molecule also to study the release kinetics from each hydrogel formulation studied, to consider a possible application as drug release or cell encapsulation platform. In this case, FD4 was incorporated in the systems before the photo-curing process, since it was dissolved together with the polymers before producing the samples. However, during the UV irradiation the aromatic rings present in the FD4 molecules interacted with the light and the loaded samples required a longer curing time (5 minutes instead of 3) than the control sample. The photo-irradiation resulted also in a change of color and a shift of the absorption peak, which finally caused the impossibility of correctly quantify the amount of biomolecule released. **Figure 102** shows the difference between a solution containing 1 mg/ml of FD4 and 0.05% w/v of LAP before and after a 5-minutes irradiation.

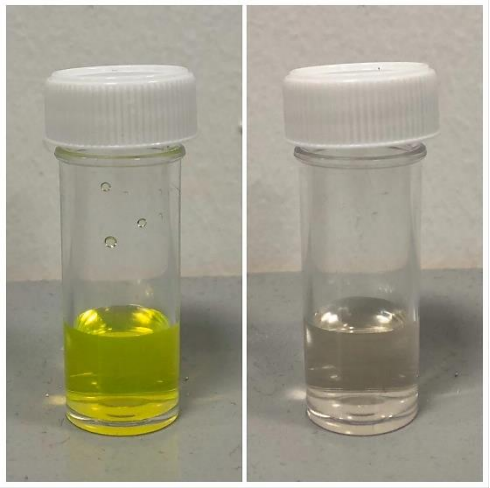

Figure 102: FD4 solution (1mg/ml) before (right) and after (left) 5 minutes of UV irradiation.

For this reason, only a qualitative evaluation of the release was possible. **Figure 103** shows the decrease of color from the production of the disk containing the FD4 solution until the last time step.

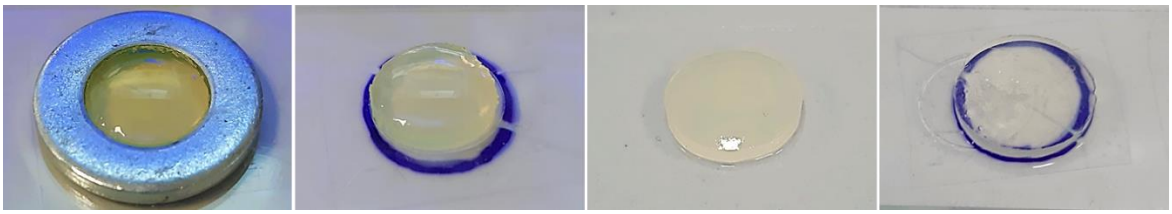

Figure 10323: FD4 release at different time steps.

3.12 Printability

In order to verify the printability of all the formulations, preliminary printing tests were performed using a commercially available bioprinter (Inkredible +, CELLINK).

All the blends resulted easily extrudable through a 27G tip to form 200 µm diameter wires. The printing was performed at room temperature, without heating the bed, because it was observed that keeping the bed at 37°C caused the wire to undergo a sol-gel transition before it touched the support (a Petri dish), causing its shrinkage and preventing a good adhesion.

Pressure required for extrusion were for all the blends comprised in the tents of kPa. However, pressure needed for PEGDA 6000-based systems were generally lower (40-50 kPa), while for PEGDA 3350 it was in some case necessary to reach pressures around 100 kPa. This can be explained considering that PEG is often used as a plasticizer and has a

known effect in decreasing the viscosity of polymeric solution, such as PLA [72], [73], [74]. This effect was especially evident with EDA6000_18% and EDA6000_10%, which despite appearing visually denser, were in fact the systems that required the lower pressure to be extruded (around 40-50 kPa). These observations have been confirmed by plotting the complex viscosity as a function of frequency at 37°C (**Figure 104, 105**).

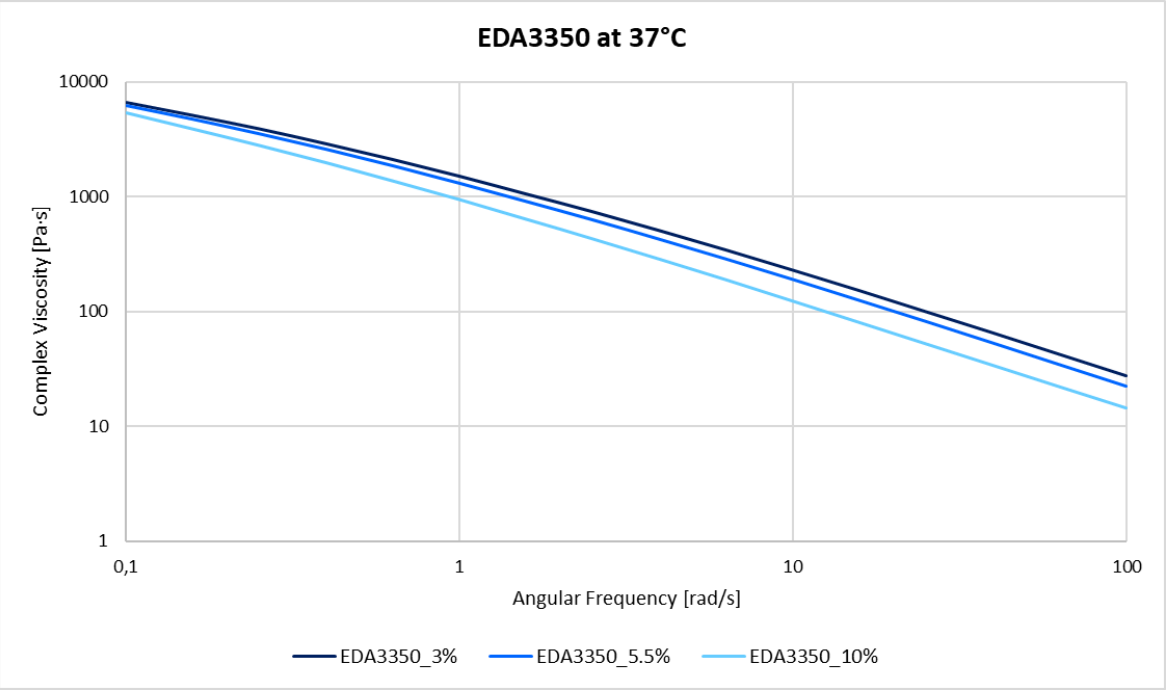

Figure 104: Complex viscosity relative to blends based on PEGDA 3350 Da

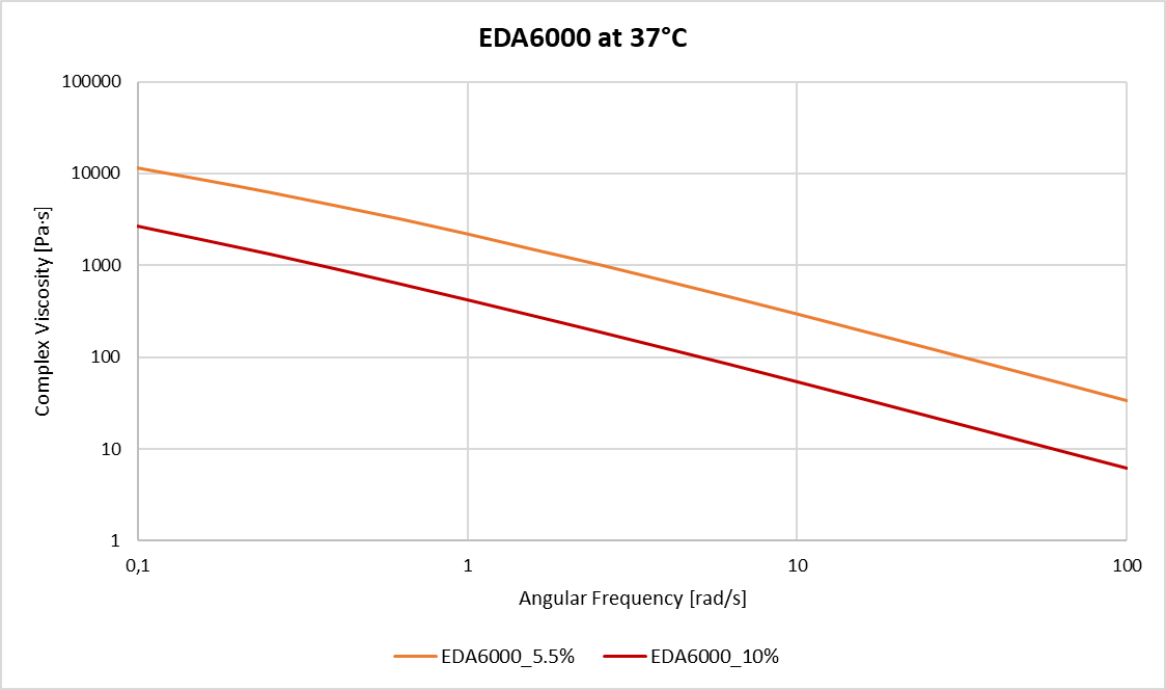

Figure 105: Complex viscosity relative to based on PEGDA 6000 Da.

For PEGDA 3350-based systems, the shear thinning behavior, evidenced by the slope in the complex viscosity values in the range considered, is very similar and indeed the pressure needed during the printing process is similar for all three formulations. On the other hand, regarding PEGDA 6000-based systems, it was possible to plot only the values relative to EDA6000_5.5% and EDA6000_10%, because of the problems found during the rheological characterization of EDA6000_18%. However, it is in this case visible that the complex viscosity obtained for EDA6000_5.5% is almost one order of magnitude higher than for EDA6000_10%, which is consistent with the lower pressure needed to print this formulation.

In this case, however, it was necessary to cool the syringe below room temperature, because these systems LCGT was considerably lower than the other formulations (15±1°C and 22±1°C) and the gelation occurred inside the syringe, affecting the resolution of the final printed scaffold, as observed when the bed was kept at 37°C.

All the optimized printing parameters, reported in **Table 23**, are compatible with a future application that includes cells in the bioprinting formulation, since the pressure and temperature used allow cells survival.

Table 23: Printability optimized parameters.

Printability parameters	
Pressure	40-100 kPa
Tip diameter	27G (200 μm)
Syringe	17-20°C
Bed temperature	25°C
UV Photo-curing Time	3 min (entire scaffold)

Figure 107 shows the model of scaffold shaped like a grid and **Figure 108** shows an example of a 4-layer scaffold printed using EDA6000_10% and the conditions mentioned above. In the code [66] used to obtain the structure shown in the picture, the curing process was to be performed after every single layer was printed. In this case, however, it was possible to

perform the photo-curing only of the entire scaffold after the process was completed, due to the printer current configuration. Despite a certain loss of resolution, after a 3-minutes UV irradiation the structure was able to better maintain its shape for a longer time and not collapse.

Considering the success of the curing procedure with the circular shaped samples used during the hydrogel characterization phase, which are considerably thicker than the single printed layer (approx. 2 mm vs 200 µm), it is expected that performing the irradiation on each layer would result in a significant improvement of the stability of these scaffolds. **Figure 107 and Figure 108** report the material printed in different phases.

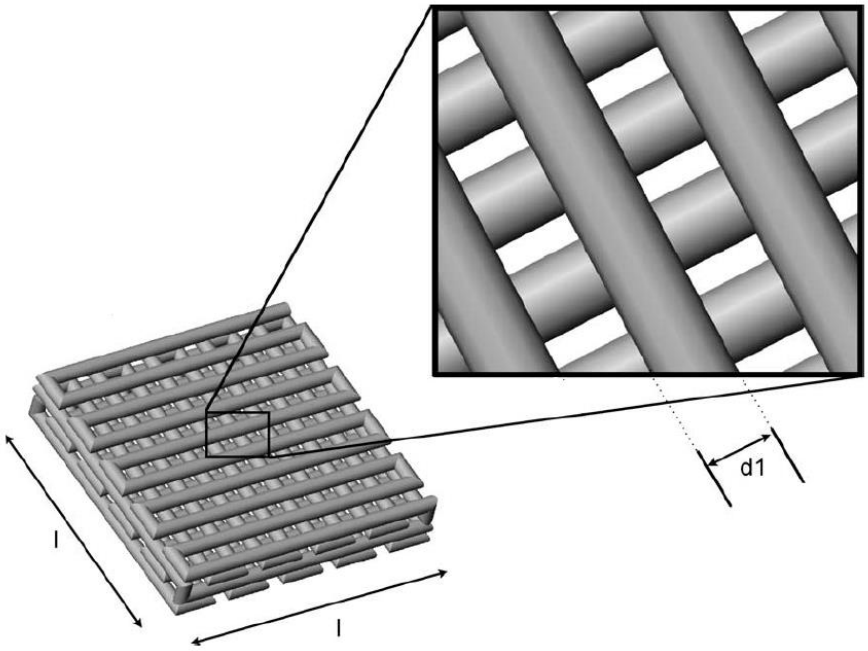

Figure 107: Scaffold theoretical model. l= 13 mm, d_1=~200 µm (adapted from [78]*).*

Figure 108: Scaffold printed model and One-layer printing.

3.13 Cytotoxcity test

As shown in **Figure 109**, the cytotoxcity tests performed on the eluates taken from the hydrogel photocured disks after 24h had positive results for each blend composition. For each material the cell resulted to have a viability near 100% with no significative differences among the different formulations. For this reason, all the blend designed in this work are considered biocompatible and able to be used with cells (bioprinting).

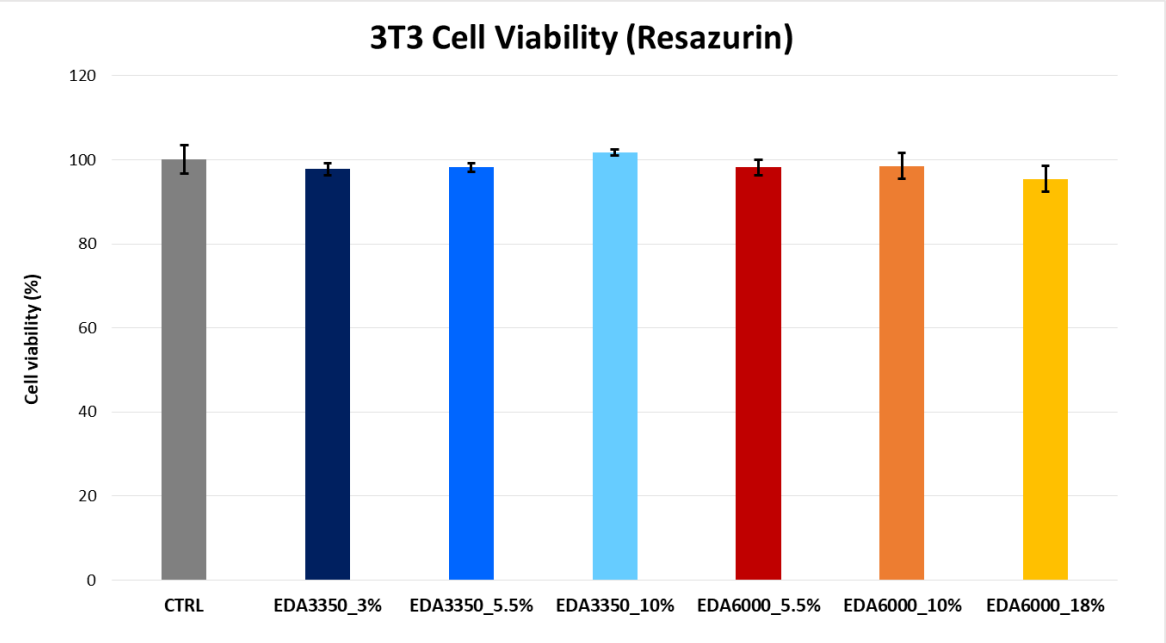

Figure 109: Cytotoxcity tests results.

Conclusions and future works

In this thesis work, a collection of novel thermosensitive and photocurable hydrogels was designed and produced. These two properties were given by the blend of a Poloxamer P407-based polyurethane (SHP407) and poly(ethylene glycol) diacrylate (PEGDA), respectively. Both these materials were successfully synthetized and characterized, in terms of chemical and physical properties, in the first phases of this exploratory work.

The hydrogel formulations were selected keeping the polyurethane component at a concentration of 12.5% w/v for all the blends, following the results of previous works in terms of gelation time and temperature compatible to biological application. The PEGDA component differed for its molecular weight (3350-4600-6000 Da) and concentration added in the blend. The solubility test lead to reject PEGDA 4600 because of its low solubility in PBS , so only the other two polymers were used to produce blend systems. The PEGDA concentrations were selected to allow the formation of a polymeric network with the aim to entrap the polyurethane component and increase the gel stability. The comparison between the different composition was carried out considering the different PEGDA molecular weight, concentration and SHP407-PEGDA molar ratio. Six formulations have been finally selected (EDA3350_3%, EDA3350_5.5%, EDA3350_10%, EDA6000_5.5%, EDA6000_10%, EDA6000_18%). The systems were characterized in terms of thermal response and photo-sensitivity, and their rheological and photo-rheological characteristics were investigated.

Table 24 reports the results obtained for each blend in terms of final storage modulus after photocuring (representative of stiffness), stability, swelling, weight loss results and swelling ratio after 24h of incubation.

Table 24: Resume of the most important results obtained for the blends based on SHP407-PEGDA 3350/6000 Da.

PEGDA Molecular Weight	Concentration (% w/v)	ΔG' (kPa)	G' post photocuring (kPa)	Stability	Swelling at 24 h (%)	Weight Loss at 24h (%)	Swelling Ratio at 24h
3350 Da	3	3.13	5.97	1 week	71.90	32.08	14.59
	5.5	9.16	12	2 weeks	88.46	20.93	14.00
	10	16.68	38.30	> 6 weeks	79.56	29.42	9.97
6000 Da	5.5	14.79	16.90	3 weeks	170.71	20.10	18.21
	10	16.68	28.90	> 6 weeks	125.96	27.15	12.64
	18	69.01	72.50	> 6 weeks	124.38	5.85	8.79

From these results, it was possible to observe how some characteristics of the blends depend on the molecular weight and on PEGDA concentration.

Investigating the variation of storage modulus (G') before and after photocuring (ΔG') through photo-rheological test, it was observed that the range of G' values that the blend covers depends on the molecular weight and concentration of the PEGDA component. The formulations based on PEGDA 3350 cover a range of ΔG' from approx. 3 to 17 kPa. On the other hand, the systems based on PEGDA 6000 cover a range of ΔG' between approx. 15 and 70 kPa. For EDA3350 systems, there an increase of PEGDA concentration from the less to the most concentrate formulation of 70%, while for EDA6000 this value is 67%. Even though the increment is almost the same, however, the two sets cover different ranges of stiffness. PEGDA 3350 formulations cover a larger range of G' values, with an increment of stiffness from the lower to the higher PEGDA concentration around 85%. On the other hand, for PEGDA 6000 formulations this increment is around 76%. Therefore, changing the PEGDA molecular weight and concentration, it is possible to cover different ranges of stiffness, from few to hundreds KPa. Taking also into account that the solubility of PEGDA

is higher than the concentration used in this work, it is theoretically possible to further expand the range of mechanical properties covered by these systems, mimicking the stiffness of a wide range of soft tissues, as shown in **Figure 110**.

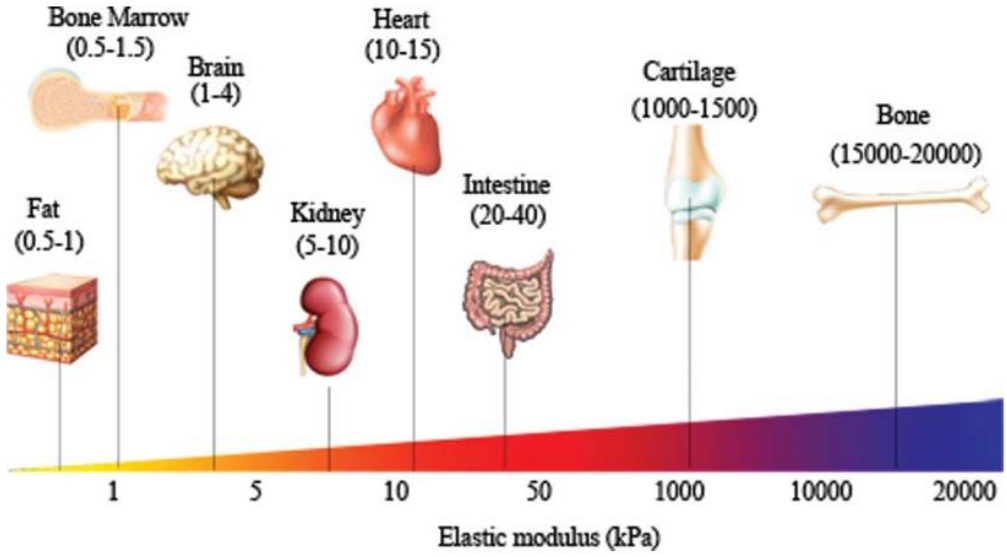

Figure 2410: Distinct modulus of human tissues suggesting tissue-specific stiffness. Different tissues with their specific elastic modulus in the body are correlated with their functions [79].

Some hypotheses have been drawn from the results obtained in terms of stability, swelling and weight loss for the different formulations investigated in this work.

Firstly, a comparison of the formulations containing PEGDA at the same molecular weight was performed. It was observed that the increase of PEGDA concentration lead to a decrease of the mesh size and swelling ratio of the hydrogel systems. It was supposed that the an higher density of PEGDA chains lead to the formation of a more entangled mesh, with an higher amount of cross-linking points, leading to a more stable systems (as evidenced by stability results) and with a weaker ability to absorb fluids due to the more chaotic structure. The hypothesis of a higher crosslinking density found validation also in the photo-rheological measurements, in which an increase of the storage modulus after photocuring was observed at the increasing of PEGDA concentration.

Secondly, a comparison among blend formulations with the same molar ratio between SHP407 and PEGDA in the formulations was performed.

In this case, contrary to what was expected, the higher PEGDA molecular weight did not involve a faster dissolution rate. This behavior was suggested because of the presence of longer PEG chains, that should susceptible to a faster dissolution rate due to higher hydrophilicity; moreover, the larger mesh produced by longer chain was expected to allow a faster ejection of the PU entrapped inside the network. From the stability results, it was instead observed that samples based on PEGDA 6000 had longer stability than PEGDA 3350 ones. This behavior was justified considering the different efficiency of the photo-crosslinking process. PEGDA 6000 has polymeric chains long enough to overcome the steric hindrance given by the SHP407 micelles, so that there is an higher probability that the terminal acrylate groups of different chains could react. The network formed is then more homogeneous and without defects, retraining the polyurethane component with better efficiency. For PEGDA 3350, on the other hand, it is assumed that the network formed by the shorter chains presents more defects and thus allows a faster dissolution of the PU component and a faster collapse of the structure.

In brief, it was observed that for samples with PEGDA at the same molecular weight the increase of concentration leads to a decrease of swelling ratio and mesh size and to an increase of stiffness and crosslinking density. Furthermore, contrary to the preliminary hypothesis, a higher PEGDA molecular weight causes a slower dissolution rate of the hydrogels, thanks to the formation of a network with better quality and homogeneity.

A graphical representation of the supposed differences in the mesh formed by PEGDA 3350 and PEGDA 6000 is reported in **Figure 111**.

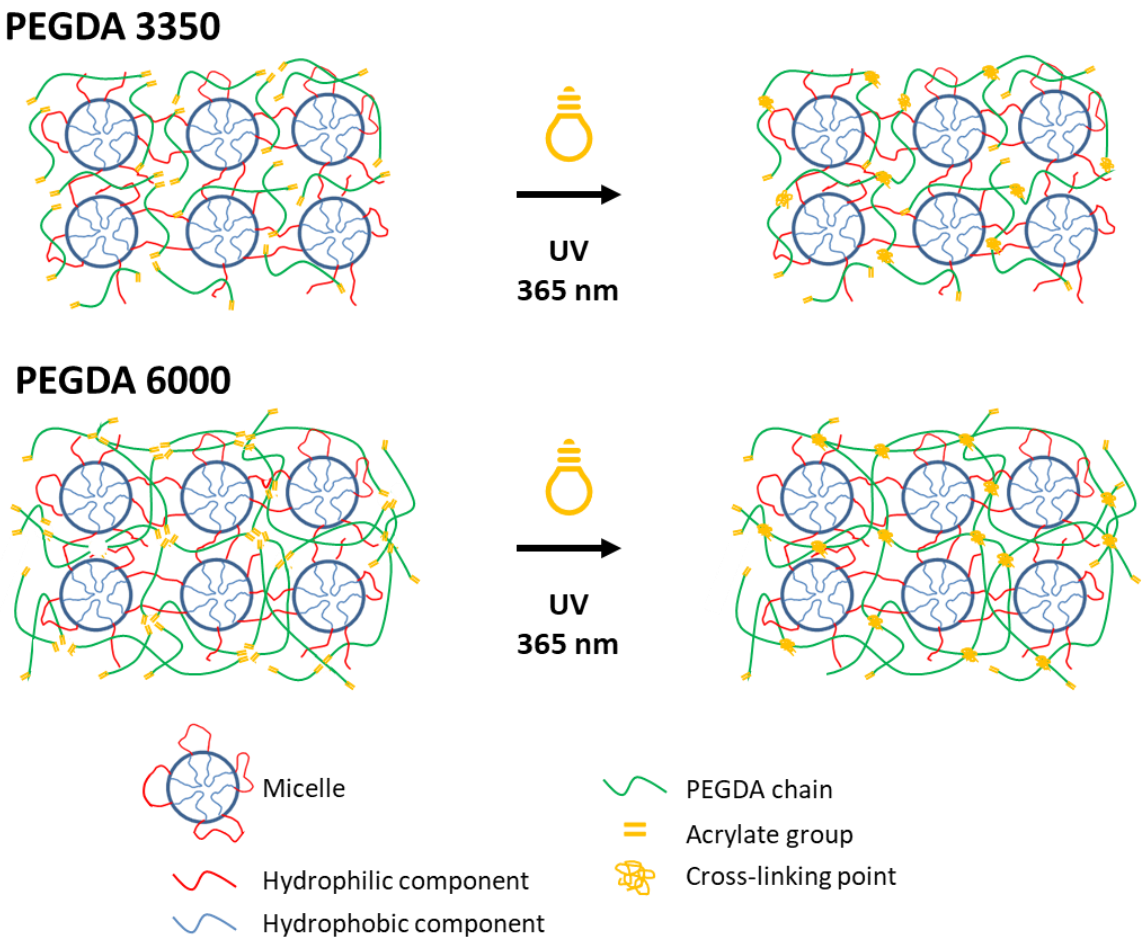

Figure 111: Different behavior in the PEGDA network formation as a result of UV irradiation for PEGDA 3350 Da and PEGDA 6000 Da (credit: Arianna Grivet Brancot).

The permeability to nutrients of the photo-cured formulations and their ability to expel wastes was proved with FD4 absorption and release tests, demonstrating their suitability to host cells. Moreover, they resulted extrudable through tips of small diameter (27G - 200 µm) applying cell-friendly parameters such as low pressures (40-100 kPa) and temperature near physiological values. Furthermore, the time required for the photo-crosslinking (3 min) resulted appropriate for the production of scaffolds loaded with cells and *in vivo* applications in the regenerative medicine field.

Future developments should include the optimization of the printing parameters, that were selected only by preliminary tests and did not guarantee a complete reproducibility of the structure produced. In addition, the stability tests performed on the photo-cured hydrogel massive samples should be repeated on the printed scaffold, to take into consideration the

higher exposed surface and how this influences the dissolution rate. Then, design and printing of scaffolds with more complex shapes should be investigated.

In this thesis work, the photo-crosslinking of the hydrogels was performed using the cytocompatible photo-initiator LAP in the UV light spectrum (365 nm). This photoinitiator was selected thanks to its efficiency, that allowed to obtain hydrogels with good crosslinking densities. Despite this advantage, the use of UV light to perform the photo-crosslinking is considered a disadvantage for *in vivo* and bioprinting applications, because the UV irradiation could damage cells at the DNA level, inducing mutations and/or apoptosis. To avoid this issue, the photocuring in the visible light spectrum (between 390 and 700 nm) should be investigated. In the first phases of this project, photo-crosslinking tests using Riboflavin as a photo-initiator and Triethanolamine as co-photoinitiator were performed. Riboflavin presents a main peak of absorption at 444 nm and another in the UV region (around 365 nm), that could enable photo-curing in the visible region. However, the preliminary test performed did not yield positive results. The concentrations used (riboflavin 2.5 µM and triethanolamine 50 mM) and the curing parameters (UV light at 365 nm, density 10 mw/cm^2, 10 min of irradiation) were taken from literature and demonstrated to not be suitable without a proper optimization. So, although the feasibility of this method was proved, the further optimization required to obtain good results went beyond the scope of this thesis work.

Bibliography

[1] W. Y. Seow and C. A. E. Hauser, “Short to ultrashort peptide hydrogels for biomedical uses,” *Mater. Today*, vol. 17, no. 8, pp. 381–388, 2014.

[2] O. WICHTERLE and D. LÍM, “Hydrophilic Gels for Biological Use,” *Nature*, vol. 185, no. 4706, pp. 117–118, 1960.

[3] Y. Li, J. Rodrigues, and H. Tomás, “Injectable and biodegradable hydrogels: Gelation, biodegradation and biomedical applications,” *Chem. Soc. Rev.*, vol. 41, no. 6, pp. 2193–2221, 2012.

[4] T. R. Hoare and D. S. Kohane, “Hydrogels in drug delivery: Progress and challenges,” *Polymer (Guildf).*, vol. 49, no. 8, pp. 1993–2007, 2008.

[5] L. R. Feksa, E. A. Troian, C. D. Muller, F. Viegas, A. B. Machado, and V. C. Rech, “Hydrogels for biomedical applications,” in *Nanostructures for the Engineering of Cells, Tissues and Organs: From Design to Applications*, 2018, pp. 403–438.

[6] Lh. Yahia, “History and Applications of Hydrogels,” *J. Biomed. Sci.*, vol. 04, no. 02, pp. 1–23, 2017.

[7] F. Castelli, G. Pitarresi, and G. Giammona, “Influence of different parameters on drug release from hydrogel systems to a biomembrane model. Evaluation by differential scanning calorimetry technique,” *Biomaterials*, vol. 21, no. 8, pp. 821–833, 2000.

[8] L. G. Griffith, “Polymeric biomaterials,” *Acta Mater.*, vol. 48, no. 1, pp. 263–277, Jan. 2000.

[9] N. Annabi *et al.*, “Controlling the Porosity and Microarchitecture of Hydrogels for Tissue Engineering,” *Tissue Eng. Part B Rev.*, vol. 16, no. 4, pp. 371–383, 2010.

[10] P. Eiselt, J. Yeh, R. K. Latvala, L. D. Shea, and D. J. Mooney, “Porous carriers for biomedical applications based on alginate hydrogels,” *Biomaterials*, vol. 21, no. 19, pp. 1921–1927, 2000.

[11] G. Huang, J. Gao, Z. Hu, J. V. St. John, B. C. Ponder, and D. Moro, “Controlled drug release from hydrogel nanoparticle networks,” *J. Control. Release*, vol. 94, no. 2–3, pp. 303–311, 2004.

[12] N. A. Neuburger and B. E. Eichinger, “Critical Experimental Test of the Flory-Rehner Theory of Swelling,” *Macromolecules*, vol. 21, no. 10, pp. 3060–3070, 1988.

[13] G. Jalani *et al.*, “Real-time, non-invasive monitoring of hydrogel degradation using

LiYF4:Yb3+/Tm3+ NIR-to-NIR upconverting nanoparticles," *Nanoscale*, vol. 7, no. 26, pp. 11255–11262, 2015.

[14] M. Yamamoto, Y. Ikada, and Y. Tabata, "Controlled release of growth factors based on biodegradation of gelatin hydrogel," *J. Biomater. Sci. Polym. Ed.*, vol. 12, no. 1, pp. 77–88, 2001.

[15] M. C. Cushing and K. S. Anseth, "Hydrogel cell cultures," *Science (80-.).*, vol. 316, no. 5828, pp. 1133–1134, 2007.

[16] R. Francis, D. K. Baby, and D. S. Kumar, "Poly(N-isopropylacrylamide) hydrogel: Effect of hydrophilicity on controlled release of ibuprofen at different pH," *J. Appl. Polym. Sci.*, vol. 124, no. 6, pp. 5079–5088, 2012.

[17] L. R. Feksa, E. A. Troian, C. D. Muller, F. Viegas, A. B. Machado, and V. C. Rech, "Hydrogels for biomedical applications," *Nanostructures Eng. Cells, Tissues Organs From Des. to Appl.*, vol. 64, pp. 403–438, 2018.

[18] T. R. R. Singh, G. Laverty, and R. F. Donnelly, *Hydrogels : design, synthesis and application in drug delivery and regenerative medicine*. 2018.

[19] B. D. RATNER and A. S. HOFFMAN, "Synthetic Hydrogels for Biomedical Applications," pp. 1–36, 2009.

[20] D. Schmaljohann, "Thermo- and pH-responsive polymers in drug delivery," *Adv. Drug Deliv. Rev.*, vol. 58, no. 15, pp. 1655–1670, Dec. 2006.

[21] E. Hopkins and S. Sharma, "Physiology, Acid Base Balance," pp. 2–7, 2018.

[22] H. R. Culver, J. R. Clegg, and N. A. Peppas, "Analyte-Responsive Hydrogels: Intelligent Materials for Biosensing and Drug Delivery," *Acc. Chem. Res.*, vol. 50, no. 2, pp. 170–178, 2017.

[23] T. Traitel, Y. Cohen, and J. Kost, "Characterization of glucose-sensitive insulin release systems in simulated in vivo conditions.," *Biomaterials*, vol. 21, no. 16, pp. 1679–87, Aug. 2000.

[24] M. R. Matanović, J. Kristl, and P. A. Grabnar, "Thermoresponsive polymers: Insights into decisive hydrogel characteristics, mechanisms of gelation, and promising biomedical applications," *Int. J. Pharm.*, vol. 472, no. 1–2, pp. 262–275, 2014.

[25] L. Bromberg, "Properties of aqueous solutions and gels of poly(ethylene oxide)-b-poly(propylene oxide)-b-poly(ethylene oxide)-g-poly(acrylic acid)," *J. Phys. Chem. B*, vol. 102, no. 52, pp. 10736–10744, 1998.

[26] A. Cabana, A. Aït-Kadi, and J. Juhász, “Study of the gelation process of polyethylene oxide(a)-polypropylene oxide(b)-polyethylene oxide, copolymer (poloxamer 407) aqueous solutions,” *J. Colloid Interface Sci.*, vol. 190, no. 2, pp. 307–312, 1997.

[27] H. Li, G. E. Yu, C. Price, C. Booth, E. Hecht, and H. Hoffmann, “Concentrated aqueous micellar solutions of diblock copoly(oxyethylene/oxybutylene) E41B8: A study of phase behavior,” *Macromolecules*, vol. 30, no. 5, pp. 1347–1354, 1997.

[28] J. Chen, R. Zhou, L. Li, B. Li, X. Zhang, and J. Su, “Mechanical, rheological and release behaviors of a poloxamer 407/poloxamer 188/carbopol 940 thermosensitive composite hydrogel,” *Molecules*, vol. 18, no. 10, pp. 12415–12425, 2013.

[29] M. Boffito *et al.*, “Novel polyurethane-based thermosensitive hydrogels as drug release and tissue engineering platforms: Design and in vitro characterization,” *Polym. Int.*, vol. 65, no. 7, pp. 756–769, 2016.

[30] V. Chiono *et al.*, “Synthetic biodegradable medical polyurethanes,” *Sci. Princ. Biodegrad. Bioresorbable Med. Polym. Mater. Prop.*, pp. 189–216, 2016.

[31] C. Pontremoli *et al.*, “Hybrid injectable platforms for the in situ delivery of therapeutic ions from mesoporous glasses,” *Chem. Eng. J.*, vol. 340, no. January, pp. 103–113, 2018.

[32] M. A. Lago, A. Rodríguez-Bernaldo de Quirós, R. Sendón, J. Bustos, M. T. Nieto, and P. Paseiro, “Photoinitiators: a food safety review,” *Food Addit. Contam. - Part A Chem. Anal. Control. Expo. Risk Assess.*, vol. 32, no. 5, pp. 779–798, 2015.

[33] C. G. Williams, A. N. Malik, T. K. Kim, P. N. Manson, and J. H. Elisseeff, “Variable cytocompatibility of six cell lines with photoinitiators used for polymerizing hydrogels and cell encapsulation,” *Biomaterials*, vol. 26, no. 11, pp. 1211–1218, 2005.

[34] M. A. Shaker and H. M. Younes, “Photo-irradiation paradigm: Mapping a remarkable facile technique used for advanced drug, gene and cell delivery,” *J. Control. Release*, vol. 217, pp. 10–26, 2015.

[35] I. Mironi-Harpaz, D. Y. Wang, S. Venkatraman, and D. Seliktar, “Photopolymerization of cell-encapsulating hydrogels: Crosslinking efficiency versus cytotoxicity,” *Acta Biomater.*, vol. 8, no. 5, pp. 1838–1848, 2012.

[36] Ş. Şenol and E. Akyol, “Study on the preparation and drug release property of Modified PEG-DA based hydrogels,” *J. Turkish Chem. Soc. Sect. A Chem.*, vol. 6, no.

1, pp. 1–14, 2019.

[37] F. Markus, F. Dreher, S. Laschat, S. Baudis, G. E. M. Tovar, and A. Southan, “Physically and chemically gelling hydrogel formulations based on poly(ethylene glycol) diacrylate and Poloxamer 407,” *Polymer (Guildf).*, vol. 108, pp. 21–28, 2017.

[38] E. A. Kamoun, A. M. Omer, S. N. Khattab, H. M. Ahmed, and A. A. Elbardan, “In-situ UV-photopolymerized PVA-g-GMA hydrogels for biomedical applications: I. Synthesis, characterizations and grafting optimization,” *J. Appl. Pharm. Sci.*, vol. 8, no. 1, pp. 034–042, 2018.

[39] W. Chen, Y. Hou, Z. Tu, L. Gao, and R. Haag, “pH-degradable PVA-based nanogels via photo-crosslinking of thermo-preinduced nanoaggregates for controlled drug delivery,” *J. Control. Release*, vol. 259, pp. 160–167, 2017.

[40] M. Rafat, L. S. Rotenstein, J. O. You, and D. T. Auguste, “Dual functionalized PVA hydrogels that adhere endothelial cells synergistically,” *Biomaterials*, vol. 33, no. 15, pp. 3880–3886, 2012.

[41] B. D. Fairbanks, M. P. Schwartz, C. N. Bowman, and K. S. Anseth, “Photoinitiated polymerization of PEG-diacrylate with lithium phenyl-2,4,6-trimethylbenzoylphosphinate: polymerization rate and cytocompatibility,” *Biomaterials*, vol. 30, no. 35, pp. 6702–6707, 2009.

[42] A. K. Nguyen *et al.*, “Two-photon polymerization of polyethylene glycol diacrylate scaffolds with riboflavin and triethanolamine used as a water-soluble photoinitiator,” *Regen. Med.*, vol. 8, no. 6, pp. 725–738, 2013.

[43] A. J. Finch, J. M. Benson, P. E. Donnelly, and P. A. Torzilli, “Light Absorptive Properties of Articular Cartilage, ECM Molecules, Synovial Fluid, and Photoinitiators as Potential Barriers to Light-Initiated Polymer Scaffolding Procedures,” *Cartilage*, vol. 10, no. 1, pp. 82–93, 2019.

[44] I. Ahmad *et al.*, “Photoinitiated Polymerization of 2-Hydroxyethyl Methacrylate by Riboflavin/Triethanolamine in Aqueous Solution: A Kinetic Study,” *ISRN Pharm.*, vol. 2013, pp. 1–7, 2013.

[45] M. B. Browning, S. N. Cereceres, P. T. Luong, and E. M. Cosgriff-Hernandez, “Determination of the in vivo degradation mechanism of PEGDA hydrogels,” *J. Biomed. Mater. Res. - Part A*, vol. 102, no. 12, pp. 4244–4251, 2014.

[46] S. Jiang, S. Liu, and W. Feng, “PVA hydrogel properties for biomedical application,” *J.*

Mech. Behav. Biomed. Mater., vol. 4, no. 7, pp. 1228–1233, 2011.

[47] J. Shen and D. J. Burgess, "Accelerated in vitro release testing of implantable PLGA microsphere/PVA hydrogel composite coatings," *Int. J. Pharm.*, vol. 422, no. 1–2, pp. 341–348, 2012.

[48] C. E. MacIas, H. Bodugoz-Senturk, and O. K. Muratoglu, "Quantification of PVA hydrogel dissolution in water and bovine serum," *Polymer (Guildf).*, vol. 54, no. 2, pp. 724–729, 2013.

[49] D. W. Hutmacher, "Scaffold design and fabrication technologies for engineering tissues - State of the art and future perspectives," *J. Biomater. Sci. Polym. Ed.*, vol. 12, no. 1, pp. 107–124, 2001.

[50] H. Tan and K. G. Marra, "Injectable, biodegradable hydrogels for tissue engineering applications," *Materials (Basel).*, vol. 3, no. 3, pp. 1746–1767, 2010.

[51] F. P. W. Melchels, M. A. N. Domingos, T. J. Klein, J. Malda, P. J. Bartolo, and D. W. Hutmacher, "Additive manufacturing of tissues and organs," *Prog. Polym. Sci.*, vol. 37, no. 8, pp. 1079–1104, 2012.

[52] S. V Murphy and A. Atala, "3D bioprinting of tissues and organs," *Nat. Biotechnol.*, vol. 32, p. 773, Aug. 2014.

[53] S. Ji and M. Guvendiren, "Recent Advances in Bioink Design for 3D Bioprinting of Tissues and Organs," *Front. Bioeng. Biotechnol.*, vol. 5, no. APR, pp. 1–8, 2017.

[54] N. Carolina, "F ETAL AND N EONATAL S TEM C ELLS Bioprinted Amniotic Fluid-Derived Stem Cells Accelerate Healing of Large Skin Wounds," pp. 792–802, 2012.

[55] F. Guillemot *et al.*, "High-throughput laser printing of cells and biomaterials for tissue engineering," *Acta Biomater.*, vol. 6, no. 7, pp. 2494–2500, 2010.

[56] R. Pantani and L. S. Turng, "Manufacturing of advanced biodegradable polymeric components," *J. Appl. Polym. Sci.*, vol. 132, no. 48, 2015.

[57] R. Sunyer, A. J. Jin, R. Nossal, and D. L. Sackett, "Fabrication of Hydrogels with Steep Stiffness Gradients for Studying Cell Mechanical Response," *PLoS One*, vol. 7, no. 10, pp. 1–9, 2012.

[58] R. E. Saunders and B. Derby, "Inkjet printing biomaterials for tissue engineering: Bioprinting," *Int. Mater. Rev.*, vol. 59, no. 8, pp. 430–448, 2014.

[59] X. Cui, D. Dean, Z. M. Ruggeri, and T. Boland, "Cell damage evaluation of thermal inkjet printed chinese hamster ovary cells," *Biotechnol. Bioeng.*, vol. 106, no. 6, pp.

963–969, 2010.

[60] I. Lee, J. Roh, J. Lee, J. Song, and J. Jang, “Antibacterial performance of various amine functional polymers coated silica nanoparticles,” *Polymer (Guildf).*, vol. 83, pp. 223–229, 2016.

[61] J. Fang, S. H. Ye, V. Shankarraman, Y. Huang, X. Mo, and W. R. Wagner, “Biodegradable poly(ester urethane)urea elastomers with variable amino content for subsequent functionalization with phosphorylcholine,” *Acta Biomater.*, vol. 10, no. 11, pp. 4639–4649, 2014.

[62] C. Pradal, K. S. Jack, L. Grøndahl, and J. J. Cooper-White., “Gelation kinetics and viscoelastic properties of pluronic and α-cyclodextrin-based pseudopolyrotaxane hydrogels,” *Biomacromolecules*, vol. 14, no. 10, pp. 3780–3792, 2013.

[63] P. Alexandridis, J. F. Holzwarth, and T. A. Hatton, “Micellization of Poly(ethylene oxide)-Poly(propylene oxide)-Poly(ethylene oxide) Triblock Copolymers in Aqueous Solutions: Thermodynamics of Copolymer Association,” *Macromolecules*, vol. 27, no. 9, pp. 2414–2425, 1994.

[64] R. Georgiev *et al.*, “Triblock copolymer micelles as templates for preparation of mesoporous niobia thin films,” *J. Phys. Conf. Ser.*, vol. 992, no. 1, 2018.

[65] X. Yang, S. K. Sarvestani, S. Moeinzadeh, X. He, and E. Jabbari, “Three-dimensional-engineered matrix to study cancer stem cells and tumorsphere formation: Effect of matrix modulus,” *Tissue Eng. - Part A*, vol. 19, no. 5–6, pp. 669–684, 2013.

[66] S. Calzone, “Design of innovative thermo- and photo-sensitive bioinks and printing setup for the fabrication of tissue engineered constructs,” 2019.

[67] L. Ouyang, C. B. Highley, W. Sun, and J. A. Burdick, “A Generalizable Strategy for the 3D Bioprinting of Hydrogels from Nonviscous Photo-crosslinkable Inks,” *Adv. Mater.*, vol. 29, no. 8, 2017.

[68] R. F. Pereira and P. J. Bártolo, “3D Photo-Fabrication for Tissue Engineering and Drug Delivery,” *Engineering*, vol. 1, no. 1, pp. 090–112, 2015.

[69] T. Master and B. Engineering, “Master of Science in Biomedical Engineering Novel thermo-sensitive and photo-curable hydrogels as potential bioinks in regenerative medicine,” no. December, 2017.

[70] S. Kirchhof *et al.*, “Diels-Alder Hydrogels for Controlled Antibody Release: Correlation between Mesh Size and Release Rate,” *Mol. Pharm.*, vol. 12, no. 9, pp. 3358–3368,

2015.

[71] F. Tan, X. Xu, T. Deng, M. Yin, X. Zhang, and J. Wang, “Fabrication of positively charged poly(ethylene glycol)-diacrylate hydrogel as a bone tissue engineering scaffold,” *Biomed. Mater.*, vol. 7, no. 5, 2012.

[72] H. Rahmani, S. H. M. Najafi, S. Saffarzadeh-Matin, and A. Ashori, “Effect of No of plies, Angle ply layers, Fiber,” 2013.

[73] W. Pivsa-Art, K. Fujii, K. Nomura, Y. Aso, H. Ohara, and H. Yamane, “The effect of poly(ethylene glycol) as plasticizer in blends of poly(lactic acid) and poly(butylene succinate),” *J. Appl. Polym. Sci.*, vol. 133, no. 8, pp. 1–10, 2016.

[74] D. Li *et al.*, “Preparation of plasticized poly (lactic acid) and its influence on the properties of composite materials,” *PLoS One*, vol. 13, no. 3, pp. 1–15, 2018.

[75] D. J. Munoz-Pinto, S. Samavedi, B. Grigoryan, and M. S. Hahn, “Impact of secondary reactive species on the apparent decoupling of poly(ethylene glycol) diacrylate hydrogel average mesh size and modulus,” *Polymer (Guildf).*, vol. 77, pp. 227–238, 2015.

[76] S. Lee, X. Tong, and F. Yang, “The effects of varying poly(ethylene glycol) hydrogel crosslinking density and the crosslinking mechanism on protein accumulation in three-dimensional hydrogels,” *Acta Biomater.*, vol. 10, no. 10, pp. 4167–4174, 2014.

[77] M. P. Glycol, D. P. Hydrogels, K. O. Donnell, A. Boyd, and B. J. Meenan, “Controlling Fluid Di ff usion and Release through,” 2019.

[78] R. Landers, A. Pfister, U. Hübner, H. John, R. Schmelzeisen, and R. Mülhaupt, “Fabrication of soft tissue engineering scaffolds by means of rapid prototyping techniques,” *J. Mater. Sci.*, vol. 37, no. 15, pp. 3107–3116, 2002.

[79] A. M. Handorf, Y. Zhou, M. A. Halanski, and W. J. Li, “Tissue stiffness dictates development, homeostasis, and disease progression,” *Organogenesis*, vol. 11, no. 1, pp. 1–15, 2015.